ANTIOXIDANTS & REDOX SIGNALING
Volume 20, Number 15, 2014

DOI: 10.1089/ars.2012.5147

Discoveries

FORUM REVIEW ARTICLE

SOD Therapeutics: Latest Insights into Their Structure-Activity Relationships and Impact on the Cellular Redox-Based Signaling Pathways

Ines Batinic-Haberle,[1] Artak Tovmasyan,[1] Emily R. H. Roberts,[2] Zeljko Vujaskovic,[1,*] Kam W. Leong,[2,3] and Ivan Spasojevic[4]

Abstract

Significance: Superoxide dismutase (SOD) enzymes are indispensable and ubiquitous antioxidant defenses maintaining the steady-state levels of $O_2^{\bullet -}$; no wonder, thus, that their mimics are remarkably efficacious in essentially any animal model of oxidative stress injuries thus far explored. ***Recent Advances:*** Structure-activity relationship (half-wave reduction potential [$E_{1/2}$] *versus* log k_{cat}), originally reported for Mn porphyrins (MnPs), is valid for any other class of SOD mimics, as it is dominated by the superoxide reduction and oxidation potential. The biocompatible $E_{1/2}$ of $\sim$+300 mV *versus* normal hydrogen electrode (NHE) allows powerful SOD mimics as mild oxidants and antioxidants (alike $O_2^{\bullet -}$) to readily traffic electrons among reactive species and signaling proteins, serving as fine mediators of redox-based signaling pathways. Based on similar thermodynamics, both SOD enzymes and their mimics undergo similar reactions, however, due to vastly different sterics, with different rate constants. ***Critical Issues:*** Although log $k_{cat}(O_2^{\bullet -})$ is a good measure of therapeutic potential of SOD mimics, discussions of their *in vivo* mechanisms of actions remain mostly of speculative character. Most recently, the therapeutic and mechanistic relevance of oxidation of ascorbate and glutathionylation and oxidation of protein thiols by MnP-based SOD mimics and subsequent inactivation of nuclear factor κB has been substantiated in rescuing normal and killing cancer cells. Interaction of MnPs with thiols seems to be, at least in part, involved in up-regulation of endogenous antioxidative defenses, leading to the healing of diseased cells. ***Future Directions:*** Mechanistic explorations of single and combined therapeutic strategies, along with studies of bioavailability and translational aspects, will comprise future work in optimizing redox-active drugs. *Antioxid. Redox Signal.* 20, 2372–2415.

Introduction

The superoxide dismutase (SOD) mimics were initially viewed as highly specific to $O_2^{\bullet -}$, whereas other reactions were, for the most part, neglected. However, driven by the expansion of knowledge on oxidative stress, cellular redox metabolism, and redox-active compounds, we and others have provided evidence that SOD mimics and other redox-active compounds undergo *in vivo* a variety of reactions, which *via* redox-sensitive signaling pathways affect cellular processes such as proliferation, differentiation, and cell death (26–28, 33, 177, 271). Therefore, the SOD therapeutics could be more appropriately described as modulators of cellular redox environment–redoxome. Recently, the term "redoxome" was established to describe the cellular redox-based signaling pathways (43, 264). Due to Buettner *et al.* (43), redoxome—a"fundamental aspect of biology—is a "quantitative information on the redox enzymes and proteins as well as the unstable, quasi-stable, and redox active species that determine the redox environment of cells and tissues."

[1]Department of Radiation Oncology, Duke University Medical School, Durham, North Carolina.
[2]Department of Biomedical Engineering, Duke University, Durham, North Carolina.
[3]King Abdulaziz University, Jeddah, Saudi Arabia Kingdom.
[4]Department of Medicine, Duke University Medical School, Durham, North Carolina.
*Current affiliation: Division of Translational Radiation Sciences, Department of Radiation Oncology, University of Maryland, Baltimore, Maryland.

The reduction potential of redox-active drugs determines whether they could be readily coupled (oxidized and/or reduced) with redox-active biological targets. As long as the compound produces beneficial therapeutic effects, it may not be utterly important to distinguish between the RS scavenged or pathways affected, and to describe the compound strictly as either SOD mimic or peroxynitrite or any other RS scavenger. We are far away from singling out the reactive species and/or other biological targets being involved in the *in vivo* actions of SOD mimics—many and diverse have already been identified as indicated here and in several other articles published in this Forum. Genetic approaches are essential for the correct conclusions on the type of species/pathways involved in oxidative damage. However, our present understanding based on numerous studies allows us to claim with a fair certainty that more potent the SOD mimic is—the closer its $E_{1/2}$ to that of SOD enzyme (+300 mV *vs*. normal hydrogen electrode [NHE])—the more biocompatible it is with cellular redox-based pathways, and, thus, the more easily it could shuttle electrons among reactive species and signaling proteins by normalizing the cellular redox environment. Thus far, our studies indicate that the k_{cat} for the catalysis of $O_2^{\bullet-}$ dismutation is a reliable measure of the therapeutic potential of redox-active compounds. Therefore, striving for the most potent SOD mimic may still be the most promising drug design approach.

The targeting of the cellular redox sensitive pathways—redoxome—is still an unusual therapeutic strategy, at least from the point of view of medical audience and pharmaceutical companies. However, cellular metabolism is dominated by redox-based processes: mitochondrial respiration, glycolysis, microsomal electron transport chain, detoxification by cyt P450 enzymes, nitric oxide synthesis, and so on. It is very unlikely that a single drug targeting a single target in a cell, where redundant systems are common, would become a potent therapeutic for a pathological condition with perturbed cellular redox status. Multi-drug strategies are, thus, becoming increasingly common in treating pathological conditions. Since normal and cancer cells differ with regard to their redox status, we have anticipated, and it is becoming increasingly true, that SOD mimics have a differential impact on their metabolism: heal a normal cell and kill a cancer cell. As our knowledge increases, and the impact of redox biology on the cell metabolism becomes exceedingly obvious, the Pharma and the medical researchers start recognizing the advantage of redox-biocompatible therapeutics and promote their development. Indeed, some time ago, NIH offered a funding opportunity for the exploration of "Metals in Medicine."

Besides its redox activity, the other major factor contributing to the drug efficacy is its bioavailability. Organ distribution, extra- and intracellular levels, and their subcellular localization will impact the final therapeutic outcome. The remarkable *in vivo* effects of SOD mimics are driving the ongoing studies.

The synthesis, isolation, and purification of cationic metalloporphyrins (MPs) have been challenges. We have learned and provided sufficient evidence that it is of utmost importance to check the quality and identity of drugs used in preclinical models to avoid misinterpretations and loss of time and resources. Comprehensive pharmacokinetic (PK) studies are often lacking, but are essential for drug development toward clinics. For example, with no earlier comprehensive PK studies, curcumin entered and failed the Clinical Trials in Alzheimer's patients (36). It was subsequently shown that it is neither sufficiently bioavailable (not much gets into the blood stream, as it undergoes glucuronidation) nor crosses the blood brain barrier (BBB), a property essential for neurodegenerative diseases; both sets of data should have been a prerequisite for conducting Clinical Trials.

By definition, an SOD mimic/therapeutic is the one that catalyzes the oxidation and reduction of $O_2^{\bullet-}$ (Eqs. [1] and [2]). As it happens, only a few compounds are "true" SOD mimics and are discussed in great detail here (ones that are not, are addressed only briefly for the sake of discussion or comparison). The true SOD mimics are MPs, Mn(III) biliverdins, metallocorroles (MCs), Mn(III) salens, Mn(II) cyclic polyamines, and metal oxides; their representatives are shown in Figure 1. MPs can either act as true SOD mimics (Eqs. [1] and [2]) or couple with cellular reductants (Eq. [2]), acting as superoxide reductase [alike enzymes in some organisms (57)]. The removal of $O_2^{\bullet-}$ can also be coupled to the reduction of $ONOO^-$, where SOD mimic would act as peroxynitrite/superoxide reducto-oxidase (147, 148, 241). The proportionality of log $k_{cat}(O_2^{\bullet-})$ *versus* log $k_{red}(ONOO^-)$ proves that powerful SOD mimics are also powerful reductants of $ONOO^-$ (28, 84, 86). None of the potential therapeutics under investigation and none of the biomarkers available can readily distinguish between $O_2^{\bullet-}$, H_2O_2, and $ONOO^-$. Modest specificity toward $ONOO^-$ relative to $O_2^{\bullet-}$, but not toward H_2O_2, has been achieved with boron-based reagents (58, 119, 293).

Here, we have addressed SOD mimics with regard to their (i) rational design and structure-activity relationships (SARs); (ii) reactivity toward reactive species other than $O_2^{\bullet-}$; (iii) impact on the cellular signaling pathways in various models of oxidative stress injuries; (iv) bioavailability; and (v) therapeutic effects related to the radiation and cancer. For injuries of central nervous systems, see review from Warner and Sheng groups (236); while for inflammation and immunity disorders, see contribution from Piganelli group (208). For the corrole-based SOD mimics, see references from Gross's group (103, 104).

Drug Design

The vital and indispensable role of SOD enzymes in all living organisms has been a driving force in the search for their mimics (see articles in Forum on SOD enzymes in ARS 20/10, and in this Forum on SOD therapeutics). In addition to MPs, different classes of SOD mimics have been developed: Mn salens, Mn corroles, and Mn cyclic polyamines (28). Over the years, reactivities other than toward $O_2^{\bullet-}$ for all SOD mimics have been demonstrated. Importantly, the proportionality between the log k_{cat} ($O_2^{\bullet-}$) and their therapeutiuc efficacy has been demonstrated (see below under Drug reactivity section for the basis of such relation). Consequently, the design of SOD mimics has been and remains an excellent strategy in designing drugs for oxidative stress injuries. The rational approach in the design of a good SOD mimic has been to mimic the kinetics and thermodynamics of the enzymatic catalysis of $O_2^{\bullet-}$ dismutation: to (i) tune the metal-centered reduction potential around the midpoint ($\sim$ +300 mV *vs.* NHE) between the potential for the oxidation (−180 mV *vs*. NHE) and the reduction of superoxide (+890 mV *vs*. NHE) and to (ii) provide favorable

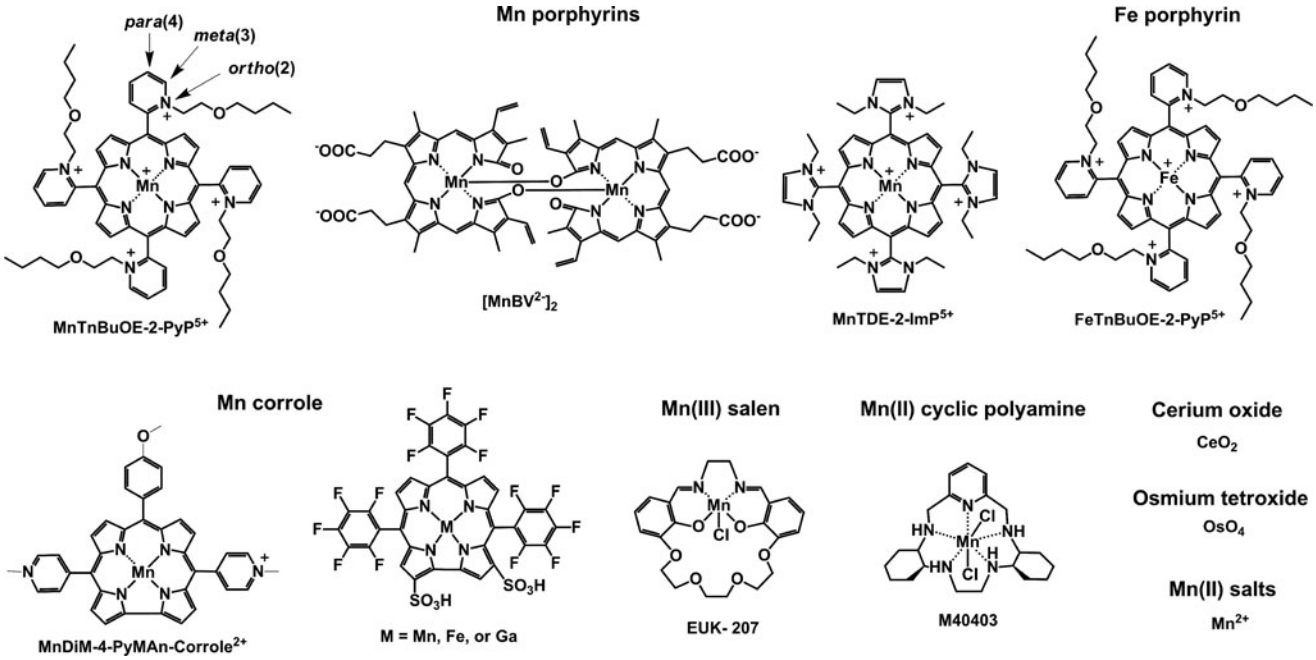

FIG. 1. Main classes of "true" SOD mimics: compounds that catalyze $O_2^{\bullet-}$ dismutation (oxidize and reduce $O_2^{\bullet-}$). The catalysis of dismutation should occur with k_{cat} higher than k for $O_2^{\bullet-}$ self-dismutation of $\sim 5\times10^5\ M^{-1}s^{-1}$ at pH 7 (109). Shown are the structures of optimized MnP, Mn corrole, Mn cyclic polyamine, and Mn salen. Cerium dioxide comes in a form of ceria nanoparticles. OsO_4 is too toxic for therapeutic purposes regardless of its k_{cat} as high as that of SOD enzyme. Mn^{2+} is a fair SOD mimic. It has not been used much in preclinical research perhaps due to the toxicity described as manganism (15, 118, 230). MnP, Mn porphyrin; SOD, superoxide dismutase.

electrostatics for the approach of negatively charged $O_2^{\bullet-}$ molecule to metal site (81, 137, 280). Such reduction potential at $\sim +300$ mV *versus* NHE would provide equal thermodynamics for both steps of the dismutation process (Eqs. [1] and [2]).

$$(H_2O)_2Mn^{III}P^{5+} + O_2^{\bullet-} \Longleftrightarrow (H_2O)Mn^{II}P^{4+} + O_2 + H_2O,\ k_{red}(O_2^{\bullet-}) \quad [1]$$

$$(H_2O)Mn^{II}P^{4+} + H_2O + 2H^+ + O_2^{\bullet-} \Longleftrightarrow (H_2O)_2Mn^{III}P^{5+} + H_2O_2,\ k_{ox}(O_2^{\bullet-}) \quad [2]$$

In the case of SOD enzyme, the similar kinetics results in identical $k_{red}(O_2^{\bullet-})$ and the $k_{ox}(O_2^{\bullet-})$ for the catalysis of $O_2^{\bullet-}$ dismutation of $\sim 10^9\ M^{-1}s^{-1}$ (71, 81, 97, 137, 280). The porphyrin structure allows limitless possibilities of modifications. We have elaborated our design strategies in detail elsewhere (26–28, 33, 177, 271). Briefly, starting from the nonsubstituted *meso*-phenyl and *meso*-pyridyl porphyrins, different substituents were attached to adjust the metal-centered reduction potential for Mn^{III}/Mn^{II} redox couple. Nonsubstituted Mn(III) porphyrins have $E_{1/2}$ of ~ -200 to -300 mV *versus* NHE, way out of the range for a successful catalytic reaction with $O_2^{\bullet-}$; at such $E_{1/2}$ Mn(III) is stabilized in +3 oxidation state and cannot be reduced to Mn(II)P in a 1st step in order to subsequently reduce $O_2^{\bullet-}$.

The superoxide dismutation by either enzyme or mimic has an antioxidative impact only if H_2O_2 is efficiently removed; under pathological conditions in which peroxide-removing systems may be suppressed, the $O_2^{\bullet-}$ dismutation may result in cytotoxic effects. Such therapeutic effects have been seen with SOD enzymes and their mimics in cancer [see below and in Ref. (177)]. In order to increase the reducibility of the metal center, that is, to increase the electron deficiency of the metal site, the porphyrin structure was modified with electron-withdrawing groups. The breakthrough step in our design strategies was the substitution (quaternization) of pyridyl and imidazolyl nitrogens in the closest (*"ortho"*) position toward the metal center, where the positive charges exert the strongest thermodynamic and electrostatic effects (Fig. 2). Incidentally, such a pentacationic electrophilic (electron-deficient) molecule also provides the favorable electrostatics for the oxidation and reduction of anionic (electron-rich) nucleophile, $O_2^{\bullet-}$. The first lead compound was identified as Mn(III) *meso* tetrakis (*N*-ethylpyridinium-2-yl)porphyrin, $MnTE\text{-}2\text{-}PyP^{5+}$. With $E_{1/2}$ of +228 mV *versus* NHE ($\sim +300$ mV *vs.* NHE for SOD enzyme), $MnTE\text{-}2\text{-}PyP^{5+}$ reduces and oxidizes $O_2^{\bullet-}$ with nearly identical rate constants as does the SOD (31, 32). Such a design later led to imidazolyl analog, $MnTDE\text{-}2\text{-}ImP^{5+}$ (26–28, 131, 211, 225, 239), and to a series of Fe porphyrins (FePs) (30, 146, 172, 173, 193, 207, 214, 215, 244, 259, 273) (see also under Drug Design section). Further, the increased bioavailability and reduced toxicity was achieved through modifications of the substituents in *ortho* positions (216, 274). The exploration of differently *meso* and *beta* substituted MPs led to the very first structure-activity relationship (SAR) not only for porphyrinic compounds but in general as well (30). It establishes the relationship between the thermodynamic property of a catalyst—the $E_{1/2}$ which describes the likelihood that the reaction will occur—and the kinetic property, log $k_{cat}(O_2^{\bullet-})$, indicating how fast the reaction

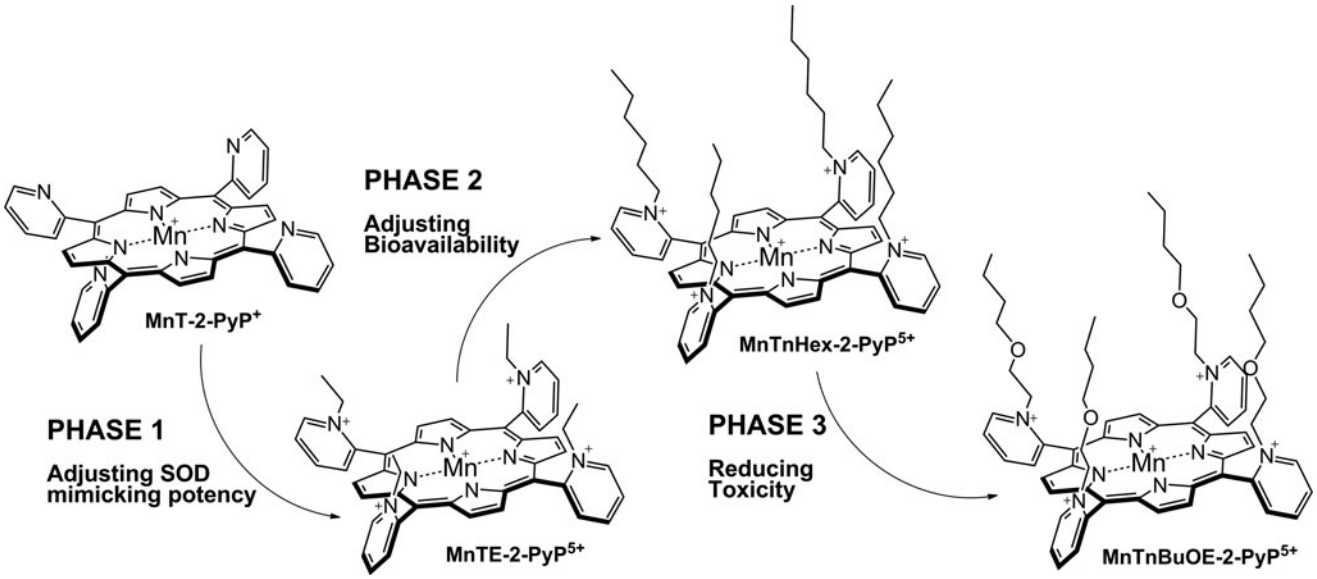

FIG. 2. The design of MnP-based redox-active drugs. Accomplished in three phases, it resulted in the creation of three lead compounds: MnTE-2-PyP^{5+}, MnTnHex-2-PyP^{5+}, and MnTnBuOE-2-PyP^{5+} (216, 271). In the first phase, the major benefit of the *ortho*- positioned quaternary nitrogens imposing a strong electro-withdrawing effect on Mn site was demonstrated. In phase 2, the lipophilicity was increased a few orders of magnitude by lengthening the *N*-alkylpyridyl chains from ethyl to n-octyl; the longer the chains are, the higher the compound bioavailability and, in turn, therapeutic efficacy of the compound. In phase 3, oxygens were introduced deep into the alkyl chains. Such a compound, MnTnBuOE-2-PyP^{5+} is approximately four to five-fold less toxic to mouse than MnTnHex-2-PyP^{5+} (26, 216, 271).

will occur and is governed by factors such as sterics and electrostatics. Those compounds with favorable $E_{1/2}$ (>0 mV *vs.* NHE) have been subsequently tested in a simple superoxide-specific assay where SOD-deficient *Escherichia coli* grows aerobically as well as wild type only if supplied by true SOD mimics (270). The SOD-deficient yeast, *Saccharomyces cerevisiae* has been recently established as an additional model (270).

Most of the published work on Mn porphyrins (MnPs) relates to our first lead, MnTE-2-PyP^{5+}, which continues to be widely used for therapeutic and mechanistic purposes. With the small porphyrin structure, we have achieved the potency near or similar to that of SOD enzymes (23, 28, 30–32, 69) (Fig. 2). The differential sterics, however, affords differential specificity; the SOD enzymes react with $ONOO^-$, thiols, and other species at much lower rates than MnPs. The impact of electrostatics on MnP potency, as dramatic as with SOD enzymes, has been clearly demonstrated (26–28, 32, 271). The cationic compounds have approximately two to three orders of magnitude higher $k_{cat}(O_2^{\bullet -})$ relative to neutral and anionic MnPs. Based on the *ortho* effect, the di-*ortho* imidazolyl derivatives were subsequently synthesized and showed potency in a number of animal models of oxidative stress (26–28, 131, 211, 225, 239). In *E. coli* model, the Mn(III) *meso*-tetrakis (*N,N*′-diethylimidazolium-2-yl)porphyrin, MnTDE-2-ImP^{5+} (AEOL10150) is inferior relative to porphyrins bearing *N*-alkylpyridyl substituents (32, 195, 270). The *N,N*′-dialkylimidazolyl substituents are positioned both above and below the porphyrin plane; in turn, the *N,N*′-dialkylimidazolylporphyrins are much bulkier than *N*-alkylpyridyl analogs (Fig. 1). The bulkiness reduces their biodistribution and, in turn, their efficacy. However, such a disadvantage has at least, in part, been outbalanced by the reduced interactions of MnTDE-2-ImP^{5+} with biological molecules and, in turn, may contribute to lower toxicity and could be utilized at higher doses for the same efficacy as MnTE-2-PyP^{5+} (237). MnTDE-2-ImP^{5+} is presently under development by Aeolus Pharmaceuticals as a radioprotector (122, 198, 212).

Once the SOD-like potency of MPs was optimized, we were challenged by medical audience on their whereabouts in the body, within cells, and particularly in mitochondria. In addition, transport across the BBB and porphyrin oral availability was questioned. Thus, we embarked on a PK journey. HPLC/fluorescence and later LCMS/MS methods were developed for each individual compound (140, 177, 238, 250, 252, 254, 288), which supported the comprehensive biodistribution studies. We have also expanded our synthetic efforts to increase porphyrin bioavailability. Compounds with longer alkyl substituents were synthesized, with MnTnHex-2-PyP^{5+} among others. This molecule has properties of surfactants (polar cationic nitrogens and hydrophobic alkyl tails), and is, thus, toxic at high doses. However, due to higher bioavailability, submiligram daily doses produce sufficient efficacy in animal models, which allows for a sufficiently wide therapeutic window (28, 210). In a 3rd phase of drug development, oxygen atoms were introduced into the pyridyl *N*-substituents to disrupt porphyrin surfactant character—the design comparable to the esterification of sodium dodecyl sulfate in order to decrease skin irritability. The insertion of polar oxygens into the alkyl chains disrupts the surfactant property. The resulting molecule, MnTnBuOE-2-PyP^{5+} (216) is equally lipophilic as MnTnHex-2-PyP^{5+}, but ~4–5-less toxic to a mouse (Figs. 1–3). The alkyl analogs, MnTnHex-2-PyP^{5+} and MnTnHep-2-PyP^{5+}, cause mouse death at 5 and 2.5 mg/kg, respectively; while no toxicity was observed with 5 mg/kg of MnTnBuOE-2-PyP^{5+} (Fig. 3). Further, in a *S. cerevisae* assay, MnTnHex-2-PyP^{5+} and MnTnHep-2-PyP^{5+}—but not MnTnBuOE-2-PyP^{5+}—became toxic at 30 and 5 μM, respectively (Fig. 3). Due to superior properties, MnTnBuOE-

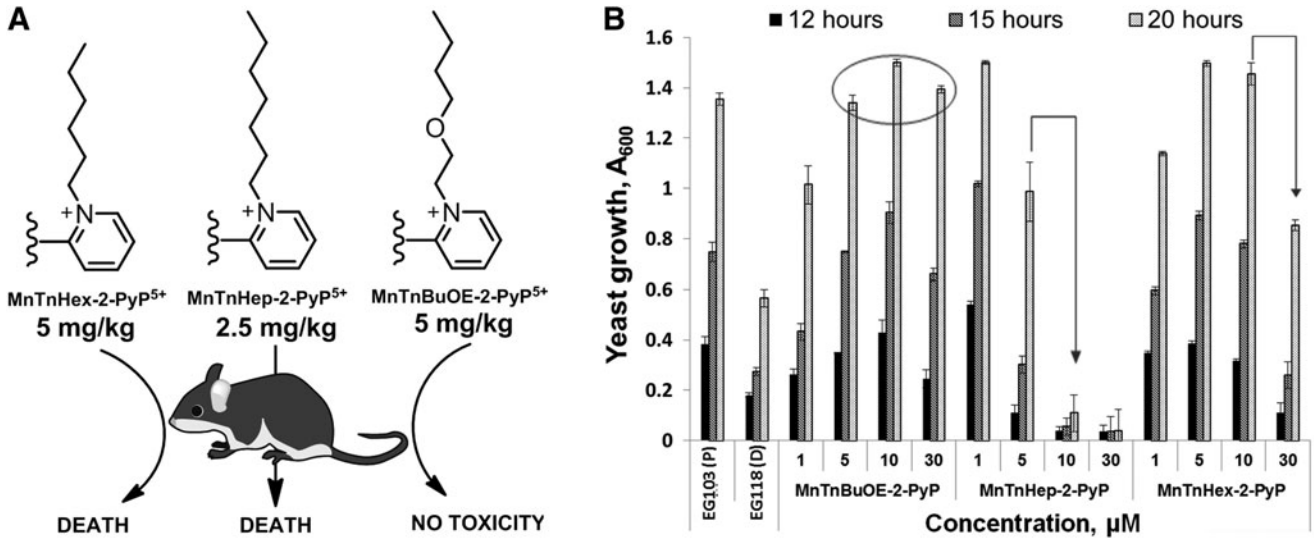

FIG. 3. The toxicity of different Mn(III) *N*-substituted pyridylporphyrins. (A) Comparison of Mn(III) *N*-butoxyethylpyridylporphyrin to its n-hexyl and n-heptyl analogs when given *via* a single ip injection. **(B)** Comparison of their efficacy and toxicity in aerobic growth of SOD-deficient (*sod1Δ*) yeast *S. cerevisiae* (EG118) relative to wild-type yeast (EG 103). Cultures in 96-well plates were grown aerobically at 30°C and 250 rpm on a thermostatic shaker in peptone agar supplemented with 2% dextrose (216). ip, intraperitoneal.

2-PyP^{5+} is presently under aggressive clinical development by BioMimetix Pharmaceutical, Inc.; its GMP scale-up is completed and safety/toxicity studies are underway. All three porphyrin-based lead candidates (MnTE-2-PyP^{5+}, MnTnHex-2-PyP^{5+}, and MnTnBuOE-2-PyP^{5+}) are excellent tools to explore the factors that determine drug bioavailability, efficacy, and toxicity. They are also indispensable for mechanistic studies.

The design of metallocorrole (MC)-based class of SOD mimics is briefly discussed next (104). The design of Mn(II) cyclic polyamines, which resulted in an optimized molecule, M40403 has been extensively covered by Riley's group (14, 167, 226–228, 232). No modification in Mn salen core structure affected the SOD-like activity of the basic EUK-8 structure (73, 74). Under high stomach acidity, the Mn salen derivatives lose Mn (229). Their insufficient metal/ligand stability was significantly enhanced in EUK-207 structure (Fig. 1) *via* derivatization with crown ether (229), as it lowers the loss of the metal when given orally (229).

SARs for Different Redox-Active Compounds

Comprehensive SAR-related studies were conducted on MnPs (18, 27, 28, 30, 32, 271). Recently, Gross' group has established limited SAR for MCs (196). Here, we showed for the first time that SAR established originally for MPs (28, 30, 32) is fairly valid for many redox-active compounds that are aimed at being SOD mimics (Fig. 4); the largest deviation is demonstrated for nonmetal-based nitroxides; however, their reduction potential relates to an irreversible oxoammonium cation/nitroxide redox couple (14, 167, 228). The scattering of the data reflects the impact of factors other than $E_{1/2}$ such as electrostatic and electronic effects, shape, size, and bulkiness of the molecule (27, 28, 221, 223). With compounds that are both anionic and distorted (the octabromosulfonato, $Mn^{III}Br_8TSPP^{3-}$ and octabromocarboxylato $Mn^{III}Br_8TBAP^{3-}$), the access of superoxide to the cationic Mn center is hindered as opposed to the anionic planar $MnTSPP^{3-}$ and $MnTBAP^{3-}$. Steric hindrance is compensated to some extent by favorable thermodynamics as a result of the strong electro-withdrawing effect of eight bromines. However, those compounds still exhibit the largest deviation from the SAR. The compounds with too negative values of $E_{1/2}$ (stabilized in higher +3 Mn oxidation state) cannot be reduced by $O_2^{\bullet-}$ to Mn +2 in a 1st step of $O_2^{\bullet-}$ dismutation process. The compounds with highly positive values of $E_{1/2}$ cannot be easily oxidized by $O_2^{\bullet-}$ to Mn +3 in a 1st step. Among them are porphyrins which contain Mn in its +2 oxidation state, and are, thus, not very stable, that is, lose Mn readily (23, 69): MnPs [$Mn^{II}Br_8$TM-3(or 4)-PyP^{4+}, $Mn^{II}Cl_5$TE-2-PyP^{4+}], and Mn(II) cyclic polyamines, such as M40403. Among them are also very stable electron-rich metal complexes, Mn(III) corroles, and Mn(III) biliverdins, which undergo facile oxidation by $O_2^{\bullet-}$ to a higher Mn +4 oxidation state in a 1st step of a dismutation process.

A closer look at the thermodynamic and kinetic data indicates that perhaps two SARs can be constructed: one for compounds utilizing M^{III}/M^{II} couple (red line) and the other one for those compounds employing M^{IV}/M^{III} couple (green line) (Fig. 4). The latter are Mn(III) biliverdin and its analogs and Mn(III) corroles. The optimal potentials for those SARs are ~300 mV away from each other.

Mn(III) biliverdins

The exploration of Mn(III) biliverdin derivatives and metal(III) corroles taught us that the magnitude of their reduction potential is a key factor in $O_2^{\bullet-}$ dismutation, with a minor role of the nature of the redox couple involved (thick curve in Fig. 4). In other words, superoxide does not care much with whom it exchanges the electrons as long as it occurs at the potential where $O_2^{\bullet-}$ could be easily reduced or oxidized. We have shown that Mn biliverdin dismutes $O_2^{\bullet-}$ employing Mn^{IV}/Mn^{III} redox couple (Eqs. [3] and [4]) as efficiently as MnP employing Mn^{III}/Mn^{II} redox couple. The $E_{1/2}$ for Mn^{IV}/Mn^{III}

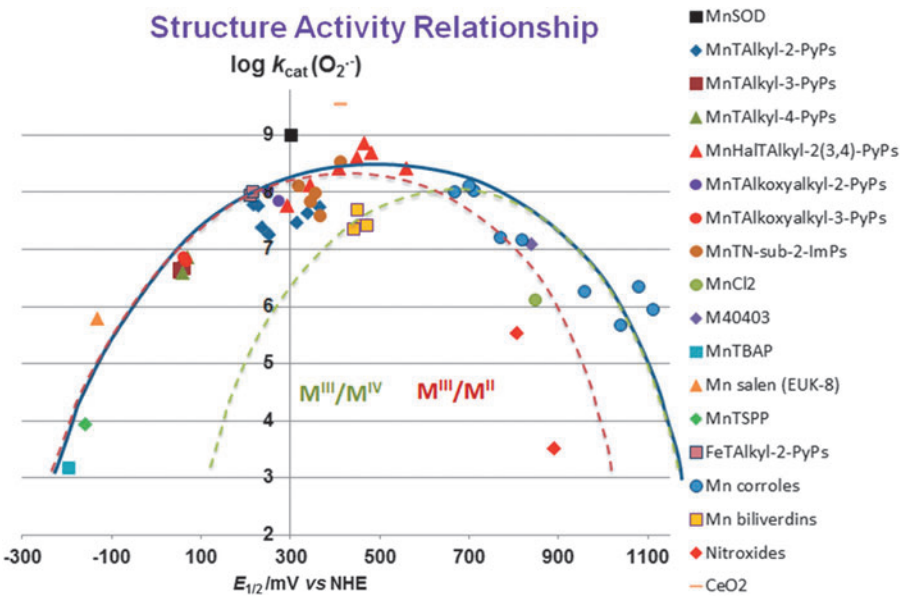

FIG. 4. Structure-activity relationships (SARs) correlate the redox potency expressed as one-electron $E_{1/2}$, and the ability of compounds to catalyze the $O_2^{\bullet-}$ dismutation, log $k_{cat}(O_2^{\bullet-})$. With Mn(III) biliverdins and Mn(III) corroles, Mn^{IV}/Mn^{III} redox couple is involved in the catalysis of $O_2^{\bullet-}$ dismutation; with all other Mn compounds, the Mn^{III}/Mn^{II} redox couple is involved. The $E_{1/2}$ for nitroxides relates to the oxidation of nitroxide to oxoammonium cation (14, 167, 228). The SAR (showed with thick blue line) is valid for many redox-active compounds regardless of their structure: metalloporphyrins, Mn(IV) biliverdins, Mn(III) salens, Mn(II) polyamines, Mn(III) corroles, and Mn(II) aqua complex (271). The $E_{1/2}$ values for $Mn^{IV}C/Mn^{III}C$ redox couple (given in Table 1) were determined in phosphate buffer for anionic Mn corrole with two sulfonatopyrrolic groups and three *meso* pentaphenyl groups, but in acetonitrile for cationic Mn corrole, which bears two *meso para*-methylpyridyl groups and one *meso* substituent with derivatized tetrapfluorophenyl group (80, 104, 196) (Fig. 1). Thus, it is not straighforward to predict the magnitude of the shift in $E_{1/2}$ from one to another corrole. According to Marcus equation, the 120 mV shift in $E_{1/2}$ should cause a 10-fold change in rate constant (29). The increase in log $k_{cat}(O_2^{\bullet-})$ for ~3 orders of magnitude (from Mn corrole) should have shifted the $E_{1/2}$ for ~360 mV, from ~ +840 mV *vs.* Ag/AgCl (+1040 mV *vs.* NHE) to ~ +500 mV *versus* Ag/AgCl (+700 mV *vs.* NHE) (Fig. 5). When translated into experimental data, it appears that $E_{1/2}$ for these compounds is identical in either solvent: water or acetonitrile (80, 104, 196). Below the SAR, indicated as a thick blue line, the two individual SARs relate to complexes that catalyze $O_2^{\bullet-}$ dismutation employing either Mn^{III}/Mn^{II} (red line) or Mn^{IV}/Mn^{III} redox couple (green line). The optimal reduction potential (peak) of these SARs differs ~300 mV. The compounds with very negative and very positive values of $E_{1/2}$ are essentially unable to dismute $O_2^{\bullet-}$; different strategies have been employed to improve their $E_{1/2}$. The electron-withdrawing groups are needed for the majority of metallporphyrins to move their potential from negative values into the region of optimal $E_{1/2}$ values (+200 to +400 mV *vs.* NHE) (28). However, with Mn corroles, the electron-donating groups are required for modifying their $E_{1/2}$ from ~ +1000 to ~ +700 mV *versus* NHE (196). Since their redox is irreversible, the nitroxides do not fit the SAR well (red rhombi). Any major deviation from SAR indicates that factors other than thermodynamics have an impact on the k_{cat} (27, 28, 221, 223). Charges are omitted in the figure legend for simplicity. $E_{1/2}$, half-wave reduction potential; NHE, normal hydrogen electrode.

redox couple is shifted ~130 mV more positive than $E_{1/2}$ of $MnTE\text{-}2\text{-}PyP^{5+}$ for Mn^{III}/Mn^{II} redox couple.

$$\frac{1}{2}(Mn^{III}BV^{2-})_2 + 2H^+ + O_2^{\bullet-} \Longleftrightarrow \frac{1}{2}(Mn^{IV}BV^{-})_2 + H_2O_2 \quad [3]$$

$$\frac{1}{2}(Mn^{IV}BV^{-})_2 + O_2^{\bullet-} \Longleftrightarrow \frac{1}{2}(Mn^{III}BV^{2-})_2 + O_2 \quad [4]$$

However, Mn(III) biliverdin exerts no electrostatic facilitation for the approach of superoxide in either step of dismutation. Thus, the thermodynamics is solely the responsible factor for the fairly high $k_{cat}(O_2^{\bullet-})$. According to Marcus equation for an outer-sphere electron transfer, for each increase in $E_{1/2}$ of 120 mV, the rate constant increases 10-fold (30). We have shown that neutral Mn(III) porphyrins have ~100-fold lower $k_{cat}(O_2^{\bullet-})$ than cationic MnPs of the same $E_{1/2}$. Were the $E_{1/2}$ = +228 mV *versus* NHE for anionic ($MnBV^{2-}$), the log $k_{cat}(O_2^{\bullet-})$ would be ~5. Based on the SAR (160), a 232 mV increase in $E_{1/2}$ from +228 ($MnTE\text{-}2\text{-}PyP^{5+}$) to +460 mV ($[MnBV^{2-}]_2$), would allow for ~100-fold increase in log $k_{cat}(O_2^{\bullet-})$ from ~5 to 7.4.

Mn(III) corroles

Gross's group reported that MCs employ $Mn^{IV}C/Mn^{III}C$ redox couple for $O_2^{\bullet-}$ dismutation (Eqs. [5] and [6]) (80, 196). The reason for that is the stabilization of a higher Mn +4 oxidation state. The redox cycling *via* $M^{III}C/M^{II}C$ occurs at too negative potentials to be of biological relevance (162). Consequently, metallocoroles could not readily oxidize cellular reductants, thiols, or ascorbate in a first step of their redox cycling. Rather, MCs would act as reductants of reactive species, such as $O_2^{\bullet-}$, H_2O_2, or $ONOO^-$ in a 1st step, while undergoing oxidation from $M^{III}C$ to $M^{IV}C$. In a subsequent step of re-reduction, MCs would behave as strong

oxidants; the coupling with cellular reductants in that step is likely, but has not yet been reported. Once reaching a cell, though, MnPs would prompty behave as oxidants of ascorbate, simple thiols, or protein thiols, undergoing reduction from $Mn^{III}P$ to $Mn^{II}P$. Both metalocorroles and MPs are efficacious in treating oxidative stress injuries. Is some common pathway operative for both classes of redox-active compounds, affecting the cellular redoxome, that we could not have yet forseen?

Mn is coordinated to trianionic (biliverdin and corrole), while porphyrins are dianionic ligands (see Figs. 1 and 10). Trianionic coordination in Mn(III) biliverdin dimer is assured by the coordination of Mn of one monomer to oxygen of another monomer (Fig. 1). Mn(III) corroles do not require oxygen binding to stabilize Mn in higher +4 oxidation state, whereas Mn in $O=Mn^{IV}P$ is stabilized in +4 oxidation state with oxygen (80). Axial protonation equilibria for corroles have not been reported.

$$Mn^{III}C + O_2^{\bullet -} + 2H^+ \Longleftrightarrow Mn^{IV}C^+ + H_2O_2 \quad [5]$$

$$Mn^{IV}C^+ + O_2^{\bullet -} \Longleftrightarrow Mn^{III}C + O_2 \quad [6]$$

The first generation of Mn corroles has $E_{1/2} \sim +1000$ mV *versus* NHE, which is out of range for the $O_2^{\bullet -}$ reduction, that is, disfavors Mn oxidation. Consequently, the marginal SOD-like activity was reported with log $k_{cat}(O_2^{\bullet -}) \sim 6$, which is only slightly above the value for $O_2^{\bullet -}$ self-dismutation [log $k_{cat}(O_2^{\bullet -}) \sim 5.7$] [log $k_{cat}(O_2^{\bullet -})$ for SOD enzymes is in a range 8.84–9.2] (80). Mn corroles were subsequently modified with electron-donating groups, which decreased the $E_{1/2}$ (196). Based on the data in Refs. (78, 194) and the similarity of $E_{1/2}$ of Mn corroles in acetonitrile and in an aqueous system, the values of $E_{1/2}$ in aqueous medium for several corroles plotted in SAR (Fig. 4) were estimated (80, 104, 196) (Fig. 1). Cytochrome *c* assay was used by Gross's group to determine the $k_{cat}(O_2^{\bullet -})$. Preliminary stopped-flow data support cyt *c* data (Gross *et al.*, unpublished).

Fe(III) porphyrins

We have originally developed SAR for both Mn and Fe complexes (30). Recently, we synthesized a series of *ortho* and *meta* Fe complexes to understand the intriguing differential *in vivo* behavior of Fe and MnPs (273). FePs have also been often used in cellular and animal models of oxidative stress (146, 172, 173, 193, 207, 214, 215, 244, 259). While MnP employs $(H_2O)_2Mn^{III}P^{5+}/(H_2O)Mn^{II}P^{4+}$, the FeP utilizes $(OH)(H_2O)Fe^{III}P^{4+}/(H_2O)Fe^{II}P^{4+}$ redox couple for $O_2^{\bullet -}$ dismutation. Consequently, the dismutation catalyzed by FePs involves MP axial protonation equilibria (Eqs. [7] and [8]) (273). Thus, the oxidized and reduced FePs have the same total charge at pH 7.8, whereas Mn species do not; the consequence of such difference on *in vivo* interactions has not yet been investigated. Both Fe-OH and Mn-H_2O centers operate at very similar $E_{1/2}$ and, thus, exhibit similar $k_{cat}(O_2^{\bullet -})$ values (see Eqs. [1], [2], [7], and [8]) (Figs. 5 and 6) (see also *FePs vs. MnPs* below):

$$(OH)(H_2O)Fe^{III}P^{4+} + O_2^{\bullet -} + H^+ \Longleftrightarrow (H_2O)Fe^{II}P^{4+} + O_2 + H_2O \quad [7]$$

$$(H_2O)Fe^{II}P^{4+} + O_2^{\bullet -} + H^+ + H_2O \Longleftrightarrow (OH)(H_2O)Fe^{III}P^{4+} + H_2O_2 \quad [8]$$

Cerium dioxide, CeO_2

Nanoparticles of CeO_2 (nanoceria), with a unique electronic structure similar to nitrone spin traps and of mixed valence state, are reportedly very potent SOD mimics. The equations [9] and [10] account for their remarkable SOD-like activity, which is somewhat higher than for SOD enzyme (138), log $k_{cat} = 9.55$. The $E_{1/2}$ for Ce^{IV}/Ce^{III} redox couple varies with medium, and in deionized water, it is $\sim +400$ mV *versus* NHE (261). Neither charge nor reduction potential easily justifies such high $k_{cat}(O_2^{\bullet -})$ values.

$$Ce^{IV} + O_2^{\bullet -} \Longleftrightarrow Ce^{III} + O_2 + e^- \quad [9]$$

$$e^- + Ce^{III} + O_2^{\bullet -} + 2H^+ \Longleftrightarrow Ce^{IV} + H_2O_2 \quad [10]$$

When the fraction of Ce^{IV} increases over Ce^{III}, the SOD-like activity gets reduced (113). As a result of simultaneous existence of Ce^{III} and Ce^{IV} in nanoparticles, cerium dioxide forms oxygen vacancies or defects in the lattice structure by the loss of oxygen and/or its electrons. Catalysis can occur at the same cerium atom or independently at different oxygen vacancy sites.

Osmium tetroxide, OsO_4

An aqueous solution of OsO_4 has a SOD-like potency which is comparable to that of cerium dioxide. However, it is a very toxic compound. Its high oxidizing power has been employed in the treatment of diseased arthritic knee (99). It is widely used for biological staining, as it binds to phospholipids. The log $k_{cat}(O_2^{\bullet -})$ is pH independent in the pH range 5.1 to 8.7. The following equations for superoxide dismutation have been proposed (99):

$$Os^{VIII} + O_2^{\bullet -} \Longleftrightarrow Os^{VII} + O_2 + e^- \quad [11]$$

$$e^- + Os^{VII} + O_2^{\bullet -} + 2H^+ \Longleftrightarrow Os^{VIII} + H_2O_2 \quad [12]$$

Osmium(VII) disproportionates to Os^{VIII} and Os^{VI}:

$$2\ Os^{VII} \Longleftrightarrow Os^{VIII} + Os^{VI} \quad [13]$$

The log $k_{cat}(O_2^{\bullet -}) = 9.15$ is described by equations [11] and [12]. The Os^{VI}/Os^{VII} redox couple could cycle with $O_2^{\bullet -}$ also (Eq. [14]) with log $k_{cat} = 8.98$:

$$e^- + Os^{VI} + O_2^{\bullet -} + 2H^+ \Longleftrightarrow Os^{VII} + H_2O_2 \quad [14]$$

Therefore, with hardly any electrostatics, the only explanation for a high $k_{cat}(O_2^{\bullet -})$ may be a very positive reduction potential for Os^{VIII}/Os^{VII} redox couple (not reported).

Manganese salts

Solvated Mn^{2+} is a fairly strong SOD mimic (phosphate buffer, pH 7.8) (Table 1). The log $k_{cat}(O_2^{\bullet -}) > 6.30$ was

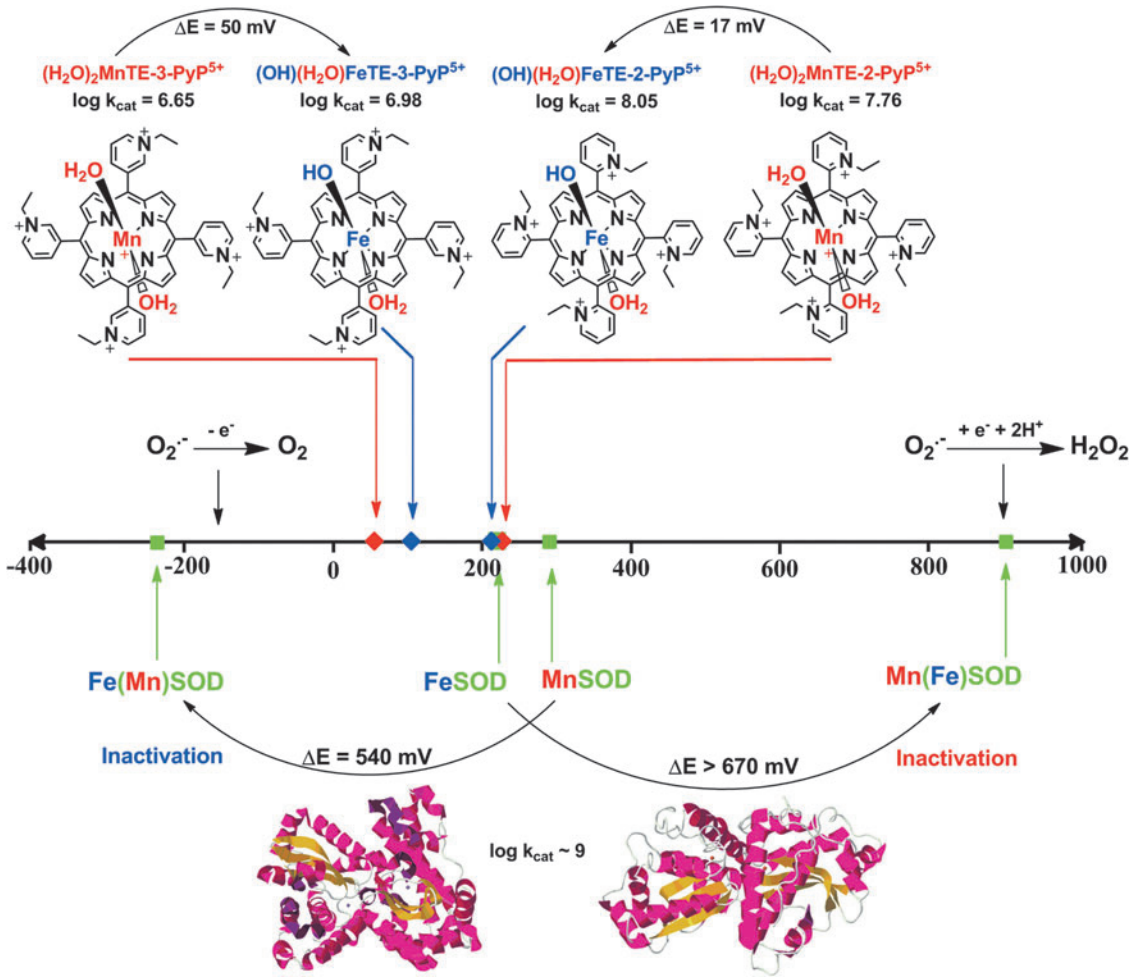

FIG. 5. Comparison of the effect of the type of metal on the SOD activity of enzymes and metalloporphyrins. Replacing the metal sites between MnSOD and FeSOD enzymes precludes the appropriate amino-acid configuration of metal site and, thus, results in vastly shifted $E_{1/2}$ out of the limits required for superoxide dismutation; consequently, the enzyme becomes inactive. However, when different metals are ligated to the same porphyrin, the change in the type of axial ligand is easily achievable: Fe hydroxo axial *versus* Mn axial water at pH 7.8 (sixth coordination site in these complexes is occupied by a water molecule). In such structures, both Mn aqua and Fe hydroxo porphyrins have essentially identical $E_{1/2}$ and, therefore, similar SOD-like activity. To see this illustration in color, the reader is referred to the web version of this article at www.liebertpub.com/ars

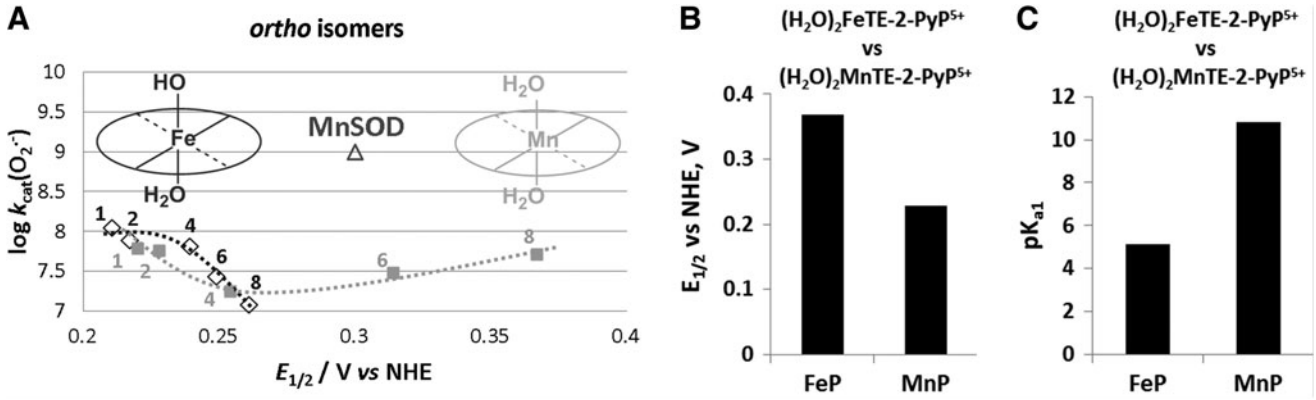

FIG. 6. SAR (A) and thermodynamic parameters (B, C) for the series of *ortho* Fe(III) *N*-alkylpyridylporphyrins as compared with Mn analogs (272, 273)**.** The different shape of SAR is due to the difference between the chemistry of Fe and MnPs. At pH 7.8, FePs bear one hydroxo ligand that neutralizes single charge on Fe and labilizes trans-axial water, which, in turn, impacts the k_{cat} and $E_{1/2}$. To stress the difference, we showed here also the electrochemical data on both Fe and MnPs bearing same axial ligands—water molecules—and therefore same charge, but their $E_{1/2}$ differ ~150 mV; we have shown earlier that the effect, which impacts the $E_{1/2}$, also affects the strength of the M-H_2O bond. The more electron-deficient the metal complex, the higher the $E_{1/2}$ it is, and the stronger it binds the axial water; consequently, the loss of its proton is promoted, which is reflected in lower pK_{a1} (84, 86, 221). FePs, Fe porphyrins.

Table 1. Metal-Centered Reduction Potential $E_{1/2}$ in mV *Versus* NHE (for $Mn^{III}P/Mn^{II}P$ Redox Couple) and log k_{cat} for the $O_2^{\cdot -}$ Dismutation of Mn and Fe Porphyrins

SOD mimics	*$E_{1/2}$/mV versus NHE*[a]	*log k_{cat} ($O_2^{\cdot -}$)*[b]
Mn porphyrins		
$MnTE\text{-}2\text{-}PyP^{5+}$	+228	7.76 (cyt *c*); 7.73 (p.r.)[c]
$MnTnHex\text{-}2\text{-}PyP^{5+}$	+314	7.48
$MnTnBuOE\text{-}2\text{-}PyP^{5+}$	+277	7.83
$MnTE\text{-}3\text{-}PyP^{5+}$	+54	6.65
$[MnBV]_2$	+460[d]	7.4
$MnTBAP^{3-}$	−194	3.16
Fe porphyrin		
$(OH)FeTE\text{-}2\text{-}PyP^{4+}$	+215	8.05
$(OH)FeTnBuOE\text{-}2\text{-}PyP^{4+}$ [e]	+237	7.41
Mn salen		
EUK-207	∼ −130	∼6.30[f]
Cyclic polyamine		
M40403	+525 (ACN)[g]	7.08
Nitroxide		
Tempol	+810[h]	
Mn corroles		
$MnDiM\text{-}4\text{-}PyMAn\text{-}Corrole^{3+}$	∼ +700[d,i]	8.11
$MnTrF_5Ph\text{-}\beta(SO_3)_2\text{-}Corrole^{2-}$	+1040[d,j]	5.68
Fe corrole		
$FeTrF_5Ph\text{-}\beta(SO_3)_2\text{-}Corrole^{2-}$	+1050[i]	
OsO_4		9.14 (pH 5.1–8.7)
CeO_2 (3–5 nm particles)	∼ +400 mV[k]	9.55
Mn^{2+}	+850[l]	6.11 (cyt c), 6.28 (p.r.)
SOD enzymes	∼ +300	8.84–9.30
$O_2^{\cdot -}$ -self dismutation		∼5.7

For comparison, the values for some other compounds are also given. All Mn porphyrins are diaqua species, while Fe porphyrins are monohydroxo monoaqua species at pH 7.8. Water molecules are not indicated in the Table. The compounds are technically not SOD mimics if they disproportionate $O_2^{\cdot -}$ with a rate constant close to self-dismutation $k = 5 \times 10^5\ M^{-1}s^{-1}$.

[a]$E_{1/2}$ is determined in 0.05 *M* phosphate buffer (pH 7.8, 0.1 *M* NaCl); [b]k_{cat} in $M^{-1}s^{-1}$ was determined by cytochrome *c* assay in 0.05 *M* potassium phosphate buffer (pH 7.8, at 25 ± 1 ^{0}C); [c]p.r., pulse radiolysis; [d]$E_{1/2}$ data associated with the Mn^{IV}/Mn^{III} reduction potential. [e]Tovmasyan *et al.*, unpublished; [f]value estimated based on cyt *c* assay for EUK-8 (249); IC_{50} ∼0.48 μ*M* (NBT assay); [g]in acetonitrile, Mn(II) complexes were 1 m*M*, 0.1 *M* tetrabutylammoniumhexafluorophosphate ($TBAPF_6$) as supporting electrolyte, Ref. (167); [h]Ref. (28), the one-electron reduction potential refers to RNO^+/RNO redox couple. [i]data in mV *versus* NHE, they are based on the data obtained in acetonitrile *versus* Ag/AgCl for M^{IV}/M^{III} redox couple with 0.3 *M* tetrabutylammonium perchlorate (for $MnDiM\text{-}4\text{-}PyMAn\text{-}Corrole^{3+}$) or 0.1 *M* $TBAP/TBAPF_6$ (for $FeTrF_5Ph\text{-}\beta(SO_3)_2\text{-}Corrole^{2-}$) as electrolyte (80, 196), and the similarity of $E_{1/2}$ in aqueous medium and acetonitrile (80), the $E_{1/2}$ in mV *versus* NHE in aqeous medium was estimated; such data are plotted in Figure 4; [j]$E_{1/2}$ for $MnTrF_5Ph\text{-}\beta(SO_3)_2\text{-}Corrole^{2-}$ is converted to mV *versus* NHE from the value given in mV *versus* Ag/AgCl in 0.01 *M* phosphate buffer, pH 7.4, 3 *M* KCl as electrolyte, (80); [k]$E_{1/2}$ for Ce^{IV}/Ce^{III} (261). [l]Oxidation potential only, Mn^{III}/Mn^{II} redox couple is irreversible; When references are not indicated, the data are taken from Refs. (26–28).

$E_{1/2}$, half-wave reduction potential; M40403, cyclic polyamine; NHE, normal hydrogen electrode; SOD, superoxide dismutase.

reported. The E_{oxid} for Mn^{II}/Mn^{III} oxidation is +850 mV *versus* NHE (17, 247, 249). Other salts, in particular Mn lactate [only 65-fold less potent than SOD enzyme (11)], are even better (28). The human body contains ∼10 mg of manganese, most of which is found in liver, bones, and kidneys. Chronic exposure to Mn levels can lead to a variety of psychiatric and motor disturbances, known as manganism (170). This is a likely reason for the lack of the use of manganese-containing drugs in medicine (15, 118, 230). Based on a number of studies, disturbed iron metabolism could underlie the neurotoxic action of manganese, resembling Parkinson's disease. Chronic exposure to Mn causes its accumulation in the nervous system, predominantly in basal ganglia, inducing a decrease in dopamine levels leading to cell death. Martins *et al.* reported that treatment of mice with $MnCl_2$ in drinking water resulted in a 2.5–5-fold increase in catalase and SOD activities and was more pronounced in cortex and cerebellum than in hippocampus and striatum (170). The highest lipid and glutathione oxidation was observed in hippocampus. The high toxicity of Mn requires a thorough removal of "free" Mn from its formulations. We have addressed levels of free Mn in MnP preparations, left from the metallation of the porphyrin ligand (222, 224). Under *in vivo* conditions, no significant release of Mn is expected from stable porphyrins and corrole complexes; based on reported stability in aqueous solutions, an extensive loss of Mn from polyamines and salens is anticipated. The data on Mn loss from Mn complexes and its *in vivo* consequences has not been explored. Thus far, no metal-free porphyrin was detected in biological tissue (253).

FePs *Versus* MnPs

The key importance of the metal site in SOD enzymes has been extensively studied. Elegant work by Anne-Frances Miller and colleagues clearly describes how the metal coordination sphere is significantly more specific to the type of metal in enzymes than in their mimics (280, 281, 300). When Fe in FeSOD gets replaced by Mn (and vice versa), the coordination sphere, originally designed for Fe, is too rigid to allow the amino-acid residues to adopt the appropriate configuration around an incoming Mn. Consequently, the engineered enzyme has dramatically modified $E_{1/2}$, and, therefore, its ability to catalyze $O_2^{\bullet -}$ dismutation is lost (Fig. 5).

However, in MPs, when Mn replaces Fe, axial coordination around Mn is readily re-adjusted due to the absence of amino-acid residues, which complicates the aqua/hydroxo protonation equilibrium of the metal center. The simple Fe-OH *versus* Mn-H_2O axial modification provides appropriate reduction potential to maintain similarly high SOD-like activity of Fe and MnPs (Fig. 5). Apart from SOD activity, however, such a different axial coordination of the metal site results in a large difference between the aqueous chemistry of these two classes of MPs and, thus, influences their entire chemistry and biology as discussed next (273). The $(OH)FeTM\text{-}4\text{-}PyP^{4+}$ was the first porphyrin reported to have SOD-like activity with log $k_{cat}(O_2^{\bullet -}) = 7.20$ (27, 203). It is frequently used *in vivo* due to its commercial availability (12, 47, 77, 102, 135, 157, 188-190, 200, 256, 257).

The acidity of simple "free" ion, hexaaqua species $[Fe^{III}(H_2O)_6]^{3+}$ is pK_{a1} ∼2.2, and of $[Mn^{III}(H_2O)_6]^{3+}$ is pK_{a1} ∼0.1. This indicates that the Mn^{3+} is more acidic than the Fe^{3+} hexaaqua species by ∼2 log units; the consequence of this is

the lack of stable Mn +3 salts. Such a remarkable difference in pK_{a1}, as a result of different electronic ligand fields of Mn and Fe metal centers, translates into the difference between the metal-centered reduction potentials of M^{III}/M^{II} redox couples (M = metal), and, eventually, into the major difference between the "free Fe" and "free Mn" biology. Due to a much higher reduction potential of "free" Mn^{III}/Mn^{II} ($E^o = +1.51$ V *vs.* NHE) than of free Fe^{III}/Fe^{II} ($E^o = +0.77$ V *vs.* NHE), Mn cannot be easily oxidized with H_2O_2 to produce $^{\bullet}OH$ radical, which means that Mn does not undergo "Fenton chemistry." On metal binding to SOD protein or its mimic, its reduction potential changes dramatically, falling between the potential for $O_2^{\bullet -}$ oxidation and reduction. Such a change in $E_{1/2}$ is enabled by the changes in the metal coordination sphere (Fig. 5) (273).

The acidity of the MP axial waters with regard to the free water ($pK_w \sim 14$) is increased by ~ 8.5 and ~ 3 log units on coordination to the pentacationic FeP and MnP moieties, respectively. Such a large difference between the pK_{a1} values shows that the axially coordinated water in Fe(III) *N*-alkylpyridyl porphyrins is about 5 log units more acidic ($pK_{a1} \sim 5$) than in the corresponding MnPs ($pK_{a1} \sim 11$). This is a reversal relative to the acidity of Mn and Fe hexaaqua species. Consequently, at pH = 7.8, the axial water in FePs (but not in MnPs) is deprotonated, giving rise to $(OH)(H_2O)Fe^{III}P$. The $(OH)(H_2O)Fe^{III}P$ and $(H_2O)_2Mn^{III}P$ species have almost identical $E_{1/2}$. Consequently, their ability to catalyze $O_2^{\bullet -}$ dismutation is similar on thermodynamic grounds (Table 1). However, the hydroxo ligand labilizes trans-axial water. It is well known that such a trans-axial effect increases the reactivity of the metal site. Thus, $k_{cat}(O_2^{\bullet -})$ for FePs is larger than for MnPs (Table 1), as is the reactivity toward other molecules such as ascorbate, thiols, and peroxide (30, 272, 273). The difference is smaller with $O_2^{\bullet -}$ dismutation, as the process is predominantly outer-sphere (*i.e.,* does not involve axial binding), with only partial inner-sphere character (273). Since axial hydroxo ligand neutralizes a single charge at the metal site, the FePs are tetracationic, while MnPs are pentacationic. We do not yet know the contribution of the lower electrostatics on the $k_{cat}(O_2^{\bullet -})$ of FePs relative to MnPs. Lengthening the alkyl chains from 1 to 8 carbon atoms has a large effect on $E_{1/2}$ of MnPs, whereas it has a significantly smaller effect on the $E_{1/2}$ of FePs. The $E_{1/2}$ of FePs appears to be predominantly determined by the axially bound OH^- ligand and not by the peripheral pyridyl substituents (Fig. 6). Such a difference in axial coordination translates into a remarkably different SAR of the *isomeric* Mn(III) and Fe(III) *N*-alkylpyridyl porphyrins (Fig. 6, shown only for *ortho* isomers). The $E_{1/2}$ is inversely related to the pK_{a3} of the pyrrolic nitrogens of porphyrin ligand (30) and to the pK_{a1} values of axial waters as exemplified for $(OH)(H_2O)FeTE\text{-}2\text{-}PyP^{4+}$ *versus* $(H_2O)_2MnTE\text{-}2\text{-}PyP^{5+}$ in Figure 6. In other words, the higher the $E_{1/2}$, the more electron deficient the metal is and the more strongly it binds the oxygen atom of axial water and pyrrolic nitrogens. Consequently, the protons (of both axial water and pyrrolic niytrogens) leave at lower pH; in turn, the pK_a values are lower. Thus, the $E_{1/2}$ is an excellent measure of the acidity of the metal center.

Due to their high SOD-like activity, FePs were evaluated on their ability to protect SOD-deficient *E. coli* when growing aerobically (Fig. 7) (30). SOD-deficient mutant lacks cytosolic SOD enzymes MnSOD and FeSOD and cannot grow as efficiently as wild type under aerobic conditions and in a restricted medium where the syntheses of branched, aromatic, and sulfur-containing amino acids are catalyzed by superoxide-sensitive enzymes (26, 28). Under identical concentrations ($\sim 20\ \mu M$), MnPs were protective, while FePs were toxic (30). However, FePs were efficacious at approximately ~ 1000-fold lower, $0.01\ \mu M$ concentrations (270, 273). Further, the *E. coli* growth pattern is different with FePs relative to MnPs. Initially, the growth delay was seen with FePs; eventually, the FeP-supported growth surpassed the growth of wild-type *E. coli* (Fig. 7). Mn and FePs have similar lipophilicities, bulkiness, and $k_{cat}(O_2^{\bullet -})$ values (Table 1). Therefore, had they acted as SOD mimics, they would have been protective under identical conditions as MnPs (Table 1).

Further studies demonstrate that the identical impact on the growth of SOD-deficient *E. coli* was produced with equal concentrations of Fe(II) citrate, Fe(II) sulfate, and FePs: 0.1 or

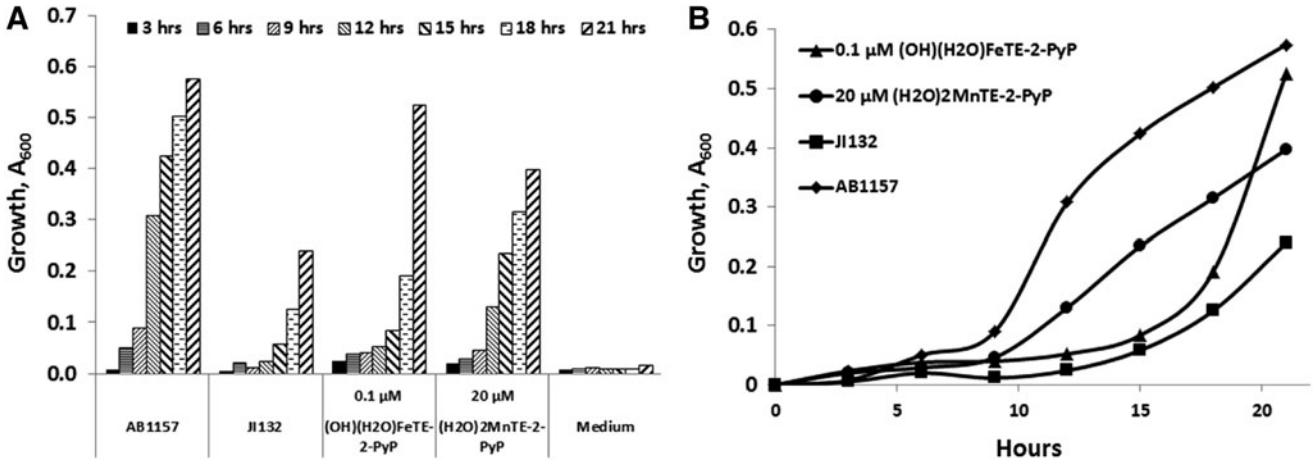

FIG. 7. Comparison of *ortho* Fe(III) and Mn(III) *N*-ethylpyridylporphyrins in protecting SOD-deficient *Escherichia coli* while growing aerobically. FeP allows *E. coli* to overgrow the wild type at ~ 1000-fold lower concentration than MnP **(A).** However, the growth pattern is different **(B)**. The growth was followed in a restricted five-amino-acid medium that better distinguishes the true SOD mimics from other redox-active compounds than rich media (270, 273). Wild-type *E. coli* was AB1157, and SOD-deficient JI132.

1 μM (272, 273). The metal/porphyrin stability studies in aqueous system in the presence of ascorbate, glutathione, or cysteine followed in order to gain insight into the possible degradation of MP (272). Hydrogen peroxide is the product of redox cycling of MPs with the reducing agents, and it degrades ("bleaches") the FePs more readily than MnPs. Subsequent studies with *E. coli* clearly showed that FeP, but not MnP, undergoes fast degradation during the first several hours of *E. coli* growth. At lower levels of free Fe, the *E. coli* likely uses it to restore 4Fe-4S clusters of Fe-bearing enzymes (such as aconitase). Upon the attack of $O_2^{\bullet -}$ these enzymes reversibly lose Fe^{2+}. A recent manuscript by Gu and Imlay substantiates the impact of $O_2^{\bullet -}$ on Fe-containing enzymes in SOD-deficient *E. coli*; at least 3 more enzymes (threonine dehydrogenase, ribulose-5-phosphate 3-epimerase, and peptide deformylase) were clearly identified as undergoing loss of Fe and subsequent inactivation (101). Inactivation is, in part, related to the Zn incorporation at the Fe site. Fur protein also seems to be a candidate (101). At higher levels of Fe, the toxicity is most likely due to the Fenton chemistry-driven $^{\bullet}OH$ production at the metal site of FeP or at "free" low-molecular Fe (273). Were the mechanism of action of FePs *versus* MnPs indeed as different in mammalian systems as shown *in E. coli*, our present understanding of the favorable effects often exerted by FePs in animal models of disease would need reconsideration (12, 47, 77, 102, 256). The *E. coli* data illustrate the complexity of the biology of redox-compatible metal complexes and call for caution when interpreting the *in vivo* data. Studies on cells other than *E. coli* are in progress. The scheme that represents differential actions of FeP *versus* MnP in SOD-deficient *E. coli* and in mouse is shown in Figure 8.

In addition to Fe(III) *N*-alkylpyridylporphyrins, Fe complexes, which bear *ortho* pyridyl nitrogens quaternized with triethyleneglycols and benzoates, have been explored (18). The nature of the *N*-pyridyl substituents only marginally affects the magnitude of $k_{cat}(O_2^{\bullet -})$. Though discussed as exclusive $ONOO^-$ scavengers, these compounds are as good superoxide scavengers as *N*-alkylpyridylporphyrins (28, 146, 172, 173, 187, 214, 215, 244, 258). The $FeTSPP^{3-}$ and its mesityl analog $FeTMSP^{7-}$ were also reported as specific $ONOO^-$ scavengers (241). $FeTM\text{-}4\text{-}PyP^{5+}$ has often been described as a peroxynitrite decomposition catalyst (77, 157, 187). $FeTSPP^{3-}$ and $FeTMSP^{7-}$ are anionic and have fairly low $E_{1/2}$ ($E_{1/2} = +0.023$ mV *vs.* NHE for $FeTSPP^{3-}$) and irreversible redox, and are thus poor SOD

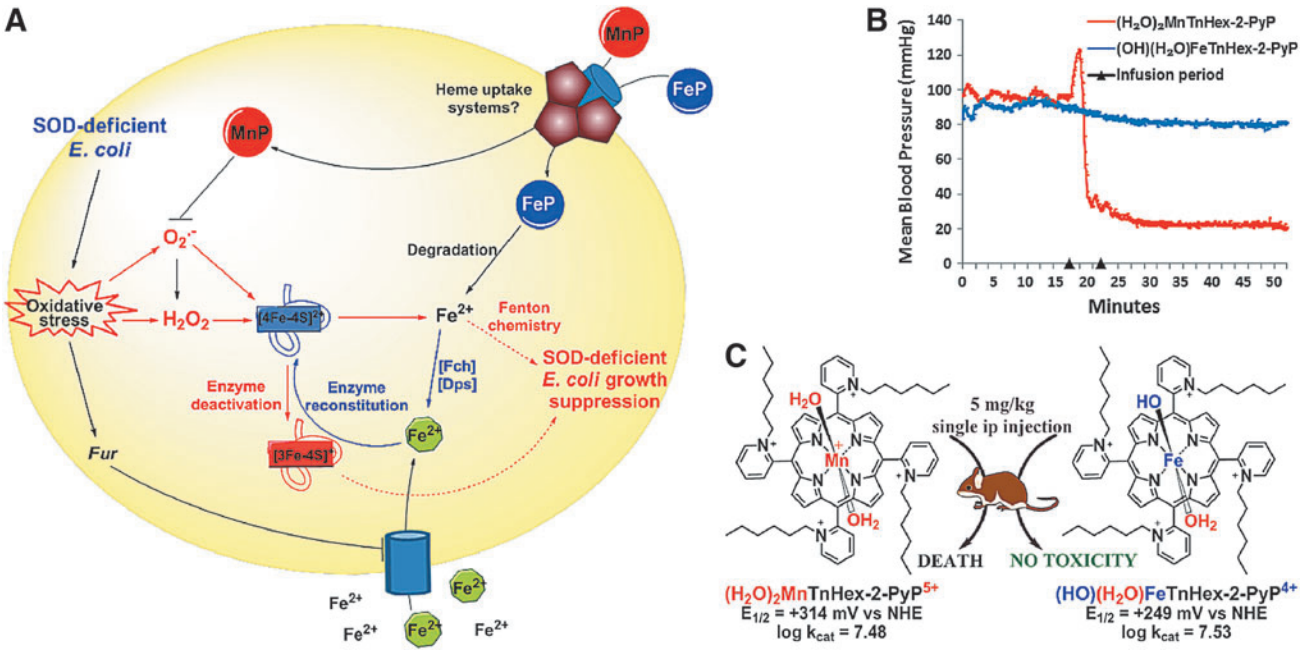

FIG. 8. FePs and MnPs differ greatly with respect to their chemistry which translates to differences in their biology. The schematic presentation of differences in the *in vivo* protective **(A)** and toxic **(B, C)** effects of FePs and MnPs on SOD-deficient *E. coli*. The $(H_2O)_2MnTE\text{-}2\text{-}PyP^{5+}$ and $(H_2O)(OH)FeTE\text{-}2\text{-}PyP^{5+}$ have very similar $E_{1/2}$ (Table 1) and similar electrostatics and, in turn, fairly similar $k_{cat}(O_2^{\bullet -})$. Consequently, FePs and MnPs should protect SOD-deficient *E. coli* when growing aerobically to a similar extent and at similar concentrations—some difference may be due to the difference in the total charge of these two classes of compounds. However, 20 μM MnPs was fully protective; while 20 μM FePs was toxic. On uptake, FePs undergo rapid degradation with H_2O_2 produced during fast redox cycling with cellular reductants (ascorbate or thiols), whereby "free" Fe^{2+} is released. The iron-transporting/sequestering siderophores (Fch—ferrochelatase; Dps—Fe-storage protein; green circles) take care of "free" Fe. At very low levels (0.01 to 1 μM), Fe^{2+} could reconstitute Fe-containing enzymes, such as aconitases, threonine dehydrogenase, ribulose-5-phosphate 3-epimerase, and peptide deformylase (69). These enzymes undergo superoxide-driven oxidative degradation and subsequent reversible release of Fe^{2+}. At higher concentrations, the deleterious effects of iron-mediated Fenton chemistry-driven $^{\bullet}OH$ radical production may prevail. The MnPs are much more resistant toward oxidative degradation and, thus, as SOD mimics, they eliminate superoxide, thereby preventing superoxide-driven damage on Fe-containing enzymes. A single ip injection of $(H_2O)_2MnTnHex\text{-}2\text{-}PyP^{5+}$ caused mouse death, while no toxicity was seen with Fe analogue. For reasons not presently understood, $H_2O)_2MnTnHex\text{-}2\text{-}PyP^{5+}$, but not $(OH)(H_2O)$-$FeTnHex\text{-}2\text{-}PyP^{4+}$ causes blood pressure drop. Modified from Tovmasyan *et al.* (273). To see this illustration in color, the reader is referred to the web version of this article at www.liebertpub.com/ars

mimics, but can still reduce $ONOO^-$ (due to its high oxidizing power), though with modest rate constants (241).

Drug Reactivity

Reactivity toward reactive species other than $O_2^{\bullet-}$

Figure 9 and Table 1 summarize available data on the SOD-like activity of different redox-active compounds toward small molecules; the reactivity toward protein thiols is discussed under Reactivity toward cellular reductants and Reactivity toward signaling proteins sections. What is shown in Table 1, and below (under reactivities toward different small and large reactive species), is perhaps only a small fraction of their reactivities in a complex milieu of a cell. Based on our present knowledge, it is incorrect to use a single redox-active compound such as MnP as a sole tool to specifically prove the involvement of a single reactive species in a certain pathological disorder. The reason for SOD-like activity, as well as for other reactivities, lies in the electron-deficient (electrophilic) nature of Mn(III) *N*-alkylpyridylporphyrins that favors the reaction and/or binding of electron-rich anionic ligands such as $ONOO^-$, ClO^-, HO_2^-, RS^-, and HA^-. Once such a porphyrinic electrophile reaches the cell, the data show that it readily undergoes reduction while oxidizing abundant ascorbate and thiols. In subsequent reoxidation of MnP with O_2 or $O_2^{\bullet-}$, and oxidation of ascorbate radical to dehydroascorbate, the peroxide is produced. MnP can employ peroxide and/or GSH to inactivate nuclear factor κB (NF-κB) (82, 125, 127, 238, 240), suppress mitochondrial respiration (124) and glycolysis (70, 124), or induce adaptive responses (52, 75). Such pro-oxidative actions agree well with what Forman *et al.* recently put forward as the mechanism of action of natural antioxidants (89). The final outcome will largely depend on the colocalization of MnPs with reactive species and their concentration levels. Given the complex cellular mileu, the existence of subcellular fragments, and the complex redox chemistry of redox-biocompatible compounds, it is difficult to impossible to understand the full biological reactivity of MnPs. The details are given next.

Reactivity toward $ONOO^-$. The log $k_{cat}(O_2^{\bullet-})$ is directly proportional to log k_{red} $(ONOO^-)$ (28, 84, 86). Thus, potent SOD mimics are potent peroxynitrite scavengers (Eqs. [15] and [16]). We have shown with MnPs that the reason lies in the fact that the most potent SOD mimics are electron-deficient and that such MnPs would favor reactions and/or binding of electron-rich anionic ligands such as $ONOO^-$. The reactivity of pentacationic MnPs toward superoxide [k_{cat} $(O_2^{\bullet-})$] is higher than toward peroxynitrite [k_{red} $(ONOO^-)$]; pentacationic MnP would prefer $O_2^{\bullet-}$ compared with $ONOO^-$ if it encounters both species under identical concentrations. The log k_{cat} $(O_2^{\bullet-})=7.76$ for MnTE-2-PyP^{5+} at

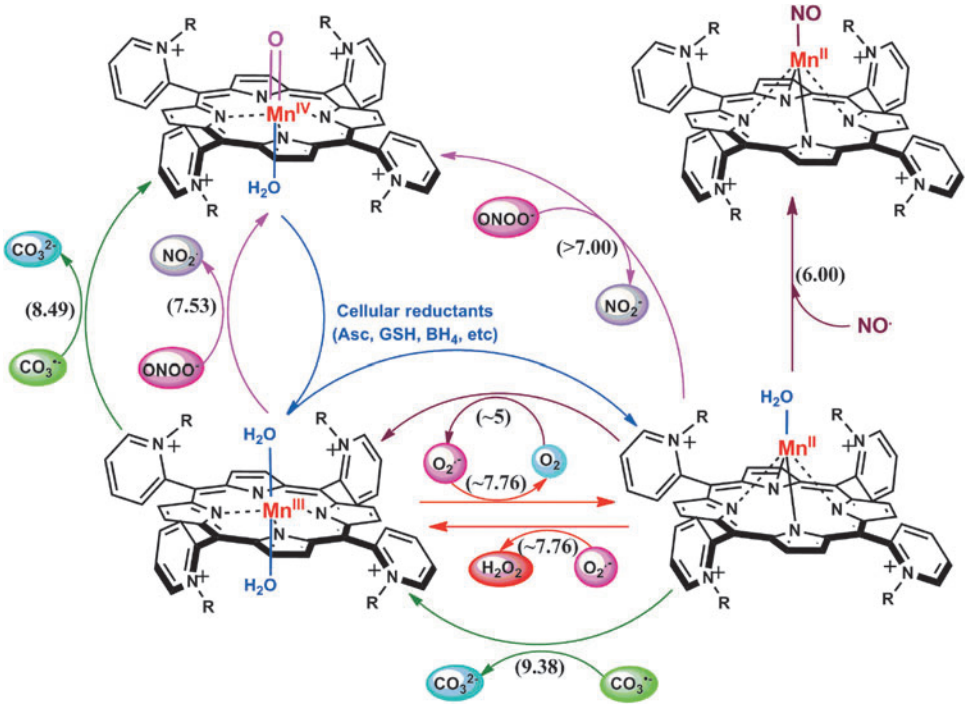

FIG. 9. The reactivities of *ortho* isomers of Mn(III) *N*-substituted pyridylporphyrins toward small molecules. R describes either alkyl or alkoxyalkyl groups. The reactivity toward protein thiols has not been included in this scheme, but is discussed under Reactivity toward cellular reductants and Reactivity toward signaling proteins sections. The reactivity is predominantly determined by the presence of cationic charges on nitrogens that dominate the electronics and electrostatics of the reactions. The removal of $O_2^{\bullet-}$ or $ONOO^-$, resulting in H_2O_2 or $O=Mn^{IV}P$ production, can only bear antioxidative character if the cell has either sufficient peroxide-removing enzymes or reductants to eliminate strong oxidants (high valent metal), respectively. If not, as is often the case with oxidative stress injuries and in a particular cancer, the pro-oxidative action may prevail. Under such conditions, MnP may employ H_2O_2 to inhibit the activation of NF-κB by oxidizing and/or glutathionylating its subunits (124, 125). Moreover, MnP may directly oxidize thiols (see below under Thiols section). NF-κB, nuclear factor κB. To see this illustration in color, the reader is referred to the web version of this article at www.liebertpub.com/ars

25^0C, while its log $k_{red}(ONOO^-) = 7.53$ but at 37°C (28). Once oxidized to $O=Mn^{IV}P$ with $ONOO^-$, MnP would regenerate itself as a catalyst with cellular reductants acting as electron pools and sparing biological targets from highly oxidizing Mn oxo species (86).

$$(H_2O)_2Mn^{III}P^{5+} + ONOO^- \Longleftrightarrow (H_2O)O=Mn^{IV}P^{4+} + {}^{\bullet}NO_2 + H_2O \quad [15]$$

$$(H_2O)Mn^{II}P^{4+} + ONOO^- \Longleftrightarrow (H_2O)O=Mn^{IV}P^{4+} + NO_2^- \quad [16]$$

In the reaction with $ONOO^-$, MnPs can cycle either one-electronically *via* $O=Mn^{IV}P/Mn^{III}P$ redox, producing highly oxidizing radical, ${}^{\bullet}NO_2$ (Eq. [15]), or two-electronically *via* $O=Mn^{IV}P/Mn^{II}P$ redox (Eq. [16]), producing benign nitrite NO_2^- (80, 196). The MnPs are *in vivo* maintained in reduced Mn +2 state by cellular reductants. Thus, the 2-electron- is more likely than the one-electron reaction.

The compounds with negative $E_{1/2}$ (such as $Mn^{III}TBAP^{3-}$, $E_{1/2} = -194$ mV *vs.* NHE) cannot participate in a 1st step of $O_2^{\bullet-}$ dismutation (Eq. [1]). However, $Mn^{III}TBAP^{3-}$ can be oxidized to $O=Mn^{IV}P$ with $ONOO^-$ (and perhaps other strong oxidants ClO^-, H_2O_2, and lipid radicals), which may explain its reported *in vivo* efficacy (19). The log k_{red} $(ONOO^-) = 5.02$ for $MnTBAP^{3-}$ is >100-fold lower than of $MnTE\text{-}2\text{-}PyP^{5+}$ (log $k_{red} = 7.53$) (28, 223). $ONOO^-$ can also oxidize Mn texaphyrin with even lower $k_{red}(ONOO^-) = 3\times10^4$ $M^{-1}s^{-1}$ (84, 196, 242) and some other MnPs, such as Mn(III) *meso*-tetracyclohexenylporphyrin as well as biscyclohexano-fused Mn(III) complex of bis(hydroxyphenyl)dipyrromethene (217, 218). The other compounds that cannot be oxidized by $O_2^{\bullet-}$ are $MitoQH_2$ (quinol), MitoQH (semiquinone), and nitroxides (177). Once it reaches mitochondria, the MitoQ readily gets reduced to $MitoQH_2$ by components of the electron transport chain (177). $MitoQH_2$can be oxidized by $ONOO^-$ to MitoQH, which then dismutes (disproportionates) to MitoQ and $MitoQH_2$. Only MitoQ (quinone) and oxoammonium cation react with $O_2^{\bullet-}$ with high rate constants to yield MitoQH and nitroxide, respectively (177). Nitroxides get oxidized with the degradation product of $ONOO^-$, $CO_3^{\bullet-}$ and ${}^{\bullet}NO_2$, and protein-derived radicals, thiyl and peroxyl radicals giving rise to oxoammnium cation (28). Oxoammonium cation though reacts with $O_2^{\bullet-}$ (28). Mn(III) cyclic polyamines are often reported as specific to $O_2^{\bullet-}$ (59, 169, 171, 186, 228, 267). The reactivity of Mn cyclic polyamine M40403 toward ${}^{\bullet}NO$ has been reported (87). Mn salen derivatives show a wide range of reactivities toward $ONOO^-$, H_2O_2, ClO^-, and ${}^{\bullet}NO$ (74, 132, 234). The MCs are reactive toward $O_2^{\bullet-}$ and $ONOO^-$ (28). The reactivity of cerium oxide (nanoceria) toward $O_2^{\bullet-}$, H_2O_2, and ${}^{\bullet}NO$ has been reported (28). Work in progress shows that potent SOD mimics are also very reactive toward ClO^- (109). One can easily envision that many other reactions are possible with each of those compounds within cells. Thus, we can only safely predict which reaction is possible but not which will occur.

MCs employ $M^{IV}C/M^{III}C$ or $O=M^{V}C/M^{III}C$ to cycle with $O_2^{\bullet-}$, H_2O_2, and $ONOO^-$ (see earlier under SARs for diverse redox-active compounds—Mn(III) corroles). Similar to MnPs, two-electron oxidation with $ONOO^-$ would lead to benign NO_2^- production (162). Reduction of strong oxidizing high-valent Mn will be achieved at the expense of reductants acting as electron pools.

Reactivity toward ${}^{\bullet}NO$. Cationic Mn(III) *N*-substituted pyridylporphyrins favor reactions with ${}^{\bullet}NO$; at submicromolar concentrations and at 1:1 ratio, a fairly stable complex is formed, $(NO)Mn^{II}P$, with Mn in +2 oxidation state (Eq. [18]). The reaction is very slow with $t_{1/2} \sim 60$ min; the same product is formed much faster if $Mn^{III}P^{5+}$ is first reduced with cellular reductants such as thiol or ascorbate (HA^- and RS^-, monodeprotonated species are major ones at pH 7.8) (Eq. [17]). The oxidation of cysteine (similar to the Eq. [17b] shown for glutathione) by $Mn^{III}P$ resembles the reported thiol oxidase action of SOD enzyme (294). The rate constant for nitrosylation of MnP (Eq. [18]), estimated by stopped flow, is $k \sim 10^6$ $M^{-1}s^{-1}$. The complex slowly undergoes the oxidation, whereby initial $Mn^{III}P$ gets restored and nitrate is eventually formed (Eqs. [19] and [20]). $Mn^{II}P^{4+}$ can undergo oxidation with either oxygen or superoxide (the latter reaction being 2nd step of $O_2^{\bullet-}$ dismutation process), depending on their relative levels in cells. The reaction of $Mn^{II}TE\text{-}2\text{-}PyP^{4+}$ with O_2 was estimated to occur with a rate constant of $\sim 8\times10^4$ $M^{-1}s^{-1}$ (248). Axially coordinated waters are omitted in the equations for simplicity, as no protonation equilibria are involved at the Mn site:

$$Mn^{III}P^{5+} + HA^- \Longleftrightarrow Mn^{II}P^{4+} + HA^{\bullet};\ 2H^+ + A^{\bullet-} + O_2^{\bullet-} \Longleftrightarrow A + H_2O_2 \quad [17a]$$

$$Mn^{III}P^{5+} + GS^- \Longleftrightarrow Mn^{II}P^{4+} + GS^{\bullet};\ 2GS^{\bullet} \Longleftrightarrow GSSG \quad [17b]$$

$$Mn^{II}P^{4+} + {}^{\bullet}NO \Longleftrightarrow (NO)Mn^{II}P^{4+} \quad [18]$$

$$(NO)Mn^{II}P^{4+} + O_2 \Longleftrightarrow Mn^{III}P^{5+} + NO_3^- \quad [19]$$

$$Mn^{II}P^{4+} + O_2 \Longleftrightarrow Mn^{III}P^{5+} + O_2^{\bullet-};\ 2O_2^{\bullet-} + 2H^+ \Longleftrightarrow H_2O_2 + O_2 \quad [20]$$

The ${}^{\bullet}NO$ scavenging by MnP may affect cellular signaling pathways. The ${}^{\bullet}NO$ binding shifts the reduction potential for the $Mn^{III}P/Mn^{II}P$ redox couple by +600 mV (133, 184, 276), stabilizing Mn in +2 oxidation state. The reactivity of nitrosylated $(NO)Mn^{II}P^{4+}$ toward $O_2^{\bullet-}$ is presently under investigation.

Reactivity toward H_2O_2. Hydrogen peroxide (H_2O_2) is a strong oxidant; thus, very few organic ligand-containing compounds are stable enough in its presence to be efficient catalysts of its dismutation. *In vivo* H_2O_2 is produced by different oxidases, such as NADPH- and xanthine oxidases, and is also a product of $O_2^{\bullet-}$ dismutation during mitochondrial respiration. Under n*M* levels, it is a main signaling species due to its long life, lack of charge, and ability to cross cellular membranes (90). It is also a source of other highly oxidizing species, such as ${}^{\bullet}OH$ radical, alkoxyl ($RO^{\bullet}$) and peroxyl ($RO_2^{\bullet}$) radicals, and protein thiyl radicals (89, 109).

The preliminary studies on the catalysis of H_2O_2 dismutation (producing H_2O and O_2) indicate that the log $k_{cat}(H_2O_2)$ is in the range of 1–2 log units for several MnPs [MnTE-2(and 3)-

PyP^{5+}, $MnTBAP^{3-}$, and MnTnHex-2(and 3)-PyP^{5+}] (Weitner *et al.*, unpublished). Data agree fairly well with those reported from Fridovich's group for MnTM-4-PyP^{5+} and $MnTBAP^{3-}$ (66). Due to the excessive bleaching, Mahammed and Gross were not able to assess the $k_{cat}(H_2O_2)$ for $FeTSPP^{3-}$ (161). Starting with an FeP, containing three mesityl groups on porphyrin *meso* positions, Nocera's group added the fourth *meso* pendant group producing structure with $k_{cat}(H_2O_2)$ increased ~3000-fold relative to Fe(III) tetrakis-*meso*(2,4,6-methylphenyl)porphyrin (49). The rate constant for the reduction of H_2O_2 to H_2O with MnTDE-2-ImP^{5+} at pH ~7 (128) is low, $k_{red}(H_2O_2) \sim 10^2\, M^{-1}s^{-1}$, and is reportedly faster with less electron-rich MnTM-2-PyP^{5+} (30).

Corrole is a trianionic ligand, while porphyrin is dianionic; as a result, the metal site is more electron rich in MCs, giving rise to more stable complexes in reduced metal +3 oxidation state with regard to the loss of metal (Fig. 10). Further, after the reaction with H_2O_2, metal in MCs is stabilized much more in higher metal +5 oxidation state relative to MPs; consequently, Fe corroles are more efficient catalysts of H_2O_2 dismutation (161). The log $k_{cat}(H_2O_2)$ of 3.8 was reported for Fe corrole-bearing pentafluorophenyl groups on three *meso* positions and two sulfonato groups at neighboring pyrrolic rings (161). Although possessing only ~0.6% of enzyme activity [assuming log k_{cat} ~6 for enzyme (109)], the Fe corrole may still have the highest $k_{cat}(H_2O_2)$ among the synthetic redox-active compounds. Whether and how this affects its therapeutic efficacy is not clear. When an aqueous solution of a compound was given orally at 20 mg/kg/day for 7 weeks, it prevented cataract incidents, favorably affected kidney function, and decreased serum cholesterol and triglyceride levels. Such a study suggests sufficient stability of that compound toward the proton-dependent loss of metal. As much as 300 mg/kg caused only a mild adverse effect (103).

Under physiological conditions, H_2O_2 is maintained at n*M* steady-state levels by abundant peroxide-removing enzymes. Under pathological conditions, particularly in cancer, some of the enzymes are reportedly down-regulated (8, 93, 191, 233, 235, 245). The reaction of MnP with oxygen (Eq. [21]), superoxide (Eq. [2]) or cycling with ascorbate (Eq. [17a]) or thiols (Eq. [17b]) would result in increased levels of H_2O_2. Subsequently, MnP can utilize H_2O_2 to glutathionylate thiols of subunits of critical anti-apoptotic transcription factor, NF-κB (124). Tome's group demonstrated that the glutathionylation occurs only in the presence of H_2O_2 and GSH and could be best presented with reactions [22] through [24], where MnP acts as glutathione peroxidase, GPx. This agrees with reported GPx-like activity of *para* isomer, MnTM-4-PyP^{5+} (9). A reaction given by equation [22] is proposed by Jin *et al.* for MnTDE-2-ImP^{5+}, which is similar in reactivities to MnTE-2-PyP^{5+} (128). The reaction described by Eq. [24] presents the disulfide interchange reaction (109):

$$(H_2O)Mn^{II}P^{4+} + O_2 + H_2O \Longleftrightarrow (H_2O)_2Mn^{III}P^{5+} + O_2^{\bullet -} \quad [21]$$

$$(H_2O)(OH)Mn^{III}P^{4+} + H_2O_2 \Longleftrightarrow O=Mn^{V}P=O^{3+} + 2H_2O + H^+ \quad [22]$$

$$O=Mn^{V}P=O^{3+} + 2\,GS^- + 4H^+ \Longleftrightarrow (H_2O)_2Mn^{III}P^{5+} + 2\,GS^{\bullet} \quad [23a]$$

$$2GS^{\bullet} \Longleftrightarrow GSSG \quad [23b]$$

$$GSSG + \text{Protein-SH} \Longleftrightarrow \text{Protein-S-S-G} + GSH \quad [24]$$

The anticancer radiation or corticosteroid-based therapy gives rise to high levels of H_2O_2. When administered along with MnP, the metal complex would catalyze glutathionylation of p65 subunit of NF-κB by H_2O_2 and GSH. Use of the redox-active metal complex along with the source of H_2O_2 has been proposed by us and others (268, 299) as a prospective anticancer treatment.

The Mn salen derivatives have reportedly the advantage because of their dual SOD and catalase-like activities (74). While the first is fair [log $k_{cat}(H_2O_2)$ ~6, Table 1] (34, 74, 249), the catalase-like activity is, however, insignificant, representing only $\sim 7\times10^{-5}$% of the enzyme activity (1, 73, 74, 98, 132, 202). Besides unfavorable thermodynamics, the low metal/ligand stability of Mn salens disfavors high catalase-like activity.

Reactivity toward cellular reductants. Due to the biocompatible $E_{1/2}$ and favorable electrostatics (26, 28, 177), the pentacationic electrophilic Mn(III) *N*-substituted pyridylporphyrins rapidly react with anionic deprotonated forms of cellular reductants: ascorbate, glutathione, cysteine, and protein thiols (29, 33, 299). In such reactions, the MnPs act as oxidants. When undergoing oxidation with strong oxidants (such as $ONOO^-$ or H_2O_2), the highly oxidizing Mn in +4 and +5 oxidation state is formed. It gets reduced back to either Mn +3 or +2 oxidation states while oxidizing reductants (instead of biological targets) that serve as suppliers of electrons (Eq. [25]) (38, 84, 86, 277).

$$(H_2O)O=Mn^{IV}P^{4+} + HA^- + 2H^+ \Longleftrightarrow (H_2O)_2Mn^{III}P^{5+} + HA^{\bullet};\ HA^{\bullet} \Longleftrightarrow A^{\bullet -} + H^+ \quad [25]$$

These reductants also likely couple with MnP in removing $O_2^{\bullet -}$ *in vivo*; consequently, the MnP may act as superoxide reductase rather than as SOD (Eq. [17] as a first step and

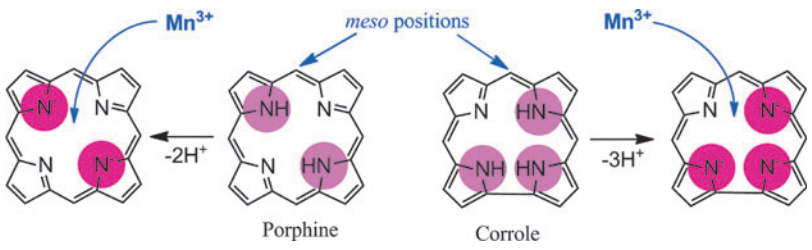

FIG. 10. The comparison of porphyrin *versus* corrole core. Porphyrin contains 2 while corrole contains 3 protonated pyrrolic nitrogens (encircled). Consequently, upon deprotonation porphyrin is a dianionic, while corrole is a trianionic ligand. Such a difference results in differential metal/ligand stability, and affects properties of metals. To see this illustration in color, the reader is referred to the web version of this article at www.liebertpub.com/ars

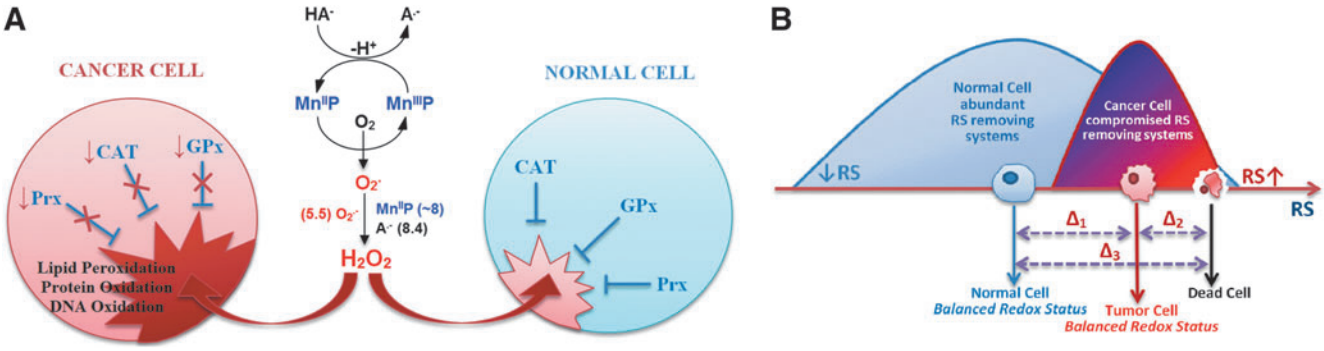

FIG. 11. Differential effect of MnP/ascorbate-driven H_2O_2 production on tumor and normal cells. (A) Ascorbate oxidation produces H_2O_2 that normal cells remove readily. Depending on the type of cancer cell, peroxide may not be well taken care of, leading to higher oxidative stress than in normal cells (16) **(B)** Redox status of cancer and tumor cell differs significantly, which determines their differential sensibility to an additional increase in reactive species. Tumor cells already have high levels of reactive species, and any further increase could cause their death (42, 114). To see this illustration in color, the reader is referred to the web version of this article at www.liebertpub.com/ars

Eq. [2] as a second step). The antioxidative effect of MnP in removing $O_2^{\bullet -}$ is assured only with sufficient physiological levels of enzymes that are capable of removing the H_2O_2. Otherwise, similar to cancer cells in which such enzymes are frequently down-regulated, the redox cycling of MnP with ascorbate or glutathione or cysteine would result in the accumulation of peroxide and its involvement in the oxidation of biological targets.

Ascorbate. The antitumor potential of ascorbate was demonstrated in a number of tumor cell lines and in animal models only when given intravenously (iv) or intraperitoneally (ip) (44–46, 82, 116, 151, 199). Supplementation of ascorbate to an immunodeficient mouse with rapidly spreading 9l glioblastoma reduced tumor growth and weight by 41%–53%; in 30% cases, cancer spreads to other organs, while no dissemination of cancer was seen in ascorbate-treated mice (46). Ascorbate antitumor action was assigned to its oxidation and subsequent cytoxic H_2O_2 formation, catalyzed by endogenous metalloproteins (116). A much higher yield of peroxide may be achieved if catalysts are optimized for ascorbate oxidation. Such are isomeric Mn(III) *N*-substituted pyridylporphyrins; their H_2O_2-producing potency has already been shown by us and others (82, 220, 273, 299) (Fig. 11).

Ascorbate distributes into cells *via* SVCT1 and SVCT2 transporters, whereas GLUT transporters are responsible for the dehydroascorbate uptake (55). Decreased tumor ascorbate levels in endometrial cancer have been associated with high hypoxia inducible factor-1α (HIF-1α), vascular endothelial growth factor (VEGF), and GLUT favoring tumor progression (141).

We were the first to show, using several tumor cell lines, that the bio-compatible pentacationic electron-deficient *ortho* isomeric MnPs catalyze ascorbate oxidation while producing high amounts of peroxide and exerting cytotoxic effects [Roberts *et al.*, unpublished (299) (Fig. 12) (see also Reactivity toward signaling proteins section). With two normal cell lines, either none or lower cytotoxicity relative to tumor cell was demonstrated (Fig. 12). A normal cell is well equipped with multiple H_2O_2-removing systems such as catalases, glutathione peroxidases, glutathione transferases, peroxyredoxins, and thioredoxins. Tumor cells, however, with a lower buffering capacity, are much more sensitive to any further

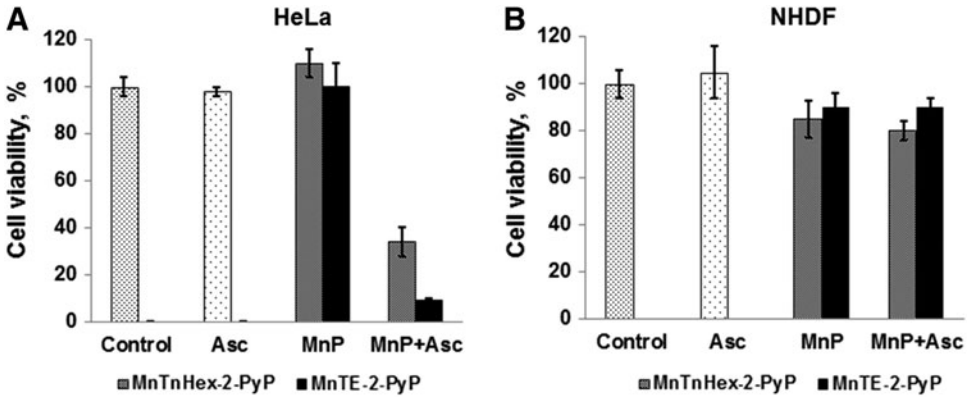

FIG. 12. Differential cytotoxicity of MnP/ascorbate in tumor (A) and normal cell line (B). Two MnPs were tested, a hydrophilic MnTE-2-PyP^{5+} and a lipophilic MnTnHex-2-PyP^{5+} at 3 μM (shown) and 15 μM. The concentration of ascorbate was 1 m*M*. MnPs and ascorbate alone were not toxic. In the presence of ascorbate, both MnPs become toxic to cervical cancer cells, HeLa, but not to normal primary fibroblasts, NHDF cells. MTT assays were performed in a 96-well plate with an initial seeding density of 25,000 cells/well. Cells were incubated with MnP ± ascorbate for 48 h before the assay was performed (272, 299). The study was done in duplicate. Ascorbate was added soon after MnP. The effect of MnP/ascorbate on several other cancer cell lines has also been demonstrated (82, 299).

increase in oxidative stress (Fig. 12) (8, 35, 93, 142, 177, 191, 233, 235, 245). In a cell culture, the MnP/ascorbate showed promise as potential treatment of inflammatory breast cancer; the noncaspase-, but AIF- and NF-κB-based apoptosis was promoted (82). Even when the SOD enzyme was up-regulated, the suppression of tumorigenesis was demonstrated by Tome *et al.*, which is likely due to the down-regulation of peroxide-removing enzymes (40). The rapamycin increased levels of reactive species in a cellular model of mantle cell lymphoma (Grant519 and NCEB1) *via* inhibition of mTORC2 signaling. These cells presumably have insufficient levels of MnSOD, which would have otherwise reduced tumor progression. The increased levels of reactive species consequently up-regulate the MnSOD enzyme. The up-regulation of MnSOD increases the levels of reactive species, which suppresses the tumor cell growth (41).

The *para* isomeric MnPs, such as MnTM-4-PyP^{5+}, could be a better catalyst for ascorbate oxidation than their *ortho* analogs when judged solely on a thermodynamic basis. The $E_{1/2}$ of +60 mV *versus* NHE shows that, once reduced, the MnTM-4-PyP^{5+} more readily reoxidizes, thus producing H_2O_2. The *ortho* analog MnTE-2-PyP^{5+} with 162 mV more positive $E_{1/2}$ is more electron deficient and prefers residing in a reduced state. Further, the *para* compounds are planar and, thus, favor intercalation within groves of nucleic acids, which may prevent their action and/or cause toxicity to normal tissue (18, 220). Also, it would undergo oxidative degradation faster then ortho analog (30, 128). Rawal et al just reported the tumor suppression in sc nude mouse xenograft model of human pancreatic cell line (220).

It is important to note that the reduction of Mn^{III}P^{5+} with ascorbate reduces a total charge of MnP from penta- to tetracationic and, thus, enhances lipopilicity and cellular and tissue accumulation (251, 270). In cellular studies, the MnP/ascorbate was added exogenously into medium where it produced peroxide outside of the cell. Thus, under such conditions, no impact of the magnitude of MnP lipophilicity on its therapeutic efficacy was observed (299). In an *E. coli* model, however, the accumulation of ascorbate-reduced tetracationic MnP is greatly enhanced (251, 270). Thus, in addition to appropriate thermodynamics and kinetics of MnP/ascorbate redox system, the bioavailability of MnP would play a role in *in vivo* studies.

Welsh *et al.* just completed Phase I Clinical Trials in pancreatic cancer, where ascorbate was administered along with gemcitabine (291). Pancreatic cancer is the fourth leading cause of death in the United States, with 80% of mortality. The data obtained from Phase I are enthusiastic and warrant Phase II Clinical trials. As compared with an earlier report by Monti *et al.* (181), Welsh *et al.* infused ascorbate to achieve at least 20 m*M* levels in plasma, which would assure the antitumoral effect of ascorbate based on an earlier study of Du *et al.* (78). While Monti's study lasted only 8 weeks, to assure the safety and tolerability, the Welsh *et al.* study was several months long. In the absence of dose-limiting toxicity, the treatment was continued until progression (defined by Response Evaluation Criteria in Solid Tumors, RECIST). Even with only 8 weeks of ascorbate administration, the reduction in tumor volume was observed in 8 out of 9 patients in the Monti *et al.* study (181). The progression-free survival and overall survival was 12.7 weeks and 6 months with Monti *et al.* and 26 weeks and 12 months with Welsh *et al.* (181, 291). It is important to note that the high levels of ascorbate and peroxide did not induce systemic oxidative stress, as levels of F_2-isoprostanes remained the same or were reduced. The same was true for blood cells glutathione, which was unchanged as was the half-cell reduction potential. The ascorbate radicals were undetectable before treatment, while they were markedly increased in treated patients.

Buettner's group has also reported that ascorbate acts as a radiosensitizer in pancreatic cancer *via* production of reactive species (4, 290). The group is further exploring the role of transition metals and their porphyrin complexes on ascorbate-induced cytotoxicity in cancer (220).

Thiols. Reactivity toward glutathione and *N*-acetylcysteine has been addressed by Ferrer–Sueta *et al.* and by us (33, 85, 272). Reactivity of different MnPs (varying in total charge and $E_{1/2}$) toward cysteine (cys-62) residue of p50 subunit of NF-κB protein in a cell-free system (thus GSH free), resulting presumably in disulfide formation, has been demonstrated by Tse *et al.* (33, 278) (See under Reactivity towards signaling proteins section). The *S*-glutathionylation of another p65 subunit of NF-κB has been demonstrated in a cellular lymphoma study by Jaramillo *et al.* (125). The opposite was recently demonstrated by Fridovich–Keil's group, where MnTE-2-PyP^{5+} prevented the protein glutathionylation in a galactose transferase *Drosophila melanogaster* knock-out when growing in the presence of galactose (130). In the absence of galactose no effect on glutathionylated proteins of GALT-null, but increase in their levels in controls were seen. When catalyzing the glutathionylation, the MnP acts as a pro-oxidant, producing the GS$^{\bullet}$ radical. The GS$^{\bullet}$ then combines with another GS$^{\bullet}$, giving rise to GSSG; or, following the Winterbourn electron sink pathway, the GS$^{\bullet}$may react with GSH, giving rise to GSSG$^{\bullet}$radical. The GSSG$^{\bullet}$radical, by oxidation with O_2, forms GSSG and $O_2^{\bullet-}$ (292). The GSSG can exchange glutathione spontaneously with protein thiol whereby glutathionylated protein, protein-S-S-G will be formed. However, this may be prevented if GSSG is safely removed by glutathione reductase. Tome's group has reported that H_2O_2 and GSH are essential for glutathionylation to occur (124). The cancer cells and a genetically modified GALT-null *Drosophila*, due to differential levels of peroxide, would exhibit a differential outcome: one, higher and the other, lower levels of protein glutathionylation, respectively.

Reactivity toward signaling proteins. The investigations of the effect of MnPs on the up-regulation of numerous cytokines (33) made it clear that either direct reactions with reactive species (which supposedly signal the start of the cellular transcription) or direct reactions with signaling proteins may be involved. The driving force for understanding such observations was the fact that MnPs were as efficient in reducing mouse or rat infarct volume when given at early (6 min) or at late time points (90 min or 6 h) after reperfusion (238–240). Our knowledge at the time when the observation was made would predict that only immediate infusion of porphyrin into the brain at the time of reperfusion (the moment of peak production of reactive species) would ameliorate the primary oxidative damage. The protection demonstrated with delayed treatment, however, suggested that MnP must have suppressed the cellular transcription which would have otherwise perpetuated the oxidative stress

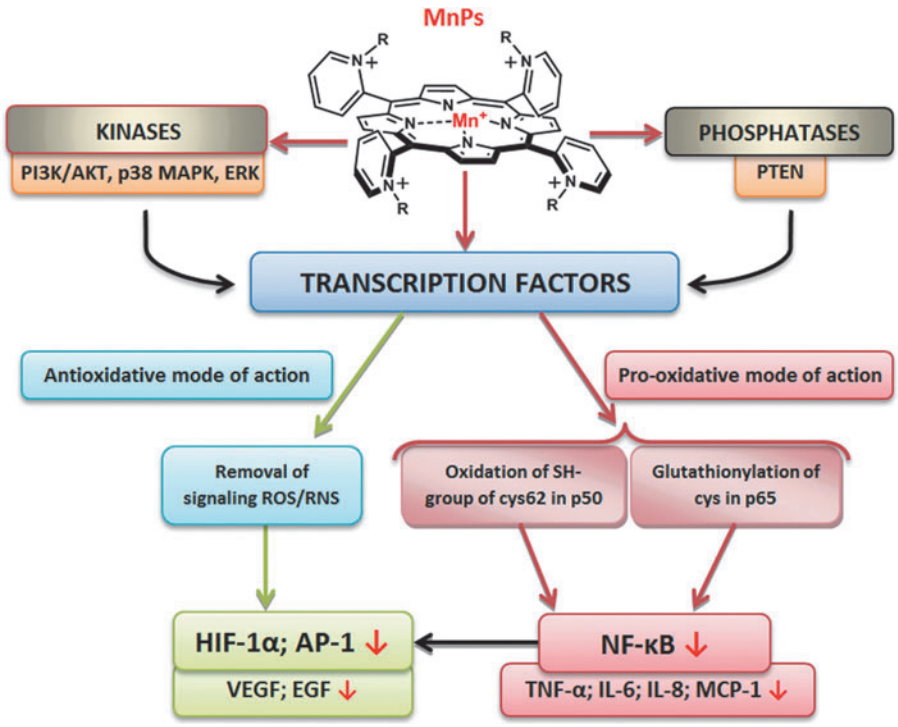

FIG. 13. The impact of MnPs on transcription factors and kinases and phosphatases and, in turn, on the related genes. To see this illustration in color, the reader is referred to the web version of this article at www.liebertpub.com/ars

(Fig. 13). Further exploration indicated that at least one major transcription factor, NF-κB, has been inactivated by the action of MnP (240). Similarly, the radioprotective effect of MnP was demonstrated when it was given for the duration of two weeks starting at any time postradiation from 2 h up to 8 weeks (96). HIF-1α and the genes it controls (VEGF, TGF-β) have been involved (95, 96). In cancer studies, the impact of MnP on activator protein-1 (AP-1) has been shown (304). In diabetes again, NF-κB and SP-1 have been identified as targets of MnPs (33, 278). Based on earlier and ongoing studies and our growing knowledge on MnPs, there is more to be identified.

The mechanism of MnP-transcription factor interactions is not fully understood. We have initially assigned the effects of MnP almost exclusively to the removal of signaling reactive species ($O_2^{\bullet -}$, $ONOO^-$), which resulted in the suppression of the cellular transcriptional activity. However, the most recent data suggest the direct and peroxide-driven oxidation of signaling proteins as a prevailing action of MnPs; depending on the cell type, the therapeutic outcome may be anti- or pro-oxidative (Fig. 13).

NF-κB—diabetes-and stroke-related cellular and animal studies. MnTDE-2-ImP^{5+} and MnTE-2-PyP^{5+} inhibited NF-κB activation in nuclear extracts of LPS-treated bone marrow-derived macrophages, and, therefore, suppressed pro-inflammatory cytokine production INF-γ and TNF-α. These results were recapitulated in human pancreatic cells cultured for 30 min in medium containing proteolytic enzymes and byproducts generated during cell isolation. The addition of 34 μM MnTDE-2-ImP^{5+} to isolated islet cells increased their survival and reduced levels of pro-inflammatory cytokines IL-6 and IL-8. Monocyte chemoattractant protein 1, MCAP-1 as well as PARP (poly(ADP-ribose)[polymerase]) were greatly suppressed and islets gained the capacity to normalize diabetic recipient mice (39, 40, 209). MnTE-2-PyP^{5+} also significantly delayed or prevented the diabetes altogether upon the treatment of young nonobese diabetic-severe combined immunodeficient mice with diabetogenic T-cell clone, BDC-2.5. All other aspects of NF-kB pathways were not affected, such as IKKα/β phposphorylation, and IKβ-α phosphorylation/degradation and p50/p65 nuclear translocation. Two additional experiments provided key support that MnP acted as a pro-oxidant, oxidizing cysteines whereby the antioxidant effects (listed earlier) were observed: (i) in a cell-free experiment (in the absence of GSH), MnP oxidized Cys-62 of p50 subunit of NF-κB, whereby disulfide formed prevented NF-κB activation (33, 278); (ii) in aqueous potassium phosphate-buffered solution, when only MnP and either cysteine or *N*-acetylcysteine or glutathione were present, the spectrophotometric evidence supported one-electron reduction of MnP (33). *In vivo* studies suggest that such NF-κB modification happens in the nucleus (33); data are supported by the biodistribution study in which MnTE-2-PyP^{5+} accumulated in the nucleus of macrophages at a 3-fold higher level than in the cytosol (33). Further on, the inactivation of NF-κB seems to play a major role in suppressing stroke injury with 2 hydrophilic and one lipophilic MnP. While in earlier studies hydrophilic MnPs were given intracerebroventricularly, most recently for the first time, the effect was demonstrated when lipophilic MnTnHex-2-PyP^{5+} was given subcutaneously for 6 days after initial iv bolus dose given at 30 minutes post-reperfusion (Fig. 14) (238, 240). Again, similar to diabetes, the pro-oxidative action of MnP in stroke accounts for the anti-oxidative therapeutic outcome.

AIF—cardiomyocyte study. An elegant study of Miriyala *et al.* of a mouse model of doxorubicin-induced cardiac toxicity has shown the effect of mitochondrially located MnPs

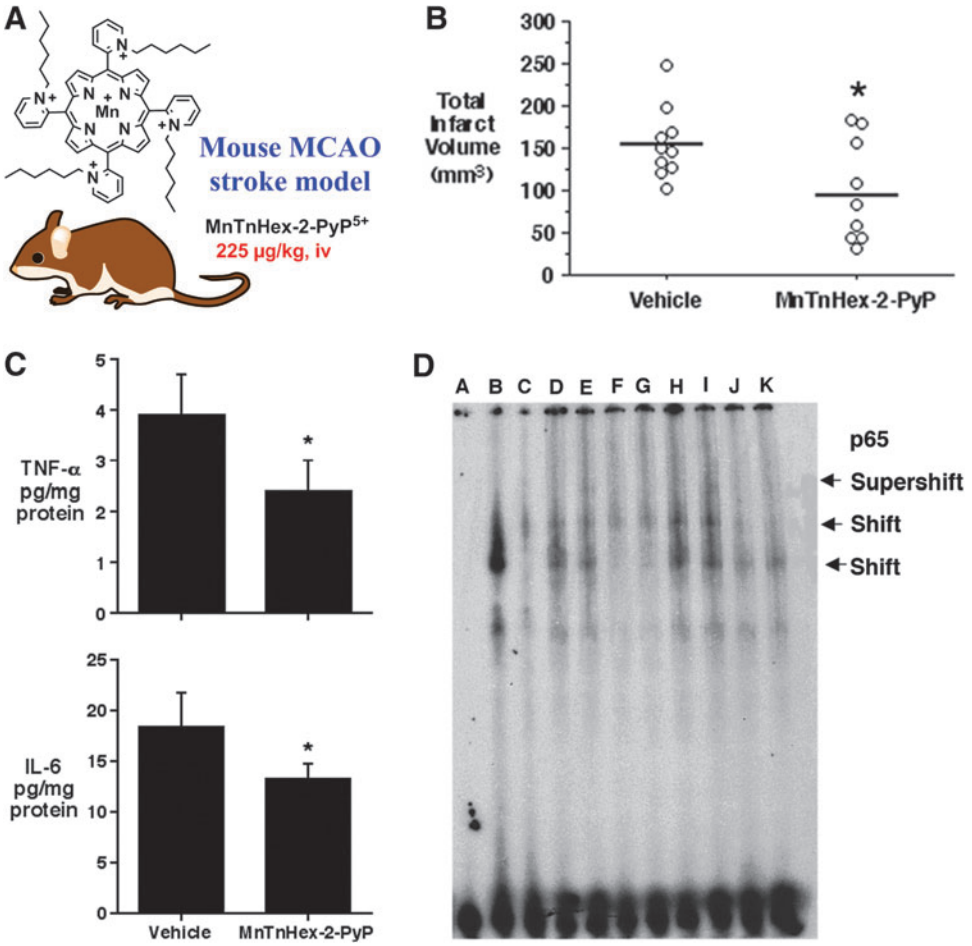

FIG. 14. The effect of MnTnHex-2-PyP^{5+} (A) on suppression of stroke injury in a mouse middle cerebral artery occlusion stroke model (238). (B) Infarct volumes were measured 7 days after 90 min MCAO. Rats were treated with intravenous vehicle (0.3 ml phosphate-buffered saline) or MnTnHex-2-PyP^{5+} (225 μg/kg) 5 min after reperfusion onset. The doses were repeated twice daily as subcutaneous injections for 7 days, after which cerebral infarct volume was measured. Open circles indicate individual animal values. Horizontal lines indicate group median values. MnTnHex-2-PyP^{5+} reduced cerebral infarct volume in the cortex ($p=0.05$) and subcortex ($p=0.01$), which was reflected in a 32% reduction in total infarct volume ($p=0.028$). Open circles indicate individual animal values. Horizontal lines indicate group mean values. **(C)** In studies on cytokines, rats were subjected to 90 min of middle cerebral artery occlusion. Five minutes after onset of reperfusion, rats were randomly treated with vehicle ($n=3$) or 225 μg/kg IV MnTnHex-2-PyP ($n=3$) followed by subcutaneous vehicle or 225 μg/kg MnTnHex-2-PyP^{5+}, respectively, at 12 and 18 h post-MCAO. Brains were harvested at 24 h post-MCAO and analyzed for TNF-α and IL-6 by fluorescent enzyme-linked immunosorbent assay. Values represent mean ± s.d. Both TNF-α and IL-6 concentrations were decreased by MnTnHex-2-PyP^{5+} (*$p<0.05$). **(D)** In NF-κB studies, four rats were subjected to 90 min middle cerebral artery occlusion and then treated with vehicle or MnTnHex-2-PyP^{5+} (225 μg/kg IV). Six hours later, ischemic brain was harvested to obtain nuclear extracts (2.5 μg) for electromobility shift assay (EMSA). The intravenous MnTnHex-2-PyP^{5+} decreased postischemic NF-κB DNA binding to a κB consensus oligo. Data shown are from Upper gel (EMSA): A-C are control lanes (A = probe only, B = positive control [HeLa nuclear extract], C = cold competitor). D and E (without and with p65 antibody, respectively) relate to rat #1 (vehicle). F and G (without and with p65 antibody, respectively) relate to rat #2 (MnTnHex-2-PyP^{5+}). H and I = vehicle rat #3 (with and without p65). J and K = rat #4 (MnTnHex-2-PyP^{5+}) with and without p65. Two slower migrating DNA-binding complexes are observed (shift). The proteins in the slower migrating complexes were identified by supershift analysis with 1 μg of p65-specific antibody. A marked reduction in NF-κB binding is seen in rats #2 and #4 (lanes F, G, J, and K, both hexyl). MCAO, middle cerebral artery occlusion. To see this illustration in color, the reader is referred to the web version of this article at www.liebertpub.com/ars

upon apoptosis inducing factor—mitochondrion-associated protein (AIFm2) (179). The AIFm2 is a p53 target gene and an AIF homologue. It appears to be a redox-responsive protein that resides in the mitochondria and plays a central role in caspase-independent cell death pathway (37, 153, 168, 194, 283, 295). The expression of AIFm2 is relatively low in tumor cells *versus* normal cells, suggesting the tumor-suppressive role of AIFm2 (178, 179, 296). If translocated into the nucleus, it serves as NADH-dependent oxidoreductase and is capable of nonsequence specific DNA binding, resulting in DNA fragmentation, that is, apoptosis. AIFm2 translocated into the nucleus after it formed the adduct with the product of lipid peroxidation, 4-hydroxynonenal. However, the three MnPs, MnTE-2-PyP^{5+}, MnTnHex-2-PyP^{5+}, and MnTnBuOE-2-PyP^{5+}, which accumulate in mitochondria (see below under Bioavailability studies section), prevented the doxorubicin-

induced mitochondrial lipid peroxidation, the 4-hydroxynonenal formation, and the formation of its adduct with AIFm2. Consequently, the translocation of AIFm2/4-hydroxynonenal adduct into the nucleus of H9C2 cardiomyocyte, as well as the initiation of the apoptosis was fully inhibited by MnPs (179). This appears to be a clear case of an antioxidative action of MnPs.

mTOR, c-Myc, and glucose-6-phosphate dehydrogenase. The studies of diabetogenic immune cells showed that MnTE-2-PyP^{5+} impedes diabetogenic autoimmune responses by restricting metabolic pathways for energy production (70). It suppresses aerobic glycolysis as demonstrated by reduced lactate production and Glut1 levels and inactivation of mTOR, c-Myc, and glucose-6-phosphate dehydrogenase (G6PD) (70). The mTOR, c-Myc, and G6PD are involved in signaling pathways that contribute to Wartburg effect (60, 111, 282). The c-Myc is widely described as an oncogene (282). The suppression of Nrf1 was also demonstrated (70).

Induction of adaptive response—up-regulation of endogenous antioxidative enzymes—rat kidney ischemia reperfusion model. Dorai's group substantiated the fact that MnP can cause adaptive response *via* a mild pro-oxidative stress (75). MnTnHex-2-PyP^{5+} was administered as a part of GMP treatment that contained specific renoprotective growth factors and mitochondria-protecting amino acids. It was given at a 24 h-time point before, at the time of ischemia (0 h) and at 24 h after 40–70 min of renal ischemia followed by 48 h of reperfusion. The up-regulation of antioxidant enzymes was demonstrated, suggesting that GMP treatment produced mild oxidative stress. In his subsequent work, Dorai introduced *N*-acetylcysteine into improved, I-GMP treatment. The aqueous solution chemistry shows that *N*-acteylcysteine readily couples with MnTnHex-2-PyP^{5+}. In turn, I-GMP further enhanced oxidative stress *via* production of H_2O_2 (33, 52). Indeed, a much more robust up-regulation of endogenous antioxidative defenses was demonstrated: glutathione peroxidase, lactoperoxidase, inducible nitric oxide synthase, mitochondrial and extracellular SOD, thioredoxin reductase 1, and a set of peroxyredoxins (52). In addition, oxidative stress genes (HSP-70 and phospho-heat shock factor-1, pHSF-1) were up-regulated. Levels of independent tissue ischemia markers (galectin-3, lipacalin-2, and high mobility group B1 protein, HMGB1) were increased upon I/R, but were reduced upon the treatment with I-GMP (52). HSP-70 exerts a cytoprotective effect (91) and also functions in a "chaperokine-like" manner due to its capacity to transport peptides and present them to antibody-producing cells, boosting the innate immune response (305). A widely accepted marker of kidney function, creatinine was greatly increased by ischemia/reperfusion and was markedly suppressed by the I-GMP treatment. Had MnP acted as an SOD mimic, the up-regulation of two SOD enzymes should not have happened.

Cancer studies

AIF—inflammatory breast cancer study. The effect of MnTnBuOE-2-PyP^{5+} on AIF, ERK, and p38(MAPK) kinases and X-linked inhibitor of apoptosis protein (XIAP) has been demonstrated in cellular inflammatory breast cancer study when MnP was co-administered with ascorbate (82). The MnP/ascorbate system enhances the oxidative stress *via* production of H_2O_2. In such pro-oxidative scenario, the GSH levels were reduced and the nuclear translocation of apoptosis-inducible factor AIF was enhanced, and so was the cellular apoptosis. With normal cells, such as cardiomyocyte, the mitochondrially localized MnP prevented the doxorubicin-based AIF-NHE adduct formation and nuclear translocation, and, in turn, inhibited the apoptosis (see earlier *AIF cardiomyocytes*). In an inflammatory breast cancer cell study (82), similar to a lymphoma study, the NF-kB was also suppressed (125, 126); in the former study, MnP/ascorbate, while in the latter, MnP/dexamethasone was the source of H_2O_2 (see below NF-kB—lymphoma).

HIF-1α–mouse breast cancer model. In a 4T1 breast cancer study, the suppression of hypoxia-related proteins was observed as well as the decrease in the levels of 8-oxo-2'-deoxyguanosine (8-OHdG), protein 3-nitrotyrosine, and NADPH oxidase. This could be a consequence of the antioxidative action of MnP. However, an MnP-driven oxidation of signaling proteins may be also operative; such an action would suppress secondary oxidative stress and, in turn, the up-regulation of various genes such as VEGF which would have otherwise contributed to the tumor growth delay (Fig. 15) (213). The data from Kim *et al.* (134) as well as the most recent data on the inhibition of NF-κB by Tome's group (125, 126) provide the basis for such reasoning (see below). NF-κB is known to control HIF-1α and NADPH oxidases (279). Kim *et al.* report indicates that a mild pro-oxidative event may cause the up-regulation of endogenous antioxidative defenses which action may result in antioxidative effects. If such scenario is operative, the effects could be wrongly assigned to the anti-oxidative action of MnP (134).

AP-1–a mouse skin carcinogenesis study. In skin carcinogenesis model, St. Clair's group has shown the inhibition of AP-1 by MnTE-2-PyP^{5+} and the reduction in the cell proliferation accompanied by the reduction in markers of oxidative stress (8-OHdG and protein carbonyls), all of which led to the remarkable suppression of skin papillomas (304). An antioxidative mechanism was proposed (304).

NF-κB—a lymphoma study. In a comprehensive study, Tome's group showed the pro-oxidative action of MnTE-2-PyP^{5+} on the enhancement of corticosteroid (dexamethasone)-induced lymphoma cell apoptosis (Fig. 16). The effect was ascribed to *S*-glutathionylation of p65 in cytosol, which prevented NF-κB DNA nuclear binding and, in turn, inhibited the up-regulation of anti-apoptotic genes (125, 126). Such modification required H_2O_2 and GSH. In turn, the cells were deprived of GSH—a major contributor to the physiological redox status. Tome's group also demonstrated that H_2O_2 was produced primarily in mitochondria by the action of dexamethasone (269)]. In addition, glucocorticoid treatment inactivates MnSOD. Were MnP a mimic of MnSOD, it would suppress (and not enhance) glucocorticoid-induced cell death.

The aqueous-based studies have confirmed that MnP readily gets reduced one electronically by thiols (glutathione, cysteine, *N*-acteylcysteine, and dithionite), thereby producing thiyl radical. Thiyl radical production is a necessary step in *S*-glutathionylation. The glutathione peroxidase-like or cysteine oxidase-like activity of MnPs seems to be operative in *S*-glutathionylation. It is only natural that with similar

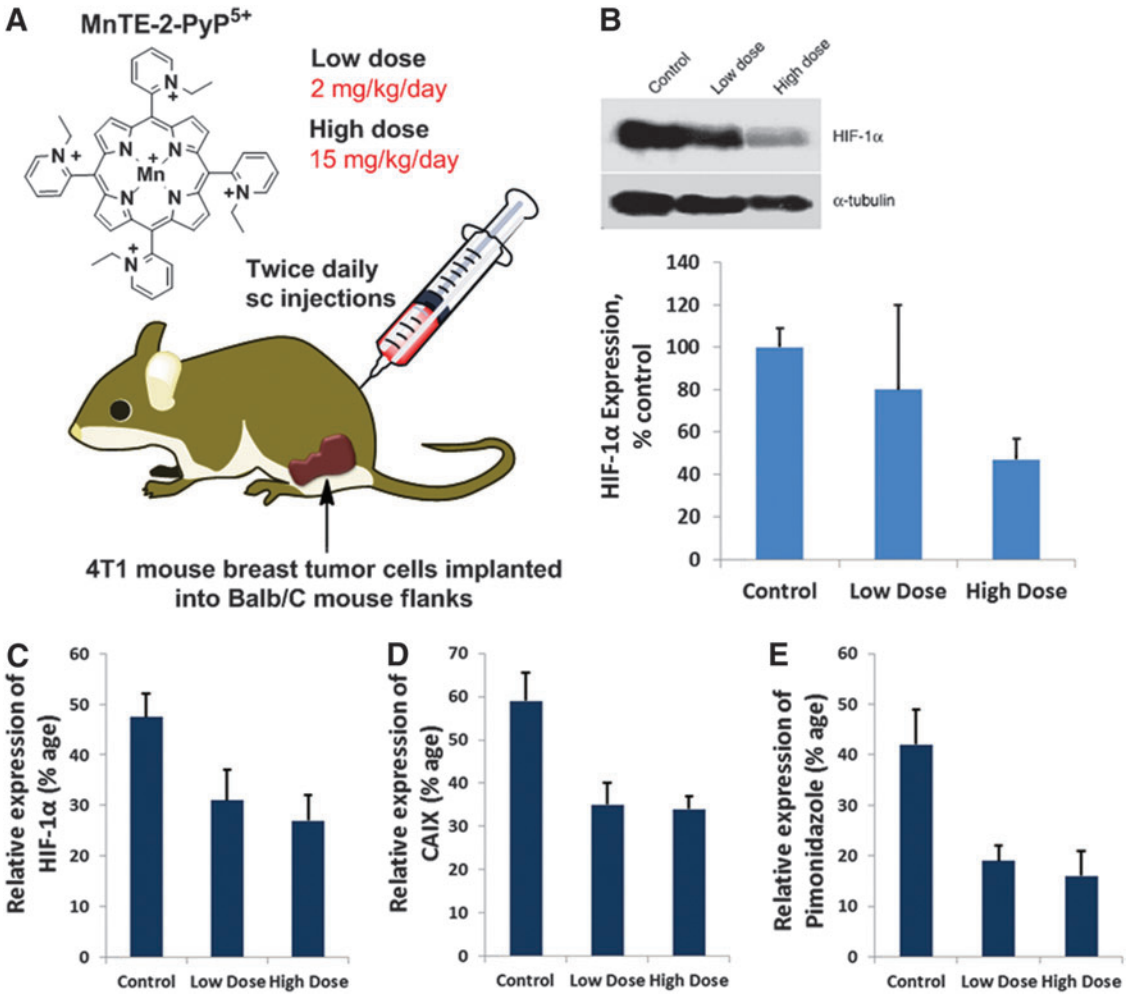

FIG. 15. The anticancer action of MnP as a sole agent. Anticancer effects of MnTE-2-PyP^{5+} **(A)** in a mouse sc 4T1 xenograft breast cancer model. 4T1 murine breast tumors were grown in Balb/C mice, allowed to reach $\geq 200\,mm^3$ in size, and randomized to one of the three treatment groups: PBS; 2×1 mg/kg/day MnTE-2-PyP^{5+} (low) and 2×7.5 mg/kg/day MnTE-2-PyP^{5+} (high). MnP was given sc throughout the duration of the study. Immunohistochemistry of HIF-1α **(C),** carbonic anhydrase CAIX **(D),** and pimonidazole **(E)** and representative Western blot for HIF-1α is shown **(B).** Densitometric readings (HIF-1α/α-tubulin) of the Western blot are expressed as percentage control. While significant changes in different signaling proteins that impact the tumor growth were demonstrated, the effect on tumor growth delay was significant but not large, even at such a high dose as 15 mg/kg/day (213). HIF-1α, hypoxia inducible factor-1α. To see this illustration in color, the reader is referred to the web version of this article at www.liebertpub.com/ars

thermodynamic features (reduction potentials), SOD enzymes and MnPs would undergo same reactions; however, the rates of such reactions would be limited by steric and electrostatic factors. While the low-molecular-weight MPs react readily with amino acids and proteins, the SOD enzymes have high specificity to small $O_2^{\bullet-}$ molecules, and will react with other large molecules that are orders of magnitude slower. For example, MnSOD reacts with $ONOO^-$ at log $k_{red}(ONOO^-)=5$, while MnPs reacts at log $k_{red}(ONOO^-)=$ 7.34 (28, 84, 86). Cu,ZnSOD was shown to have Px-like activity, and, most recently, Bonini's group showed that MnSOD has Px-like activity also (7). The cysteine oxidase activity of Cu,ZnSOD was reported to be log k ~5 (294). Our preliminary studies in simple aqueous systems have demonstrated such thiol oxidase activity for cationic Mn(III) *N*-alkylpyridylporphyrins (272). Araujo-Chaves *et al.* have indicated GPx activity of MnTM-4-PyP^{5+} (9). The scheme in Figure 17 proposes the GPx-like and thiol oxidase activity of MnP. We have shown that MnP/ascorbate system kills cancer cells, while it may be nontoxic or mildly toxic to normal cells (Fig. 12) (220, 272, 299). Please see the anticancer mechanism elucidated by Tome's group originating from the impact of MnP/dexamethasone on cellular bioenergetics (124). In the presence of dexamethasone, the mitochondrially located MnP glutathionylates, and in turn, inactivates critical proteins in electron transport chain, complexes I and III of mitochondrial respiration. Tome's group suggested to further combine MnP/dexamethasone therapy with 2-deoxyglucose inhibitor of glycolysis to deprive cancer cells from both energy sources and to down-regulate the anti-apoptotic pathways (124). Their study has vast therapeutic implications. Somewhat similar studies were reported by Kalyanaraman's group, where breast cancer MiaPaCa-2 cells were co-treated with redox-active mitochondrially targeted nitroxide, Mito-carboxypropyl (Mito-CP), and 2-deoxy-D-glucose (2-DG), which resulted in suppression of energy resources (48).

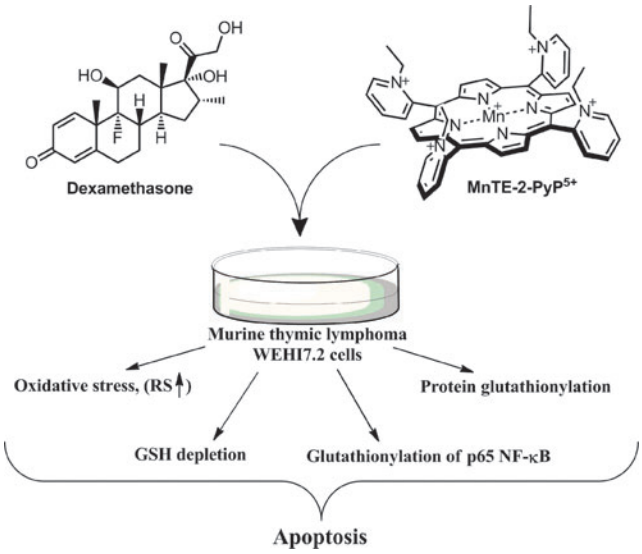

FIG. 16. The chemosensitizing effect of MnE-2-PyP^{5+} in cellular lymphoma study (125). Dexamethasone alone (1 μM) and MnTE-2-PyP^{5+} (50 nM) each increased levels of reactive species, which resulted in glutathionylation of p65 and subsequent suppression of NF-κB DNA binding. The effects are largely enhanced with their co-administration to murine thymic lymphoma WEHI7.2 cells maintained in suspension in DMEM + 10% calf serum. DMEM, Dulbecco's Modified Eagle Medium-low glucose. To see this illustration in color, the reader is referred to the web version of this article at www.liebertpub.com/ars

NF-kB- brain tumor. In an MnP/radiation study of nude/nude Balb/c sc xenograft mouse study of pediatric D-341-MED medulloblastoma, the preliminary data show the effect on NF-κB pathways (see under Therapeutic effects section; cancer studies).

Will pro-oxidative action of MnP promote oxidation or prevent oxidation of biological targets? Our data imply that, while the reactions of MnP are likely identical, the magnitude and the end results of such reactions may be profoundly different in normal *versus* cancer cells, as much as in one *versus* another cancer cell type. Based on our present understanding, the resulting effects of electron shuttling by MnPs may be pro-oxidative rather than antioxidative, and particularly so in cancer cells that are already under the conditions of increased oxidative stress (16). The modes of action, other than antioxidative, have also been speculated for Mn salens (229) and polyphenols, and discussed by Forman *et al.* for natural compunds commonly viewed as antioxidants (16, 107, 108, 260). It may, thus, be concluded that the redox environment of the cell, including the levels and activities of the endogenous antioxidative enzymes, are main factors determinining how the cell will respond to MnP that is, the outcome of the therapy.

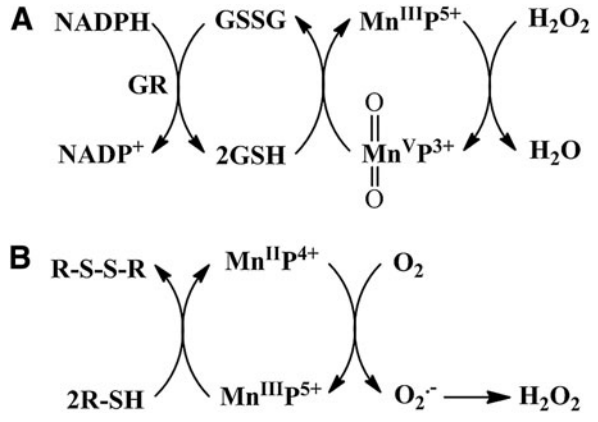

FIG. 17. The glutathione peroxidase (GPx) and thiol oxidase (TO) activities may contribute to the biological actions of MnPs. The proposed GPx-like **(A)** and thiol oxidase **(B)** activities of MnPs. The scheme is proposed based on the aqueous chemistry and experimental data in cellular and animal studies (272).

Bioavailability Studies

Besides the compatibility of their redox properties with biological targets, bioavailability is the second critical property that determines the therapeutic potential of redox-active drugs. Bioavailability refers not only to the drug levels in organs, but also to their ability to reach the appropriate subcellular compartments. The impact of MnP bioavailability on its efficacy has been illustrated with SOD-deficient *E. coli.* The 10-fold lower $k_{cat}(O_2^{\bullet-})$ of a *meta* MnTE-3-PyP^{5+} porphyrin was fully compensated by its 10-fold higher lipophilicity relative to MnTE-2-PyP^{5+}. Consequently, both compounds exerted identical efficacy in allowing SOD-deficient *E. coli* to grow aerobically (139). In *E. coli* and 4T1 mouse breast cancer cellular studies in the presence of ascorbate Mn^{III}P^{5+} was reduced which resulted in a loss of 1+ charge and increase in lipophilicity, and in turn bioavailability (251, 299).

In all bioavailability studies (reported below), chloride salts of MnPs were administered. In all oral bioavailability studies, the water solutions of MnPs were used, except with *Drosophila melanogaster*, where MnPs were dissolved in phosphate-buffered saline (130). The effect of counterion on the MnP bioavailability has not yet been explored.

PK studies

Comprehensive PKs of MnTE-2-PyP^{5+} and MnTnHex-2-PyP^{5+} *via* iv, ip, and oral routes of administration were reported. The LCMS/MS technique was employed to analyze MnP levels in plasma, organs, tumors, and subcellular fragments (288, 299). Figure 18 compares the key properties that affect the therapeutic potential of these MnPs. They exhibit similar redox potency described by the log $k_{cat}(O_2^{\bullet-})$, but are of different lipophilicities and, consequently, bioavailabilities that affect their mouse brain and mouse heart mitochondrial accumulation (Fig. 18) (288).

Regardless of high water solubility and pentacationic charge, these MnPs are orally available. The oral availability (based on plasma AUC_{ORAL}/AUC_{IV}) is similar for all three compounds: 23% for MnTE-2-PyP^{5+}, 21% for MnTnHex-2-PyP^{5+}, and 22% for MnTnBuOE-2-PyP^{5+} (Fig. 19) (288). The oral availability was further substantiated in a model of galactosemia, *Drosophila melanogaster*, developed by Fridovich–Kiel's group (130). Galactosemia is a potentially lethal, autosomal recessive disorder that results from profound deficiency of galactose-P uridylyltransferase (GALT), the middle enzyme in the Leloir pathway of galactose metabolism. While newborns appear healthy, once exposed to milk that contains large amounts of galactose, they undergo devastating demise. At present, no cure exists. The survival of GALT-null mutant was extended for 30%–50% when *Drosophila* was fed with 10 μM MnTE-2-PyP^{5+} and 10 μM MnTnBuOE-2-PyP^{5+}.

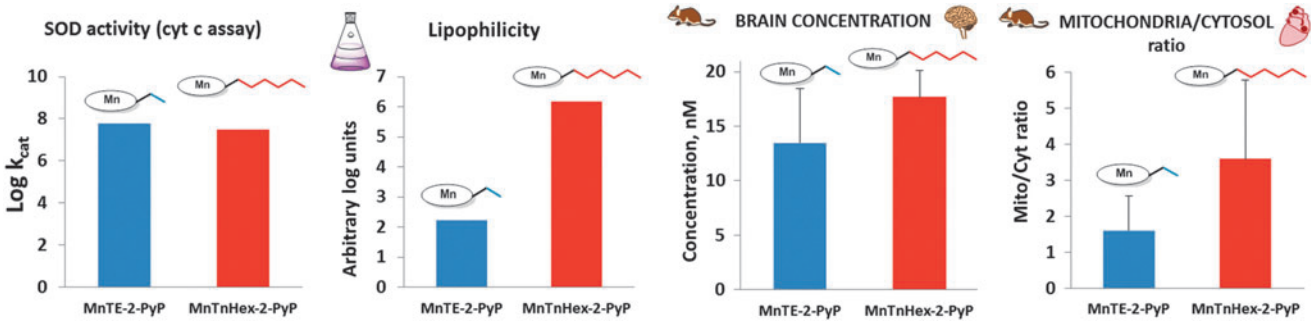

FIG. 18. Comparison of the SOD-like potency, log$k_{cat}(O_2^{\bullet-})$, lipophilicity, and accumulation in mitochondria and brain for two MnPs. MnTE-2-PyP^{5+} and MnTnHex-2-PyP^{5+} have similar redox-based properties, identical charge, and are, thus, among the most potent SOD mimics and peroxynitrite reductants. However, they differ greatly with regard to lipophilicity, bulkiness, and shape. These differences translate into differences in their bioavailability and, in turn, therapeutic potential. In mouse studies, MnPs were given to C57BL6 mice sc for 5 days, twice daily at 2 mg/kg. MnP levels were measured in brain (289) and in heart mitochondria and cytosol at 6 h after the last injection (250, 254). To see this illustration in color, the reader is referred to the web version of this article at www.liebertpub.com/ars

The availability of MnPs in organs when given orally, calculated as AUC_{ORAL}/AUC_{IP}, ranges from 5% (kidney) to 46% (brain) for MnTE-2-PyP^{5+}, and from 12% (heart) to 37% (liver) for MnTnHex-2-PyP^{5+} (Fig. 20). The AUC values for liver, heart, and spleen are higher for MnTnHex-2-PyP^{5+} than for MnTE-2-PyP^{5+} (and quite comparable for other organs) despite a fivefold lower dose, clearly demonstrating the better tissue penetration and tissue retention of a more lipophilic MnTnHex-2-PyP^{5+} (Fig. 20). We have also performed a dose-dependence study *via* an oral route (single dose administration) and showed that at higher doses, both MnPs exert toxicity in mice; they are well tolerated at ~2 mg/kg for MnTnHex-2-PyP^{5+} and ~10 mg/kg for MnTE-2-PyP^{5+} (288).

Mitochondrial availability

Factors that govern mitochondrial distribution relative to cytosol are cationic charge and lipophilicity (177). In a mouse study, both MnTE-2-PyP^{5+} and MnTnHex-2-PyP^{5+} prefer to accumulate in heart mitochondria relative to cytosol (5 days sc twice daily 2 mg/kg) (Fig. 18), which is in agreement with their beneficial effects demonstrated in animal models of mitochondrial disorders and ascribed to mimicking of MnSOD (177). The ratio of mitochondria/cytosol distribution for more lipophilic MnTnHex-2-PyP^{5+} is 3.6, while for hydrophilic MnTE-2-PyP^{5+}, it is 1.6 (289) (Fig. 18). The accumulation of MnTnBuOE-2-PyP^{5+} in mitochondria relative to cytosol is similar to MnTnHex-2-PyP^{5+}, likely due to their similar lipophilicity (Spasojevic *et al.*, unpublished). Our data obtained by LCMS/MS agree with synchrotron-radiation-induced-X-ray emission studies of MnTE-2-PyP^{5+} and MnTnHex-2-PyP^{5+} (3).

Brain availability

The trend in mouse brain distribution (5 days sc twice daily 2 mg/kg) of 13 and 18 n*M* for MnTE-2-PyP^{5+} and MnTnHex-2-PyP^{5+} (MnTnHex-2-PyP^{5+}/MnTE-2-PyP^{5+} = 1.4) is in good agreement with their mouse heart mitochondrial distribution (MnTnHex-2-PyP^{5+}/MnTE-2-PyP^{5+} = 3.6/1.6 = 2.2) (Fig. 18) (288, 289). For the purpose of comparison, we averaged their organ oral availability (expressed as AUC_{oral}/AUC_{ip}, where AUC_{ip}/AUC_{iv} is 83–84% for both compounds) (288). The ratio of AUC_{oral}/AUC_{ip} values for several major organs for MnTnHex-2-PyP^{5+} and MnTE-2-PyP^{5+} was calculated to be (33%)/(13%) = 2.2. The similar ratios of these two MnPs in

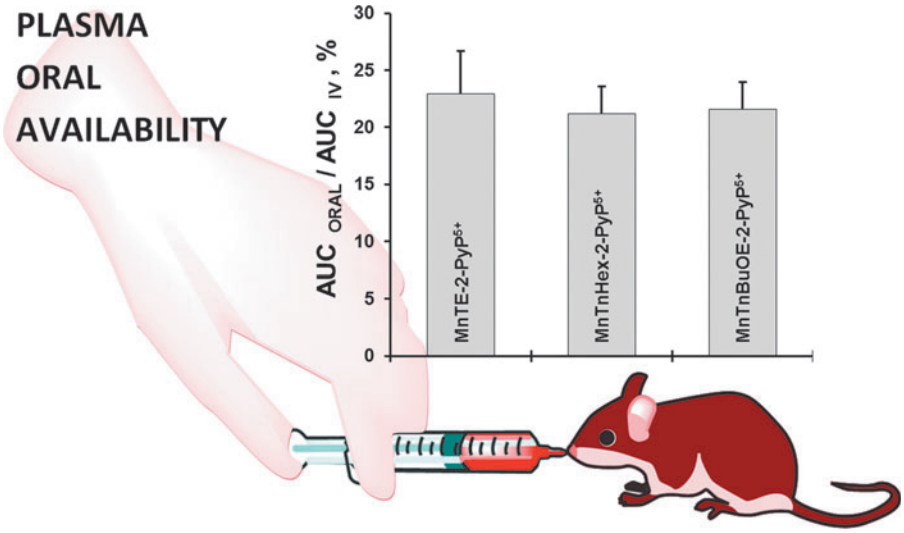

FIG. 19. Plasma oral availability of three water-soluble but differently hydrophilic Mn(III) *N*-substituted pyridylporphyrins, MnTE-2-PyP^{5+}, MnTnHex-2-PyP^{5+}, and MnTnBuOE-2-PyP^{5+}. The unpublished data (Spasojevic *et al.*) for MnTnBuOE-2-PyP^{5+} are also shown. The data for MnTE-2-PyP^{5+} and MnTnHex-2-PyP^{5+} are from Ref. (288). To see this illustration in color, the reader is referred to the web version of this article at www.liebertpub.com/ars

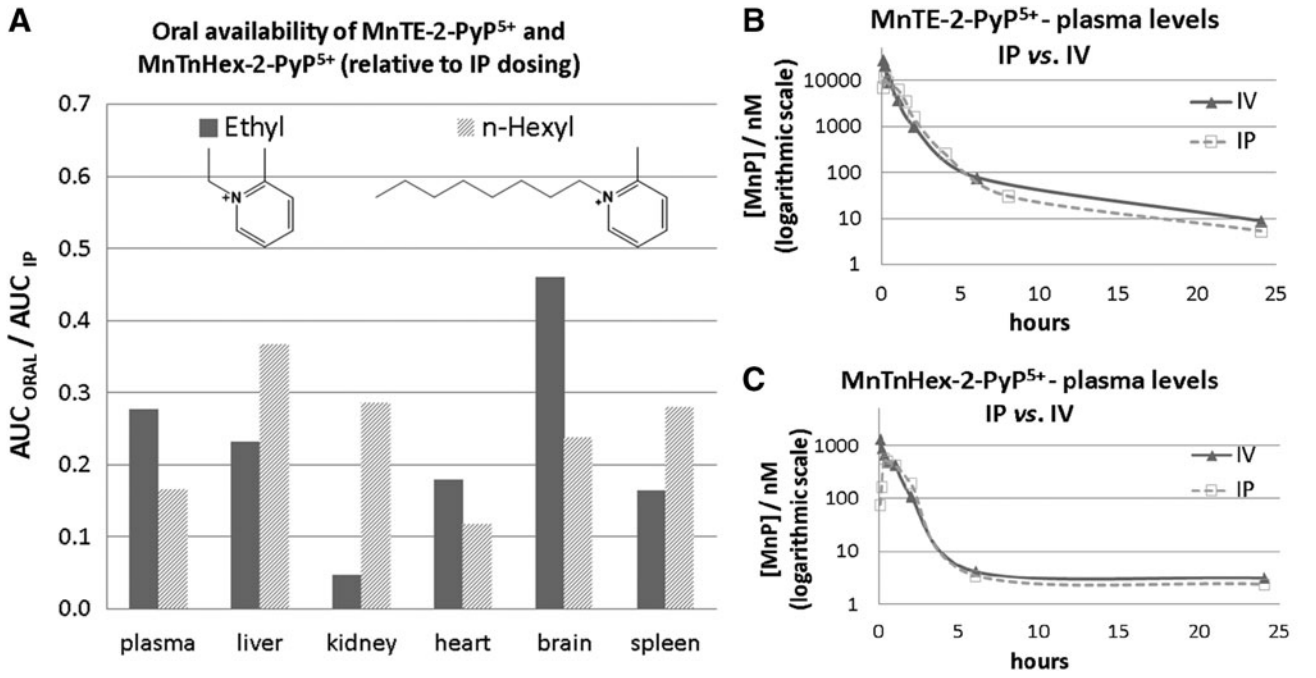

FIG. 20. Organ oral availability of two water-soluble, differently hydrophilic Mn(III) *N*-alkylpyridylporphyrins, MnTE-2-PyP^{5+} and MnTnHex-2-PyP^{5+}. (A) The AUC_{IP} was taken as 100% (1 unit). The plasma, liver, kidney, heart, brain, and spleen AUC_{ORAL}/AUC_{IP} values for MnTE-2-PyP^{5+} and MnTnHex-2-PyP^{5+}. MnTE-2-PyP^{5+} was given orally at 10 mg/kg, while MnTnHex-2-PyP^{5+} at 2 mg/kg. The plasma AUC_{IP} was found to be **(B)** 83% of AUC_{IV} for MnTE-2-PyP^{5+} and **(C)** 84% for MnTnHex-2-PyP^{5+}. At a 5-fold dose difference, the average distribution of drug in organs is either similar or higher with hexyl than with ethyl species (288). Only pyridyl substituents at *meso* positions of porphyrin ring are shown.

mouse heart mitochondria (1.4), brain (2.2), and all organs (2.2) strengthen the conclusion on the large impact of lipophilicity on their biodistribution.

Tumor availability

The fivefold higher levels of MnTnHex-2-PyP^{5+} were found in a tumor (4T1 mouse breast cancer sc xenograft study) than in normal muscle extracted from the opposite leg (299) (Fig. 21B). MnPs bear potential as MR imaging agents (183). In agreement with a 4T1 mouse tumor study, the MRI mouse prostate tumor study shows that MnTE-2-PyP^{5+} accumulated almost exclusively in tumor and not in a surrounding tissue (Fig. 21A).

Comprehensive PK studies of redox-active compounds are rare (217). No reported PK data on Mn salen derivatives and Mn cyclic polyamines exist. The ip accumulation studies were performed with anionic Ga corrole; the drug reaches brain

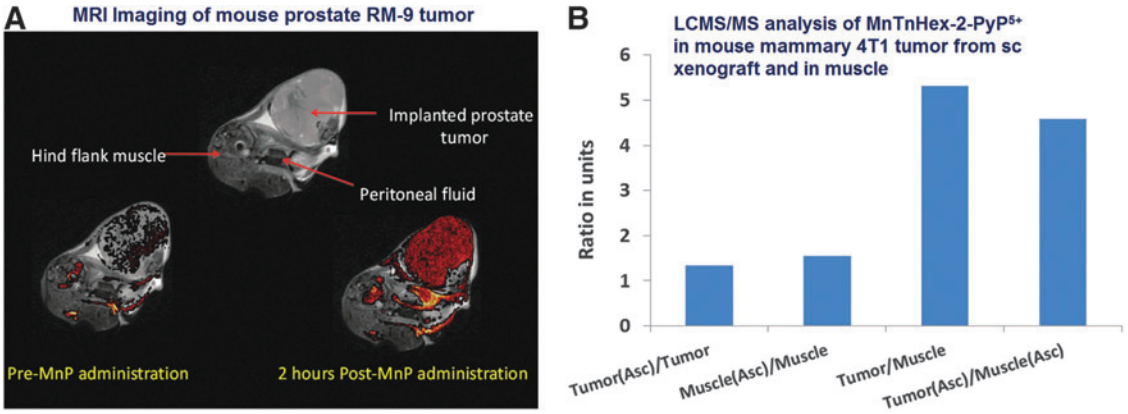

FIG. 21. Differential accumulation of MnPs in tumor and normal tissue. (A) T2-weighted image of prostate cancer with hind flank muscle (Top) of C57Bl mice. Overlay of T1-weighted image over T2-weighted image (*Bottom-Left*, predose and *Bottom-Right*, post ip) shows contrast enhancement within the tumor (*in vivo* RM-9 model) after 8 mg/kg ip administration of MnTE-2-PyP^{5+} (183). **(B)** The accumulation of MnTnHex-2-PyP^{5+} measured by LCMS/MS in 4T1 breast cancer sc xenograft tumor and in the muscle from the opposite leg when MnP was given as a single agent (twice daily sc at 1 mg/kg), or in the presence of ascorbate (twice daily ip at 2 g/kg for the duration of study) (299). Ascorbate did not affect MnP accumulation. LCMS, liquid chromatography-tandem mass spectrometry.

vessels but does not cross BBB (197). Due to the low total charge, the Fe corrole, derivatized with three *meso* pentaflurophenyl groups and two slufonatopyrrolic substituents, is orally efficacious; however, related PK studies are not available (105). Due to the dianionic charge, it does not cross BBB (105, 197).

Toxicity

The subcutaneous route of administration appears to be the least toxic for MnPs while affording the highest body exposure (AUC) (288). The single TD_{50} (the dose toxic to 50% of mice) determined for such a route is 91.5 mg/kg for MnTE-2-PyP^{5+} and 12.5 mg/kg for MnTnHex-2-PyP^{5+} (210). Given the up to 120-fold higher efficacy of MnTnHex-2-PyP^{5+} *versus* MnTE-2-PyP^{5+} in animal studies, the therapeutic window for the former is superior to the latter (28, 210). A single maximal tolerated dose *via* oral route was found to be $\sim$10 mg for MnTE-2-PyP^{5+}, and $\sim$2 mg/kg MnTnHex-2-PyP^{5+} (288).

The first lead drug candidate of Mn(III) *N*-substituted pyridylporphyrins was MnTE-2-PyP^{5+} (AEOL10113, BMX-010) and has been GMP scaled up and Drug Master File filed. A full GLP nonclinical assessment was conducted in order to evaluate the safety of MnTE-2-PyP^{5+} (92). The safety evaluation included *in vitro* genotoxicity studies (Bacterial Reverse Mutation Assay, mammalian chromosome aberration test using Chinese hamster ovary cells), hemolysis, flocculation, safety pharmacology (*in vitro* hERG, respiratory and CNS in mice, and cardiovascular in monkeys), venous irritation in rabbits, and iv toxicity in mice (single dose, five-day, and 28-day) and monkeys (single dose, 5-day, and 14-day). MnTE-2-PyP^{5+} was not genotoxic or hemolytic, did not cause flocculation or elicit adverse pharmacologic effects on respiration, the central nervous system, or the cardiovascular system. The intended iv clinical solution did not cause venous irritation in rabbits. The NOAEL [No observable (toxic) effect level)] in mice after 28 days of dosing was 10 mg/kg. The NOAEL in monkeys after 14 days of iv dosing was 5 mg/kg. Based on the results of these studies, a conservative safe initial starting clinical dose of 5.0 mg (0.083 mg/kg in a 60 kg adult) is proposed for human trials. Due to patient life issues, the use of MnTE-2-PyP^{5+} as a transplantation aid was not pursued past the preclinical stages (92).

The 2nd lead in the class of Mn(III) *N*-substituted pyridylporphyrins, MnTnBuOE-2-PyP^{5+} is also GMP scaled up. The safety evaluation on mice and monkeys is in progress.

The lead compound in the class of *N,N'*-di-*ortho* substituted imidazolylporphyrins, MnTDE-2-ImP^{5+} was in phase I clinical Trials on ALS (198) and was well tolerated. The limited PKs has been reported (174). It is currently in development as a radioprotector by Aeolus Pharmaceuticals and supported in large part by Federal funds.

Therapeutic Effects

Introduction

Among the most striking therapeutic effects reported thus far is the effect of MnTE-2-PyP^{5+} in a rat spinal cord injury model, where 1 mg/kg/day given subcutaneously for a week after T10 injury (starting 30 min after T10 crush) resulted in a remarkable near-full recovery of rat limb function. The data are discussed with regard to inhibition of NF-κB activation (204). In a rat stroke model, the efficacy of MnTnHex-2-PyP^{5+} is at least in part due to the inhibition of NF-κB (238)]. It seems that in many models of diseases the activation of the master transcription factor, NF-κB, which controls inflammatory and immune pathways, is implicated. A very similar effect on rat spinal cord injury was observed with estrogen and is supposedly orchestrated *via* glucocorticoid receptor (67, 110, 129, 185, 243). A significant association between testosterone level and severity of SCI has been reported (79, 83). Since males greatly outnumber females in serious spinal cord injuries, it is unlikely that estrogen will be accepted as a treatment. The prevalence of testosterone deficiency was significantly greater in participants with complete motor dysfunction compared with those with less severe injuries (79, 83). Significant reduction in neuropathic pain and complete inhibition of chronic morphine tolerance were exerted by MnTE-2-PyP^{5+} and MnTnHex-2-PyP^{5+} (24, 76). Remarkable data were also obtained in a prostate radioprotection study, where the effect on complete reversal of erectile dysfunction and prevention of testes shrinkage was observed (100, 164, 165). Near-full elimination of papillomas was reported in a mouse skin carcinogenesis model when 5 ng MnTE-2-PyP^{5+} was applied on skin for 14 weeks at 4 days per week (304). All existing studies of cancer, radiation, and radiosensitization are listed in Tables 2 and 3; while possible mechanisms are discussed under reactivity toward signaling proteins section and next. The effects of MPs on central nervous system injuries are summarized by Warner *et al.*, and their effects on inflammation and autoimmunity by Delmastro-Greenwood *et al.* in this Forum (208a). Next, we show some of the data related to the radioprotective and radiosensitizing effects of MnPs. We have chosen to include other redox-active drugs also, though some may be neither true SOD mimics (catalysts of $O_2^{\bullet -}$ dismutation) nor $O_2^{\bullet -}$ scavengers. The reason is that the observed effects are frequently similar to the effects of true SOD mimics. The most recent example is the study reported at 2012 Annual Meeting of the Society of Free Radical Biology Medicine from Kalyanaraman's group on the effect of nitroxide Mito-CP on cancer cell bioenergetics (48). The results resemble those observed with MnPs by Tome's group (124). Finally, we discuss in detail only those cancer studies that have not been covered in our earlier reviews (26–28, 208a, 236, 270). The anticancer research is becoming increasingly important and prevalent due to (i) the increase in aging population, and, thus, the number of cancer patients; and (ii) the lack of anticancer drugs, which is at least in part due to the ability of cancer cells to mutate and become resistant to therapy. Thus far, we have tested them in animal models of lymphoma, leukemia, skin, brain, breast, prostate, and head and neck cancer studies.

Radioprotection studies

Pulmonary studies. In a rat pulmonary radioprotection study, 6 mg/kg MnTE-2-PyP^{5+} normalized breathing rate frequencies, as well as suppressed HIF-1α pathways and its gene VEGF when the two-week-long sc administration started at different time points between 2 h and 8 weeks after radiation. MnTnHex-2-PyP^{5+} was radioprotective also and at as low a dose as 0.05 mg/kg/day; the sc dosing started at 2 h after radiation and lasted for 2 weeks (95, 96). A significant decrease in HIF-1α, TGF-β, and VEGF A, as well as an overall reduction in lung damage (histopathology), was observed in

Table 2. Anticancer Effects of Redox-Active Compounds

Model	*Combinations*	*Redox compound*	*Dose, multiplicity*	*Animal/cells*	*References*
Porphyrins					
Skin		MnTE-2-PyP^{5+}	5 ng/day, m	Mouse	(304)
Breast		MnTE-2-PyP^{5+}	15 mg/kg/day, m	Mouse	(213)
B16F10 melanoma	Hyperthermia	MnTE-2-PyP^{5+}	5 mg/kg/day, m	Mouse	(121)
D 245-MC glioma	Chemotherapy (temozolomide, 5 mg/kg/day, 5 days) Radiation (1 Gy/day, 3 days) Chemotherapy (temozolomide, 5 mg/kg/day, 5 days) + radiation (1 Gy/day, 3 days)	MnTnHex-2-PyP^{5+}, MnTnBuOE-2-PyP^{5+}	2 × 1.6 mg/kg/day, m	Mouse	(21, 22)
Lymphoma WEHI7.2	Chemotherapy (dexamethasone)	MnTE-2-PyP^{5+}	50 n*M*	Murine cell	(127)
4T1 breast tumor	Chemotherapy (ascorbate, 2 g/kg/day, 5 days)	MnTnHex-2-PyP^{5+}	2 × 1 mg/kg/day, m	Mouse	(299)
Prostate cancer	Radiation (10 Gy)	MnTE-2-PyP^{5+}	6 mg/kg/day, m	Mouse	(164, 165)
		MnTDE-2-ImP^{5+}	6 mg/kg/day, m	Mouse	(100)
Mn salens					
Cells		EUK-189	μM solution	Cell	(6)
Nitrones					
rat C6 glioma		phenyl-tert-butylnitrone (PBN)	75 mg/kg/day, drinking water, m	Rat	(72)
rat C6 glioma		2,4-disulfophenyl-PBN (NXY-059)	10 mg/kg/day, drinking water, m	Rat	(94)
APC$^{min/+}$ mouse model of colorectal cancer		phenyl-tert-butylnitrone (PBN)	100 mg/kg/day, drinking water, m	Mouse	(88)
Nitroxides					
human glioblastoma U87MG and U373MG cell lines	Chemotherapy (temozolomide, 5–300 μM)	Tempol	0.5, 1 or 2 m*M*	Cell	(219)
Prostate cancer			10 mg/g diet	Mouse	(266)
Pancreatic cancer		Mito-CP		Cell	(48)
Corroles					
MDA-MB-231 (breast), SK-MEL-28 (melanoma), OVCAR-3 (ovarian) cells		MnDiM-4-PyMAn-Corrole^{2+}	30 μM	Cells	(154)
Natural antioxidants, polyphenols					
Murine colon carcinoma	Radiation (8 Gy)	Honokiol	0.3 mg/mouse, m	Mouse	(143)
Colorectal cancer cells	Radiation (2.5 Gy)		25 μM	Cell	(112)
Dalton's lymphoma		Curcumin	50–150 mg/kg/day, m	Mouse	(63)
Skin carcinogenes			1% curcumin diet	Mouse	(155)
Human ovarian carcinoma cell lines	Chemotherapy (cisplatin) Radiation (2–8 Gy)		10 or 20 μM 2–8 μM	Cell	(298)

Data relate to Mn porphyrins as monotherapy and to their combination with other agents and radiation. In addition, data for some of the other redox-active compounds most frequently studied, natural and synthetic, are listed.
Mito-CP, Mito-carboxypropyl; m, multiple dosing.

animals in which MnP treatment started at the time of fully developed lung injury 8 weeks post-IR (96).

In another mouse pulmonary radioprotection study, the forty-four genes associated with metabolism, cell growth, apoptosis, inflammation, oxidative stress, and extracellular matrix synthesis were up-regulated throughout 6 months postradiation (122). The messenger RNA expression of adrenomedulin (Adm), 1-acylglycerol-3-phosphate *O*-acyltransferase 2 (Agpat2), *N*-acetyltransferase ARD 1 homolog (Ard1), connective tissue growth factor (CTGF), Enolase 1, α noneuron (Eno1), HIF-2α, guanine nucleotide binding protein, α11 (Gna11), protein kinase, AMP-activated, α catalytic subunit (Prkaa1), sorbitol dehydrogenase (Sdh1), and tubulin α3 (Tub α 3) were elevated in irradiated animals relative to control. The expression of DNA damage repair (Dr1), fatty acid-binding protein 4 (Fabp4), formin-binding protein 3 (Fnbp3),

Table 3. Radioprotective Effects of Redox-Active Compounds

Model (radioprotection)	*Radiation dose, Gy*	*Redox compound*	*Dose, multiplicity**	*Animal/cell*	*References*
Porphyrins					
Whole body		$MnTE\text{-}2\text{-}PyP^{5+}$		Zebrafish	(150, 152)
	8	$MnTM\text{-}2\text{-}PyP^{5+}$	5 mg/kg/day, m	Mice	(205)
Hematopoietic stem cell	6.5	$MnTE\text{-}2\text{-}PyP^{5+}$	6 mg/kg/day, m		
Lung	15	$MnTDE\text{-}2\text{-}ImP^{5+}$ (AEOL10150)	40 mg/kg/day, s (20 mg/kg/day, m)	Mouse	(122, 302)
	28	$MnTE\text{-}2\text{-}PyP^{5+}$	1–6 mg/kg/day, m	Rat	(95, 96, 211,
		$MnTDE\text{-}2\text{-}ImP^{5+}$	1–30 mg/kg/day, m		212, 286,
	28	$MnTnHex\text{-}2\text{-}PyP^{5+}$	0.3–1.0 mg/kg/day, m 0.05 mg/kg/day, m		297)
	10 Gy	$MnTnHex\text{-}2\text{-}PyP^{5+}$	0.05 mg/kg/day, m	Nonhuman primate	(51)
Prostate	37.5 (in 5 fractions)	$MnTE\text{-}2\text{-}PyP^{5+}$	5 mg/kg/day, m	Rat	(192)
Salivary gland	9–15	$MnTnBuOE\text{-}2\text{-}PyP^{5+}$	2×1.5 mg/kg/day,	Mouse	(13)
Eye	8, 28	$MnTE\text{-}2\text{-}PyP^{5+}$	2.5 μM	Rat	(166)
GI tract—rectum	20–30	$MnTE\text{-}2\text{-}PyP^{5+}$	5 mg/kg, m		(10)
Brain	100	$MnTDE\text{-}2\text{-}ImP^{5+}$	3.4 μg		(206)
Cell	2–20	EUK-451	10 μM	Cell	(210, 285)
	5	$MnTnHex\text{-}2\text{-}PyP^{5+}$	1 μM		
	2	$MnTM\text{-}2\text{-}PyP^{5+}$	5 μM		(149)
Mn salens					
Whole body	7.96 ($LD_{50/30}$ with saline) *vs*. 9.13 ($LD_{50/30}$ with EUK-189)	EUK-189	70 mg/kg, s	Mouse	(255)
Lung	10–20.5		2 or 30 mg/kg/day	Rat	(145)
Lung	10	EUK-207	8 mg/kg/day	Rat	(163)
Lung	10		8 mg/kg/day	Mouse, rat	(115)
Cell	2–20		30 μM	Cell	(285)
Nitroxides					
Radiation-related hair loss	30 (in 10 fractions)	Tempol	100 ml/day (of 70 mg/ml of 70% of ethanol, (topically), m	Human	(175, 246)
Whole body	7.84 ($LD_{50/30}$ with saline) *vs*. 9.97 ($LD_{50/30}$ with Tempol)		275 mg/kg	Mouse	(106, 246)
Salivary gland	30 (6 Gy/day, 5 days)		275 mg/kg	Mouse	(56)
Nitrones					
Cell	0–10 Gy	α-phenyl-N-tert-buty lnitrone (PBN)	10 mM	Cell	(301)
		5,5-dimethyl-1-pyrroline-N-oxide (DMPO)	200 mM		
		α-(4-pyridyl-1-oxide)-N- tert-butylnitrone (POBN)	40 mM		

(*continued*)

Table 3. (Continued)

Model (radioprotection)	*Radiation dose, Gy*	*Redox compound*	*Dose, multiplicity**	*Animal/cell*	*References*
Polyamines					
Radiation-induced mucositis	40	M40403	6–60 mg/kg/day, m	Hamster	(186)
Whole body	6.5, 7.5 or 8.5		40, 30, 20 or 10 mg/kg	Mouse	(266)
Fullerenes					
Whole body	7	$C_{60}(H_2O)_n$, $n = 22–24$ (C_{60}HyFn)	0.1 or 1 mg/kg, s	mouse	(5)
Whole body	20–80	DF-1	100 μM	Zebrafish embrio	(61, 62)
Cell	4		100 μM	Cell	(264)
Whole body	7, 8	$C_{60}(OH)_{24}$	10 or 100 mg/kg	Rat	(274)
Cell	2, 4	Carboxyfullerene (C3)	50 μg/ml	Cell	(156)
Cell	100–2000	$C_{60}(OH)_x$, x = 18–22	0.1 or 0.25 mg/ml	Stylonychia mytilus	(302)
Metal oxide					
Radiation-induced pneumonitis	30 (10 fractions)	CeO_2 (3–5 nm nanoparticles)	0.01 μg/ml, m	Mouse	(53)
GI epithelium	20		0.01 μg/ml, m		(54)
Head and neck	30 (6 fractions)		0.001 or 0.01 μg/ml, m		(160)
Cell	10	CeO_2 (3–5 nm nanoparticles)	10 nM	Cell	(262)
Natural antioxidants, polyphenols					
Lung	~30 (9 fractions, 10 Gy/day)	Genistein	10 mg/kg	Mouse	(201)
Lung	10		18.5–22.5 mg/rat/day, m	Rat	(163)
Whole body	9.5		25–400 mg/day	Mouse	(144)
Whole body	7.75		200 mg/day	Mouse	(68)
Whole body	8.75		200 mg/day	Mouse	(64)
Whole body	7.75		200 mg/day	Mouse	(65)
Whole body	1.15	Curcumin	5–20 mg/kg/day, m	Mouse	(2)
Whole body	2.6		1% curcumin diet	Rat	(120)
Partial body	2 Gy/day (5, 10 or 20 days)		100 mg/day	Mouse	(123)
PE/CA-PJ15 oral squamous cell carcinoma	1, 2.5 or 5		3, 3.75, 4.50 or 5.25 μM	Cell	(158)

*multiplicity; multiple (m), single (s).

and solute carrier family 2, member 1 (Slc2a1) was elevated only at 6 month postradiation. The animals were treated with imidazolium derivative, MnTDE-2-ImP^{5+} (AEOL10150) (Fig. 1) starting at 24 h after 15 Gy whole thorax radiation with sc loading dose of 40 mg/kg, followed by 20 mg/kg (sc) every other day for 4 weeks. The impact of MnTDE-2-ImP^{5+} was evaluated at 6 weeks after radiation. The elevated expression of 31 of these genes was attenuated in animals treated with MnTDE-2-ImP^{5+}, suggesting that expression of a number of hypoxia-associated genes is regulated by early development of oxidative stress after radiation. Such genes are: IL-1 β, TGF- β1, PPAR-α (peroxisome proliferator-activated receptor α), HIF-2β, carbonic anhydrase 12 (Car12), neuroblastoma myc-related oncogene (Nmyc1), cell division cycle 42 homolog (Cdc42), dynactin 2 (Dctn2), death-associated kinase 3 (dapk3), matrix metalloproteinase 14 (MMP14), CTGF, Sdh1, and so on (122). Data substantiated the earlier observation (96) that MnP radioprotects even when its injections started at 24 h after injury.

The impact of MnTDE-2-ImP^{5+} on apoptotic pathways as a consequence of mouse pulmonary irradiation was also explored (Fig. 22) (302). The involvement of oxidative stress was verified *via* observed up-regulation of NOX4 and 8-OHdG, which were increased at 6 weeks after radiation. The apoptosis was observed primarily in type I and II pneumocytes and endothelium. Apoptosis correlated well with increased phosphoinositide 3-phosphatase (PTEN) and transforming growth factor TGF-β1 (excreted by many cells, including macrophages and involved in apoptosis *via* Sma- and Mad-

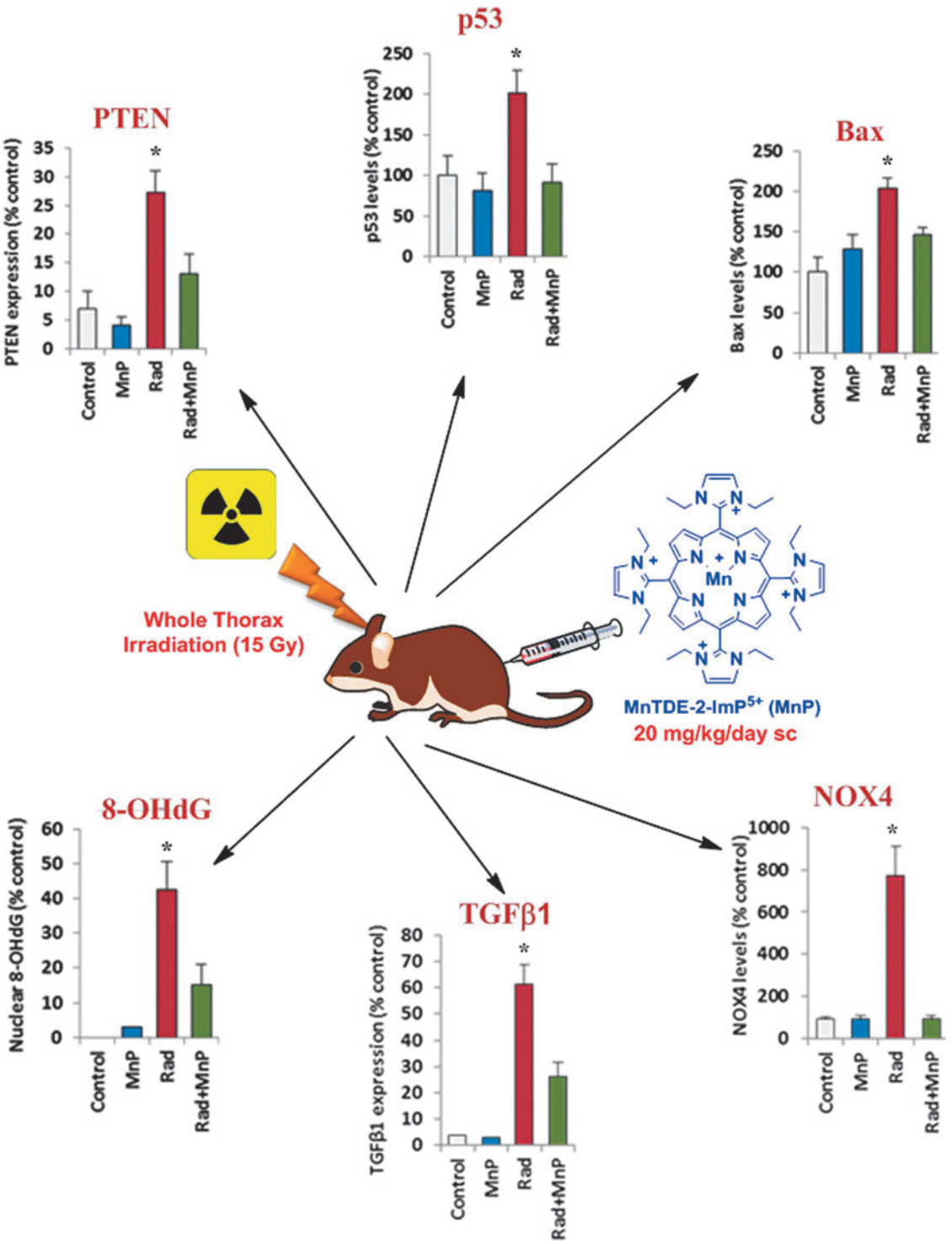

FIG. 22. The effect of MnTDE-2-ImP^{5+} on oxidative stress and, in turn, on PTEN signaling pathways involved in a mouse pulmonary radioprotection. Shown are changes in PTEN signaling as measured by PTEN expression and protein levels obtained by immunostaining; the same finding was supported with Western blotting. Also shown are protein levels of Bax and p53 (western blotting). PI3K-AKT is a key signaling pathway that is negatively regulated by PTEN. Finally, the changes in transforming growth factor expression (TGF)-β1 (by immunostaining), NOX4 expression and protein levels (by immunostaining, and Western blotting), and 8-OHdG levels (by immunostaining) are also presented (302). 8-OHdG, 8-oxo-2′-deoxyguanosine; PTEN, phosphoinositide 3-phosphatase. To see this illustration in color, the reader is referred to the web version of this article at www.liebertpub.com/ars

related proteins), SMAD [SMAD proteins are homologs of both the Drosophila protein, mothers against decapentaplegic (MAD), and the *Caenorhabditis elegans* protein SMA (from gene *sma* for small body size)] and death-associated protein 6 (DAXX transcriptional activities), as well as inhibition of downstream PI3K/AK signaling, and increased p53 and Bax protein levels. MnTDE-2-ImP^{5+} suppressed oxidative stress also and, thus, the pro-apoptotic signaling, which consequently reduced the number of apoptotic cells (Fig. 22) (302).

One study of pulonary radioprotection of *nonhuman primates* has been completed, and the other is in progress. Both studies administer low doses of MnTnHex-2-PyP^{5+}. The treatment with MnP (sc twice daily at 0.05 mg/kg) delayed onset of radiation-induced lung lesions, prevented elevation of respiratory rate, and reduced lung weight, inflammation, edema, and epithelial hyperplasia (50).

Head and neck cancer studies. Significant radioprotection of mouse salivary glands were observed in a C57BL/6 study with MnTnBuOE-2-PyP^{5+} injected sc twice daily at 1.5 mg/kg for the duration of the study, starting one week before radiation (13). The study is a part of head and neck cancer studies (Ashcraft *et al.* in preparation). In preliminary studies, no protection of cancer was observed (Park *et al.*, unpublished).

Hematopoietic studies. MnTE-2-PyP^{5+} protected bone marrow-derived hematopoietic stem cells (HSCs) against sublethal 6.5 Gy total body radiation (TBI) (152, 205). Mice were treated with 6 mg/kg MnTE-2-PyP^{5+} sc at 6 h after radiation and then, every day for 30 days. After treatment, the irradiated mice showed a significant recovery in the frequency and number of HSCs and a dramatic improvement in HSC and function of hematopoietic progenitor cells, HPC. The clonogenic function of HSCs from irradiated mice after MnP treatment was comparable to that of HSCs from normal controls, suggesting that MnP treatment inhibited the induction of HSC senescence by TBI. The effects were attributed to the inhibition of senescence p16 pathways, which is supported by the finding that MnP treatment also reduced the expression of p16Ink4a (p16) mRNA in HSCs induced by TBI and improved the long-term and multilineage engraftment of irradiated HSCs after transplantation (205). The authors reported that the reactive species produced by NADPH oxidases played a critical role.

Protection of erectile dysfunction during prostate radiation. The role of oxidative stress in prostate radiation-caused erectile dysfunction was demonstrated by Koontz group in a rat model (Fig. 23D–F) (136). Irradiated animals (eight to nine per group) received prostate-confined radiation in a single

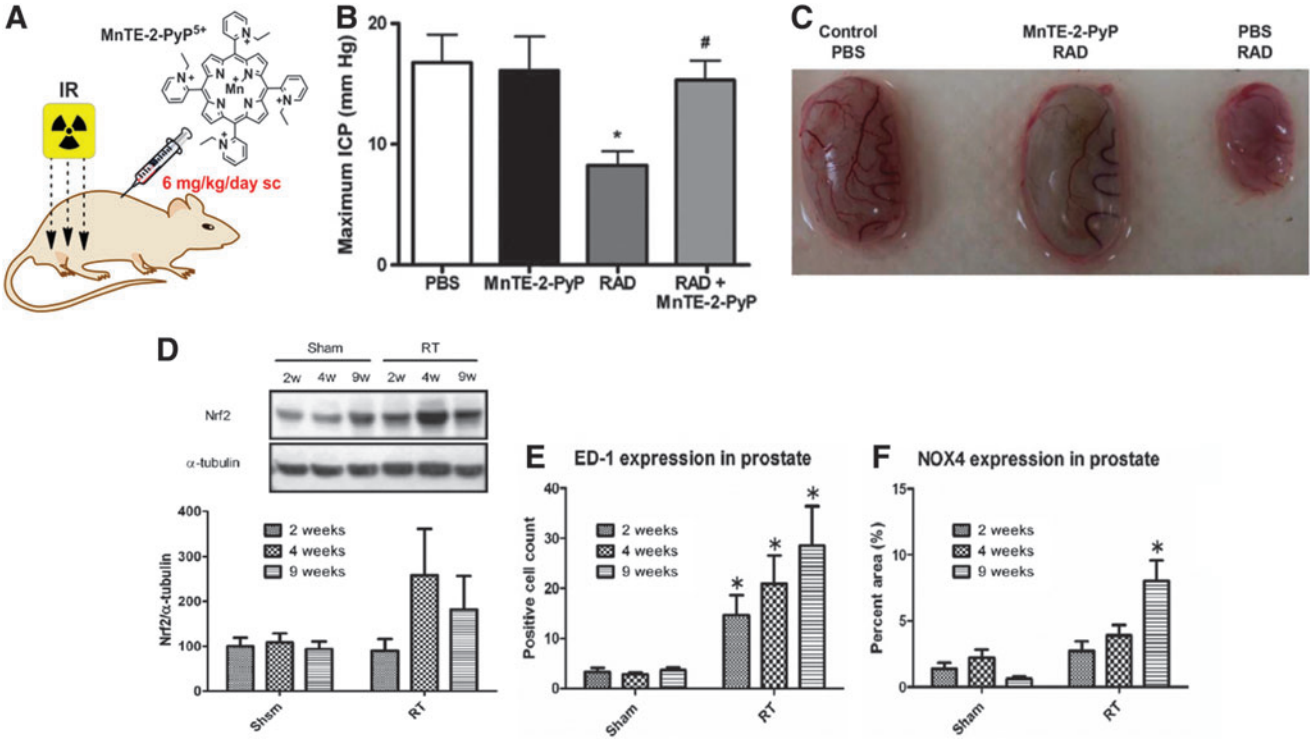

FIG. 23. MnP protects against prostate radiation-induced injury to male reproductive system. The reversal of erectile dysfunction and the reduction in testes shrinkage by MnTE-2-PyP^{5+}, induced after rat prostate radiation **(A–C)** as a consequence of radiation-induced oxidative stress **(D–F)** (192)**.** Intracavernous pressure (ICP) was obtained after cavernous nerve stimulation as a measurement of erectile function 12 weeks postirradiation. Irradiation caused a significant decrease in ICP (RAD group) **(B)** as compared with the nonirradiated group (PBS). MnTE-2-PyP^{5+} protected from the irradiation-induced loss in ICP (MnTE-2-PyP RAD). n = 8 rats/group, "*" denotes a significant difference from PBS group, $p = 0.05$, and "#" denotes a significant difference from RAD group, $p = 0.05$. The MnP also prevented testes shrinkage **(C)**, hair loss (not shown), and the damage to prostate tissue (not shown) (192). The oxidative stress is demonstrated as the increase in NAPDH oxidase expression **(F),** macrophage infiltration (ED-1) **(E),** and Nrf-2 (the primary cellular defense against the cytotoxic effects of oxidative stress) up-regulation **(D)** (136) Nrf-2, nuclear factor-erythroid-derived 2-like 2. To see this illustration in color, the reader is referred to the web version of this article at www.liebertpub.com/ars

20 Gy fraction. Radiation caused a significant decrease in intracavernous pressure and increased expression of NADPH oxidase isoaform 4 (NOX4), DNA damage (8-OHdG), and lipid peroxidation (measured by 4-hydroxynonenal) in prostate tissue and corpora cavernosa accompanied by a trend toward an increase in endogenous antioxidant defense, nuclear factor-erythroid-derived 2-like 2 (Nrf-2) (136).

The MnTE-2-PyP^{5+} fully reversed the erectile dysfunction as a consequence of prostate tumor radiation (Fig. 23) (192). Mice were irradiated for five sequential days at 7.5 Gy/day in a lower pelvic region, which mimics the irradiation scheme of prostate tumor patients. MnP was injected at 5 mg/kg 24 h before starting with radiation and then, 2.5 mg/kg every other day for the next two weeks and 5 mg/kg once a week for 12 weeks postradiation. MnP reduced DNA damage as seen by the decrease in 8-OHdG levels in prostate epithelial cells. It also prevented the ~60% of shrinkage of rat testes due to radiation, and prevented damage of penile tissue. Intracavernous pressure in was obtained after cavernous nerve stimulation as a measurement of erectile function 12 weeks postirradiation. A significant decrease in erectile function was demonstrated as compared with the nonirradiated mice and was greatly attenuated with MnP. The reduction in tissue damage and hair loss by MnP was demonstrated as well.

Is Mn pro-oxidant or antioxidant in radioprotection? While thus far we have understood the radioprotective effects as resulting from scavenging reactive species, rising number of data argue that perhaps mild pro-oxidative action of MnP may predominate. The oxidation of NF-κB (which controls HIF-1α, and its genes) by MnP would prevent excessive inflammation, secondary oxidative stress and result in prevention of extensive oxidative damage of biological targets (208, 209, 236–240, 278). Data on rat kidney ischemia/reperfusion indicate that MnP can also up-regulate endogenous antioxidative defenses (52, 75). Similar findings have been argued by Huang's group (134) and Forman (89) . The action of another class of SOD mimics, cyclic polyamines, is discussed in terms of activation of Nrf-2 *via* oxidation of cysteine of Keap (176). The same is proposed based on the actions of curcumin, resveratrol, diallyl sulfide from garlic by Forman *et al.* (89) . Studies are needed to further substantiate such mechanisms, including the effect of MnP on the activation of the primary cellular defense against the cytotoxic effects of oxidative stress, Nrf-2. Nrf-2 translocates to the nucleus upon oxidative stress and binds there to antioxidant response elements, increasing transcription of those genes (159).

Cancer studies

In several different animal models, MnPs protected normal tissue again radiation; importantly, no protection of tumor tissue was demonstrated. Moreover, MnPs proved to be radio- and chemosensitizers (21, 22). MnTE-2-PyP^{5+} also enhanced hyperthermia in a B16F10 mouse melanoma study (182).

Prostate cancer. A study on the prostate cells evaluated the antitumor potential of MnTE-2-PyP^{5+}. MnP was used in a dose-dependent fashion (1–30 μM). It significantly inhibited the growth of three prostate cancer cells: PC3 (98.2% ± 0.9%), Du145 (94.3% ± 0.7%), and LnCAP (100% ± 0%). MnTE-2-PyP^{5+} further reduced the growth of tumor cells when co-administered with radiation (5 Gy), but did not inhibit the proliferation of the prostate tumor cells. However, MnP significantly inhibited the invasiveness of PC3 cells on matrigel (67% ± 3.1%) and significantly inhibited Du145 cells (56.7% ± 5.6%) ability to migrate across a filter. MnTE-2-PyP^{5+} reduced NF-κB activity, which may inhibit tumor colony formation. It further reduced the phosphorylation of the focal adhesion kinase (involved in breaking down the extracellular matrix to allow cells to migrate), and VEGF-A in hypoxic prostate cells. VEGF-A is another protein of VEGF family that is involved in the growth migration of tumor cells (287).

Breast cancer. Significant radiosensitization *via* HIF-1α suppression and, in turn, vastly reduced vascular density exhibited by MnTE-2-PyP^{5+} was demonstrated in a 4T1 mouse breast cancer sc xenograft study (180). The MnTE-2-PyP^{5+} exerted an anticancer effect as a single agent at a high (but not at low dose of 2 × 1 mg/kg/day) dose of 2 × 7.5 mg/kg/day for the duration of the study. Strong suppression of oxidative stress and angiogenesis (reduced NADPH oxidase expression, HIF-1α, VEGFR, macrophage infiltration, and protein nitration) was demonstrated (Fig. 15) (213).

Brain tumor—MnP-driven radiosensitization. Recently, a brain tumor study was conducted on sc xenografts of glioblastoma multiforme D-245 MG (eight mice per group). Similarly, lipophilic and redox-active drugs, MnTnHex-2-PyP^{5+} (shown in Fig. 2) and MnTnBuOE-2-PyP^{5+} exert similar radio- and temozolomide-sensitizing effects (21, 22). Tumor growth was delayed for ~12 days as a result of MnP impact on radiation and temozolomide and in both of these treatments combined (Fig. 24). The significance in tumor growth delay with MnP/radiation therapy of pediatric medulloblastoma D-341 MED cell line (in a sc xenograft Balb/c nude/nude mouse was not reached under single conditions

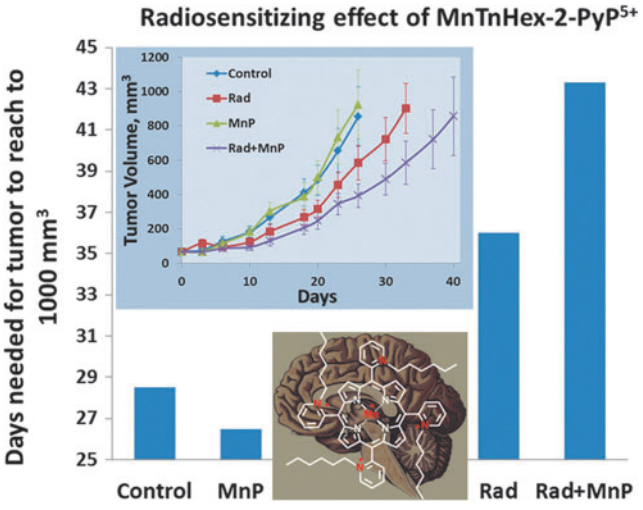

FIG. 24. The radiosensitizing effect of a lipophilic MnTnHex-2-PyP^{5+} in a sc xenograft nu/nu mouse Balb/c D 245-MG glioblastoma multiform model (21, 22). The mice (8/group) were treated twice daily via sc injections of 1.6 mg/kg of MnP (starting at 24 h before radiation and continued during the duration of the study), or 1 Gy radiation (3 days 1 Gy per day) and their combination. To see this illustration in color, the reader is referred to the web version of this article at www.liebertpub.com/ars

tested. However, the metastatic pathways (*ctss*, catepsin L, *becn1*, and beclin1) were largely down-regulated, as were antiapoptotic and NF-κB pathways (*Nfkb1*, *Bcl211*, and *Bcl2*) and PI3kinase and mTOR (*Rsp6kb1*). The protein translation changes were also implicated (*EIF5b* and *Rsp6kb1*)(22). The data are in agreement with the data on NF-κB inhibition by MnP obtained with a number of other models (see also under Reactivity towards signaling proteins section).

Lymphoma. As discussed under Reactivity toward signaling proteins section, MnTE-2-PyP^{5+} enhanced corticosteroid (dexamethasone) therapy in a lymphoma cellular study *via* NF-κB pathways (Fig. 11) (125). The most recent study indicates that MnP additionally inactivates complexes I and III of mitochondrial electron transport chain, suppressing largely mitochondrial ATP production (123). MnP also suppresses glycolysis in its own right and when combined with glycolysis inhibitor 2-deoxyglucose (124); in turn, energy production of the cell seems to be greatly suppressed by the action of MnP (123).

Head and neck cancer. Preliminary data indicate the radiosensitizing effect of MnP, MnTnBuOE-2-PyP^{5+} in head and neck mouse sc xenograft study, which along with its ability to protect salivary glands and oral mucosis indicates its high therapeutic potential (13) (Ashcraft *et al.*, in preparation).

Skin cancer. The anticancer effects of MnP as a single anticancer agent were previously reported in skin carcinogenesis model (304). See also under Reactivity towards signaling proteins section; Cancer studies. Please see Holley *et al.* contribution in this Forum, which suggests that the pharmacological intervention by an MnSOD mimic, MnTnBuOE-2-PyP^{5+}, may play an important role in prevention of aberrant cell signaling that may contribute to carcinogenesis (117).

As discussed under *Reactivity towards cellular reactants*, the MnP is a promising anticancer agent in combination with ascorbate. Such a system, very similar to radiation therapy, is a source of cytotoxic H_2O_2 that MnP employs to oxidize a variety of biological targets (Tovmasyan *et al.*, unpublished). Under certain conditions, such as in pediatric tumors, radiation should be avoided and could be potentially replaced with MnP/ascorbate. Related studies are still at cellular stage, and exploration of optimal ratio MnP/ascorbate is required as well as a thorough insight into the redox status of the each targeted cancer cell line. Another cycling system employing ascorbate is ascorbate/menadione combination, which is already in clinics for the treatment of prostate cancer (262, 284).

Is MnP acting as an oxidant or antioxidant in cancer? Present lymphoma data clearly suggest that in the presence of H_2O_2 (produced synergistically by dexamethasone and MnP) and GSH, the MnP glutathionylates p65 of NF-κB and, thus, suppresses anti-apoptotic pathways (125, 127). These data, along with the data showing (i) that MnP/dexamethasone inactivates complexes I and III of mitochondrial respiration and, in turn, ATP production (124, 125), (ii) reduces cytosolic ATP production in glycolysis (124), and (iii) suppresses aerobic glycolysis *via* suppression of pathways involved in Wartburg effect (70), offer substantial proof of high anticancer pro-oxidative potential of MnP in an appropriate redox environment of excessive oxidative stress. Suppression of NF-κB pathway, when MnP was given along with radiation, was seen in a nude/nude Balb/c mouse sc xenograft study of D341-MED pediatric medulloblastoma. Similar to lymphoma, the radiation was the source of H_2O_2 in MnP/radiation studies (16, 231). In cellular studies, the MnP/ascorbate system was the source of cytotoxic H_2O_2 (25, 82, 299). Cancer cells produce abnormal levels of reducing equivalents that are necessary for proliferation and for maintenance of appropriate (cell-type dependent) levels of RS to prevent cell apoptosis and cell death but induce genomic instability (16). During cancer progression, its oxidative status increases and imparts the neighboring and distant normal tissue (16). Thus, even with no source of H_2O_2 added, cancer is under increased levels of H_2O_2 relative to normal tissue, supporting the likelihood of pro-oxidative action of MnP. Finally, the magnitude of the anticancer effect would be also highly dependent on the type of cancer cell, that is, its redox environment, which may differ largely from cell to cell.

Concluding Remarks

Being a true and very efficacious SOD mimic does not in itself mean that a drug will eventually be an excellent therapeutic. Bioavailability and low toxicity are other critical parameters that will determine its *in vivo* efficacy and therapeutic potential. However, the animal efficacy studies of cationic Mn and FePs, with $E_{1/2} \sim +300$ mV *versus* NHE, undoubtedly, show that those compounds of high SOD-like activity have the ability to readily shuttle electrons between their metal sites and a variety of biological targets (reactive species, proteins, lipid, nucleic acids, *etc.*), which, in turn, normalize cellular metabolism and, thus, have high prospects to become therapeutics. The high accumulation of cationic MPs in mitochondria and transport across BBB further contributes to their remarkable efficacy. Any efficacious SOD mimic is also an efficacious scavenger of peroxynitrite as well as of many other RS (such as hypochlorite, lipid radicals, $^{\bullet}NO$, $CO_3^{\bullet -}$, *etc.*). However, even compounds, which are not true and potent SOD mimics, and are not even very biocompatible redox-active drugs, scavenge a wide variety of highly oxidizing species ($ONOO^-$, ClO^-, lipid radicals, etc.), and if localized at critical cellular sites, may still be effective modulators of cellular redox status. The sum of bioavailability, redox compatibility with biological targets, and toxicity of MnPs, as well as the cellular redox environment would determine their final therapeutic potential.

Based on all said, it is more correct to describe SOD mimics as modulators of cellular redox environment (cellular signaling pathways or redoxome), or promoters/catalysts of processes already in place—rather than antioxidants. Years ago, we had assigned the therapeutic effects observed entirely to the MnP-driven removal of reactive species (in particular $O_2^{\bullet -}$ in accord with H_2O_2 removal) and, thus, to their antioxidant actions. Rising evidence, however, points to the prevailing pro-oxidative mechanism of action, even in normal cells, with final antioxidative therapeutic effects. Such effects may originate from (i) the inhibition of pro-inflammatory, antiapoptotic NF-κB-based pathways *via* oxidation of thiols of NF-κB subunits; and (ii) adaptive responses to MnP-driven increase in oxidative stress, with subsequent up-regulation of endogenous antioxidative defenses. In cancer in particular, the pro-oxidative action, *via* NF-kB pathway, may predominate, leading to cancer cell death; further studies in different models and on different cancer cell types are needed to gain

thorough insights into the biological pathways of MnPs and other redox-active compounds.

The prediction, the anti-(normal tissue) or pro-oxidative (cancer) therapeutic outcome of MnP, would have higher chances to be correct if it is based on the knowledge of the expression and the activities of enzymes that control the cellular redox environment of a cell type of interest (redoxome, or, as Forman *et al.* (89) put it "nucleophilic–electron-rich- tone" of the cell): catalases, SODs, glutathione peroxidases, glutathione reductases, glutathione transferases, peroxyredoxins, thioredoxins, and so on. The redoxome may differ largely from one cancer cell to another, which would greatly affect the magnitude of the therapeutic effect. While a drug may reach clinics without full knowledge of its whereabouts, the mechanistic studies are critical for understanding the biology of diseases, which, in turn, would favorably affect drug development. While the tools are often available to track the pathways modified by the action of SOD mimics, the identification of the sources of modification is more challenging. Given the complexity of cells and the rich chemistry of SOD mimics, we are still far from comprehending the *in vivo* whereabouts of SOD mimics.

Acknowledgments

The authors are grateful to numerous researchers who have worked for years on *in vitro* and *in vivo* models of oxidative stress and help them revise their development strategies and keep them motivated. They are particularly thankful to those who made them believe that scientists of the highest integrity, kindness, and humbleness still exist; to mention the few who cross their pathways: Daret St. Clair, Margaret Tome, Jon Piganelli, Huaxin Sheng, David S. Warner, Judith Fridovich-Keihl, and Kam Leong. They are thankful to Garry Buettner for the useful information on the therapeutic potential of ascorbate in just completed Phase I Clinical Trials. As always, they are lucky to just step down the corridor to discuss many topics and confirm the correctness of their thoughts with Irwin Fridovich. They appreciate the financial support from Duke University's CTSA grant 1 UL 1 RR024128-01 from NCRR/NIH (AT, IBH, IS), W.H. Coulter Translational Partners Grant Program (IBH, IS, AT), and NIH/NCI Duke Comprehensive Cancer Center Core Grant (5-P30-CA14236-29) (IS), NIH U19AI067798 (ZV, IBH, IS, AT), and IBH general research funds (AT).

Author Disclosure Statement

Both Drs. Batinic-Haberle and Spasojevic are consultants for BioMimetix Pharmaceutical, Inc. Duke University, and Drs. Batinic-Haberle and Spasojevic also have patent rights and have licensed technology to BioMimetix Pharmaceutical, Inc. related to this technology.

References

1. Abashkin YG and Burt SK. (salen)MnIII compounds as nonpeptidyl mimics of catalase. Mechanism-based tuning of catalase activity: a theoretical study. *Inorg Chem* 44: 1425–1432, 2005.
2. Abraham SK, Sarma L, and Kesavan PC. Protective effects of chlorogenic acid, curcumin and beta-carotene against gamma-radiation-induced *in vivo* chromosomal damage. *Mutat Res* 303: 109–112, 1993.
3. Aitken JB, Shearer EL, Giles NM, Lai B, Vogt S, Reboucas JS, Batinic-Haberle I, Lay PA, and Giles GI. Intracellular targeting and pharmacological activity of the superoxide dismutase mimics MnTE-2-PyP5+ and MnTnHex-2-PyP5+ regulated by their porphyrin ring substituents. *Inorg Chem* 52: 4121–4123, 2013.
4. Allen BG, Sibenaller ZA, Cullen JJ, Buettner GR, Welsh JJ, Wagner BA, van't Erve TJ, Buatti JM, Carlisle TL, Smith MC, Walsh SA, Bayouth JE, TenNapel M, and Spitz DR. Pharmacological ascorbate enhances chemo-radio-sensitization in brain and lung cancer. *Free Radic Biol Med* 53: S39, 2012.
5. Andrievsky GV, Bruskov VI, Tykhomyrov AA, and Gudkov SV. Peculiarities of the antioxidant and radioprotective effects of hydrated C60 fullerene nanostuctures *in vitro* and *in vivo*. *Free Radic Biol Med* 47: 786–793, 2009.
6. Ansari KI, Kasiri S, Grant JD, and Mandal SS. Apoptosis and anti-tumour activities of manganese(III)-salen and -salphen complexes. *Dalton Trans* 8525–8531, 2009.
7. Ansenberger-Fricano K, Ganini D, Mao M, Chatterjee S, Dallas S, Mason RP, Stadler K, Santos JH, and Bonini MG. The peroxidase activity of mitochondrial superoxide dismutase. *Free Radic Biol Med* 54: 116–124, 2013.
8. Aranganathan S, Panneer Selvam J, and Nalini N. Hesperetin exerts dose dependent chemopreventive effect against 1,2-dimethyl hydrazine induced rat colon carcinogenesis. *Invest New Drugs* 27: 203–213, 2009.
9. Araujo-Chaves JC, Yokomizo CH, Kawai C, Mugnol KC, Prieto T, Nascimento OR, and Nantes IL. Towards the mechanisms involved in the antioxidant action of MnIII [meso-tetrakis(4-N-methyl pyridinium) porphyrin] in mitochondria. *J Bioenerg Biomembr* 43: 663–671, 2011.
10. Archambeau JO. Manganese(III)-porphyrin superoxide dismutase mimic ameliorates acute proctitis and late radiation toxicity following focal irradiation of the rat rectum. Submitted 2012.
11. Archibald FS and Fridovich I. The scavenging of superoxide radical by manganous complexes: *in vitro*. *Arch Biochem Biophys* 214: 452–463, 1982.
12. Arora M, Kumar A, Kaundal RK, and Sharma SS. Amelioration of neurological and biochemical deficits by peroxynitrite decomposition catalysts in experimental diabetic neuropathy. *Eur J Pharmacol* 596: 77–83, 2008.
13. Ashcraft KA, Palmer G, Spasojevic I, Batinic-Haberle I, and Dewhirst MW. Radioprotection of the salivary gland and oral mucosa with a novel porphyrin-based antioxidant. *58th Annual Meeting of the Radiation Research Society*, Puerto Rico. Published by RRS, Lawrence, KS. 129, 2012.
14. Aston K, Rath N, Naik A, Slomczynska U, Schall OF, and Riley DP. Computer-aided design (CAD) of Mn(II) complexes: superoxide dismutase mimetics with catalytic activity exceeding the native enzyme. *Inorg Chem* 40: 1779–1789, 2001.
15. Bagga P and Patel AB. Regional cerebral metabolism in mouse under chronic manganese exposure: implications for manganism. *Neurochem Int* 60: 177–185, 2012.
16. Bakalova R, Zhelev Z, Aoki I, and Saga T. Tissue redox activity as a hallmark of carcinogenesis: from early to terminal stages of cancer. *Clin Cancer Res* 19: 2503–2517, 2013.
17. Barnese K, Gralla EB, Cabelli DE, and Valentine JS. Manganous phosphate acts as a superoxide dismutase. *J Am Chem Soc* 130: 4604–4606, 2008.
18. Batinic-Haberle I, Benov L, Spasojevic I, and Fridovich I. The ortho effect makes manganese(III) meso-tetrakis(N-methylpyridinium-2-yl)porphyrin a powerful and poten-

tially useful superoxide dismutase mimic. *J Biol Chem* 273: 24521–24528, 1998.
19. Batinic-Haberle I, Cuzzocrea S, Reboucas JS, Ferrer-Sueta G, Mazzon E, Di Paola R, Radi R, Spasojevic I, Benov L, and Salvemini D. Pure MnTBAP selectively scavenges peroxynitrite over superoxide: comparison of pure and commercial MnTBAP samples to MnTE-2-PyP in two models of oxidative stress injury, an SOD-specific *Escherichia coli* model and carrageenan-induced pleurisy. *Free Radic Biol Med* 46: 192–201, 2009.
20. Batinic-Haberle I, Gauter-Fleckenstein B, Kos I, Fleckenstein K, Spasojevic I, and Vujaskovic Z. MnTnHex-2-PyP^{5+} structural characteristics, lipophilicity and bioavailability contribute to its high potency in pulmonary radioprotection. *55th Radiation Research Society Meeting*, Savannah. Published by RRS, Lawrence, KS. 143, 2009.
21. Batinic-Haberle I, Keir ST, Rajic Z, Tovmasyan A, and Bigner DD. Lipophilic Mn porphyrins in the treatment of brain tumors. *Free Radic Biol Med* 51: S119, 2011.
22. Batinic-Haberle I, Tovmasyan A, Weitner T, Rajic Z, Keir ST. Huang T-T, Leu D, Weitzel DH, Beauséjour CM, Miriyala S, Roberts ERH, Dewhirst MW, Clair DSt. Leong KW. Spasojevic I, Piganelli J, Tome M. Mechanistic considerations of the therapeutic effects of Mn porphyrins, commonly regarded as SOD mimics. In anticancer therapy. Lessons from brain and lymphoma studies. *Free Rad Biol Med* 65:S2, 2013.
23. Batinic-Haberle I, Liochev SI, Spasojevic I, and Fridovich I. A potent superoxide dismutase mimic: manganese beta-octabromo-meso-tetrakis-(N-methylpyridinium-4-yl) porphyrin. *Arch Biochem Biophys* 343: 225–233, 1997.
24. Batinic-Haberle I, Ndengele MM, Cuzzocrea S, Reboucas JS, Spasojevic I, and Salvemini D. Lipophilicity is a critical parameter that dominates the efficacy of metalloporphyrins in blocking the development of morphine antinociceptive tolerance through peroxynitrite-mediated pathways. *Free Radic Biol Med* 46: 212–219, 2009.
25. Batinic-Haberle I, Rajic Z, and Benov L. A combination of two antioxidants (an SOD mimic and ascorbate) produces a pro-oxidative effect forcing *Escherichia coli* to adapt via induction of oxyR regulon. *Anticancer Agents Med Chem* 11: 329–340, 2011.
26. Batinic-Haberle I, Rajic Z, Tovmasyan A, Reboucas JS, Ye X, Leong KW, Dewhirst MW, Vujaskovic Z, Benov L, and Spasojevic I. Diverse functions of cationic Mn(III) N-substituted pyridylporphyrins, recognized as SOD mimics. *Free Radic Biol Med* 51: 1035–1053, 2011.
27. Batinic-Haberle I, Reboucas JS, Benov L, and Spasojevic I. Chemistry, biology and medical effects of water soluble metalloporphyrins. In: *Handbook of Porphyrin Science*, edited by Kadish KM, Smith KM, and Guillard R. Singapore: World Scientific, 2011, pp. 291–393.
28. Batinic-Haberle I, Reboucas JS, and Spasojevic I. Superoxide dismutase mimics: chemistry, pharmacology, and therapeutic potential. *Antioxid Redox Signal* 13: 877–918, 2010.
29. Batinic-Haberle I, Spasojevic I, and Fridovich I. Tetrahydrobiopterin rapidly reduces the SOD mimic Mn(III) ortho-tetrakis(N-ethylpyridinium-2-yl)porphyrin. *Free Radic Biol Med* 37: 367–374, 2004.
30. Batinić-Haberle I, Spasojević I, Hambright P, Benov L, Crumbliss AL, and Fridovich I. Relationship among redox potentials, proton dissociation constants of pyrrolic nitrogens, and in vivo and in vitro superoxide dismutating activities of manganese(III) and iron(III) water-soluble porphyrins. *Inorg Chem* 38: 4011–4022, 1999.
31. Batinić-Haberle I, Spasojević I, Stevens RD, Hambright P, and Fridovich I. Manganese(III) *meso*-tetrakis(*ortho*-*N*-alkylpyridyl)porphyrins. Synthesis, characterization, and catalysis of $O_2^{\bullet -}$ dismutation. *J Chem Soc Dalton Trans* 2689–2696, 2002.
32. Batinic-Haberle I, Spasojevic I, Stevens RD, Hambright P, Neta P, Okado-Matsumoto A, and Fridovich I. New class of potent catalysts of O2.-dismutation. Mn(III) ortho-methoxyethylpyridyl- and di-ortho-methoxyethylimidazolylporphyrins. *Dalton Trans* 1696–1702, 2004.
33. Batinic-Haberle I, Spasojevic I, Tse HM, Tovmasyan A, Rajic Z, St Clair DK, Vujaskovic Z, Dewhirst MW, and Piganelli JD. Design of Mn porphyrins for treating oxidative stress injuries and their redox-based regulation of cellular transcriptional activities. *Amino Acids* 42: 95–113, 2012.
34. Baudry M, Etienne S, Bruce A, Palucki M, Jacobsen E, and Malfroy B. Salen-manganese complexes are superoxide dismutase-mimics. *Biochem Biophys Res Commun* 192: 964–968, 1993.
35. Behrend L, Mohr A, Dick T, and Zwacka RM. Manganese superoxide dismutase induces p53-dependent senescence in colorectal cancer cells. *Mol Cell Biol* 25: 7758–7769, 2005.
36. Belkacemi A, Doggui S, Dao L, and Ramassamy C. Challenges associated with curcumin therapy in Alzheimer disease. *Expert Rev Mol Med* 13: e34, 2011.
37. Bilyy R, Kit Y, Hellman U, and Stoika R. AMID: new insights on its intracellular localization and expression at apoptosis. *Apoptosis* 13: 729–732, 2008.
38. Bloodsworth A, O'Donnell VB, Batinic-Haberle I, Chumley PH, Hurt JB, Day BJ, Crow JP, and Freeman BA. Manganese-porphyrin reactions with lipids and lipoproteins. *Free Radic Biol Med* 28: 1017–1029, 2000.
39. Bottino R, Balamurugan AN, Bertera S, Pietropaolo M, Trucco M, and Piganelli JD. Preservation of human islet cell functional mass by anti-oxidative action of a novel SOD mimic compound. *Diabetes* 51: 2561–2567, 2002.
40. Bottino R, Balamurugan AN, Tse H, Thirunavukkarasu C, Ge X, Profozich J, Milton M, Ziegenfuss A, Trucco M, and Piganelli JD. Response of human islets to isolation stress and the effect of antioxidant treatment. *Diabetes* 53: 2559–2568, 2004.
41. Briehl MM, Gustafson HL, Lee K, and Tome ME. Rapamycin treatment of mantle cell lymphoma inhibits mTORC2 signaling, resulting in increased MnSOD expression and hydrogen peroxide generation. *Free Radic Biol Med* 53: S39, 2012.
42. Buettner GR. Superoxide dismutase in redox biology: the roles of superoxide and hydrogen peroxide. *Anticancer Agents Med Chem* 11: 341–346, 2011.
43. Buettner GR, Wagner BA, and Rodgers VG. Quantitative redox biology: an approach to understand the role of reactive species in defining the cellular redox environment. *Cell Biochem Biophys* 2011 DOI: 10.1007/s12013-011-9320-3.
44. Chen Q, Espey MG, Krishna MC, Mitchell JB, Corpe CP, Buettner GR, Shacter E, and Levine M. Pharmacologic ascorbic acid concentrations selectively kill cancer cells: action as a pro-drug to deliver hydrogen peroxide to tissues. *Proc Natl Acad Sci U S A* 102: 13604–13609, 2005.
45. Chen Q, Espey MG, Sun AY, Lee JH, Krishna MC, Shacter E, Choyke PL, Pooput C, Kirk KL, Buettner GR, and Levine M. Ascorbate in pharmacologic concentrations selectively generates ascorbate radical and hydrogen peroxide in extracellular fluid *in vivo*. *Proc Natl Acad Sci U S A* 104: 8749–8754, 2007.
46. Chen Q, Espey MG, Sun AY, Pooput C, Kirk KL, Krishna MC, Khosh DB, Drisko J, and Levine M. Pharmacologic

doses of ascorbate act as a prooxidant and decrease growth of aggressive tumor xenografts in mice. *Proc Natl Acad Sci U S A* 105: 11105–11109, 2008.
47. Chen YJ, Santos M, and Quilley J. Treatment of diabetic rats with a peroxynitrite decomposition catalyst prevents induction of renal COX-2. *Am J Physiol Heart Circ Physiol* 300: H1125–H1132, 2011.
48. Cheng G, Zielonka J, Dayton AR, Joseph J, and Kalyanaraman B. Alterations in Kreb's cycle carbon pool and bioenergetics metabolites in pancreatic cancer cells treated with mitochondria-targeted drug. *Free Radic Biol Med* 53: S40, 2012.
49. Chng LL, Chang CJ, and Nocera DG. Catalytic O-O activation chemistry mediated by iron hangman porphyrins with a wide range of proton-donating abilities. *Org Lett* 5: 2421–2424, 2003.
50. Cline JM, Dugan G, Bourland D, Perry DL, Stitzel JD, Weaver AA, Jiang C, Owzar K, Spasojevic I, Batinic-Haberle I, and Vujakovic Z. Post-irradiation treatment with MnTnHex-2-PyP5+ mitigates radiation pneumonitis and fibrosis in the lungs of non-human primates after whole-thorax exposure to ionizing radiation. *Radiat Res* 2013 (In revision).
51. Cline M, Dugan G, Perry D, Batinic-Haberle I, and Vujaskovic Z. MnTnHex-2-PyP^{5+} provides protection in nonhuman primate lungs after whole-thorax exposure to ionizing irradiation. *56th Radiation Research Society Meeting*, Maui, HI. Published by RRS, Lawrence, KS. 54, 2010.
52. Cohen J, Dorai T, Ding C, Batinic-Haberle I, and Grasso M. The administration of renoprotective agents extends warm ischemia in a rat model. *J Endourol* 27: 343–348, 2013.
53. Colon J, Herrera L, Smith J, Patil S, Komanski C, Kupelian P, Seal S, Jenkins DW, and Baker CH. Protection from radiation-induced pneumonitis using cerium oxide nanoparticles. *Nanomedicine* 5: 225–231, 2009.
54. Colon J, Hsieh N, Ferguson A, Kupelian P, Seal S, Jenkins DW, and Baker CH. Cerium oxide nanoparticles protect gastrointestinal epithelium from radiation-induced damage by reduction of reactive oxygen species and upregulation of superoxide dismutase 2. *Nanomedicine* 6: 698–705, 2010.
55. Corti A, Casini AF, and Pompella A. Cellular pathways for transport and efflux of ascorbate and dehydroascorbate. *Arch Biochem Biophys* 500: 107–115, 2010.
56. Cotrim AP, Hyodo F, Matsumoto K, Sowers AL, Cook JA, Baum BJ, Krishna MC, and Mitchell JB. Differential radiation protection of salivary glands versus tumor by Tempol with accompanying tissue assessment of Tempol by magnetic resonance imaging. *Clin Cancer Res* 13: 4928–4933, 2007.
57. Coulter ED, Emerson JP, Kurtz DM, and Cabelli DE. Superoxide reactivity of rubredoxin oxidoreductase (Desulfoferrodoxin) from *Desulfovibrio vulgaris*: a pulse radiolysis study. *J Am Chem Soc* 122: 11555–11556, 2000.
58. Cummins TD, Higdon AN, Kramer PA, Chacko BK, Riggs DW, Salabei JK, Dell'italia LJ, Zhang J, Darley-Usmar VM, and Hill BG. Utilization of fluorescent probes for the quantification and identification of subcellular proteomes and biological processes regulated by lipid peroxidation products. *Free Radic Biol Med* 59: 56–68, 2013.
59. Cuzzocrea S, Mazzon E, di Paola R, Genovese T, Muia C, Caputi AP, and Salvemini D. Synergistic interaction between methotrexate and a superoxide dismutase mimetic—pharmacologic and potential clinical significance. *Arthritis Rheum* 52: 3755–3760, 2005.
60. Dang CV, Le A, and Gao P. MYC-induced cancer cell energy metabolism and therapeutic opportunities. *Clin Cancer Res* 15: 6479–6483, 2009.
61. Daroczi B, Kari G, McAleer MF, Wolf JC, Rodeck U, and Dicker AP. *In vivo* radioprotection by the fullerene nanoparticle DF-1 as assessed in a zebrafish model. *Clin Cancer Res* 12: 7086–7091, 2006.
62. Daroczi B, Kari G, Zengin AY, Chinnaiyan P, Batinic-Haberle I, Rodeck U, and Dicker AP. Radioprotective effects of two superoxide dismutase (SOD) mimetics and the nanoparticle DF-1 in a vertebrate zebrafish model. *48th ASTRO, Annual Meeting of the American Society for Radiation Oncology* 2006.
63. Das L and Vinayak M. Anti-carcinogenic action of curcumin by activation of antioxidant defence system and inhibition of NF-kappaB signalling in lymphoma-bearing mice. *Biosci Rep* 32: 161–170, 2012.
64. Davis TA, Clarke TK, Mog SR, and Landauer MR. Subcutaneous administration of genistein prior to lethal irradiation supports multilineage, hematopoietic progenitor cell recovery and survival. *Int J Radiat Biol* 83: 141–151, 2007.
65. Davis TA, Mungunsukh O, Zins S, Day RM, and Landauer MR. Genistein induces radioprotection by hematopoietic stem cell quiescence. *Int J Radiat Biol* 84: 713–726, 2008.
66. Day BJ, Fridovich I, and Crapo JD. Manganic porphyrins possess catalase activity and protect endothelial cells against hydrogen peroxide-mediated injury. *Arch Biochem Biophys* 347: 256–262, 1997.
67. Day NL, Floyd CL, D'Alessandro TL, Hubbard WJ, and Chaudry IH. 17beta-estradiol confers protection following traumatic brain injury in the rat and involves activation of G Protein-coupled estrogen receptor 1 (GPER). *J Neurotrauma* 30: 1531–1541, 2013.
68. Day RM, Barshishat-Kupper M, Mog SR, McCart EA, Prasanna PG, Davis TA, and Landauer MR. Genistein protects against biomarkers of delayed lung sequelae in mice surviving high-dose total body irradiation. *J Radiat Res* 49: 361–372, 2008.
69. DeFreitas-Silva G, Reboucas JS, Spasojevic I, Benov L, Idemori YM, and Batinic-Haberle I. SOD-like activity of Mn(II) beta-octabromo-meso-tetrakis(N-methylpyridinium-3-yl)porphyrin equals that of the enzyme itself. *Arch Biochem Biophys* 477: 105–112, 2008.
70. Delmastro-Greenwood MM, Votyakova T, Goetzman E, Marre ML, Previte DM, Tovmasyan A, Batinic-Haberle I, Trucco M, and Piganelli JD. Mn porphyrin regulation of aerobic glycolysis: implications on the activation of diabetogenic immune cells. *Antioxid Redox Signal* 19: 1902–1915, 2013.
71. Desideri A, Falconi M, Parisi V, Morante S, and Rotilio G. Is the activity-linked electrostatic gradient of bovine Cu, Zn superoxide dismutases conserved in homologous enzymes irrespective of the number and distribution of charges? *Free Radic Biol Med* 5: 313–317, 1988.
72. Doblas S, Saunders D, Kshirsagar P, Pye Q, Oblander J, Gordon B, Kosanke S, Floyd RA, and Towner RA. Phenyl-tert-butylnitrone induces tumor regression and decreases angiogenesis in a C6 rat glioma model. *Free Radic Biol Med* 44: 63–72, 2008.
73. Doctrow SR, Baudry M, Huffman K, Malfroy B, and Melov S. Salen manganese complexes: multifunctional catalytic antioxidants protective in models for neurodegenerative diseases of aging in medicinal inorganic chemistry. In: *American Chemical Society Symposium Series 903, ACS*, Washington, DC, edited by Sessler J, Doctrow SR, McMurry T, and Lippard S. Oxford University Press, 2005, pp. 319–347.
74. Doctrow SR, Huffman K, Marcus CB, Tocco G, Malfroy E, Adinolfi CA, Kruk H, Baker K, Lazarowych N, Mascar-

enhas J, and Malfroy B. Salen-manganese complexes as catalytic scavengers of hydrogen peroxide and cytoprotective agents: structure-activity relationship studies. *J Med Chem* 45: 4549–4558, 2002.
75. Dorai T, Fishman AI, Ding C, Batinic-Haberle I, Goldfarb DS, and Grasso M. Amelioration of renal ischemia-reperfusion injury with a novel protective cocktail. *J Urol* 186: 2448–2454, 2011.
76. Doyle T, Bryant L, Batinic-Haberle I, Little J, Cuzzocrea S, Masini E, Spasojevic I, and Salvemini D. Supraspinal inactivation of mitochondrial superoxide dismutase is a source of peroxynitrite in the development of morphine antinociceptive tolerance. *Neuroscience* 164: 702–710, 2009.
77. Doyle T, Chen Z, Muscoli C, Bryant L, Esposito E, Cuzzocrea S, Dagostino C, Ryerse J, Rausaria S, Kamadulski A, Neumann WL, and Salvemini D. Targeting the overproduction of peroxynitrite for the prevention and reversal of paclitaxel-induced neuropathic pain. *J Neurosci* 32: 6149–6160, 2012.
78. Du J, Martin SM, Levine M, Wagner BA, Buettner GR, Wang SH, Taghiyev AF, Du C, Knudson CM, and Cullen JJ. Mechanisms of ascorbate-induced cytotoxicity in pancreatic cancer. *Clin Cancer Res* 16: 509–520, 2010.
79. Durga A, Sepahpanah F, Regozzi M, Hastings J, and Crane DA. Prevalence of testosterone deficiency after spinal cord injury. *PM R* 3: 929–932, 2011.
80. Eckshtain M, Zilbermann I, Mahammed A, Saltsman I, Okun Z, Maimon E, Cohen H, Meyerstein D, and Gross Z. Superoxide dismutase activity of corrole metal complexes. *Dalton Trans* 7879–7882, 2009.
81. Ellerby RM, Cabelli DE, Graden JA, and Valentine JS. Copper-zinc superoxide dismutase: why not pH-dependent? *J Am Chem Soc* 118: 6556–6561, 1996.
82. Evans MK, Tovmasyan A, Batinic-Haberle I, and Devi GR. Mn Porphyrin in combination with ascorbate acts as a pro-oxidant and mediates caspase-independent cancer cell death. *Free Radic Biol Med* 2013 (In revision).
83. Fargo KN and Sengelaub DR. Testosterone manipulation protects motoneurons from dendritic atrophy after contralateral motoneuron depletion. *J Comp Neurol* 469: 96–106, 2004.
84. Ferrer-Sueta G, Batinic-Haberle I, Spasojevic I, Fridovich I, and Radi R. Catalytic scavenging of peroxynitrite by isomeric Mn(III) N-methylpyridylporphyrins in the presence of reductants. *Chem Res Toxicol* 12: 442–449, 1999.
85. Ferrer-Sueta G, Manta B, Botti H, Radi R, Trujillo M, and Denicola A. Factors affecting protein thiol reactivity and specificity in peroxide reduction. *Chem Res Toxicol* 24: 434–450, 2011.
86. Ferrer-Sueta G, Vitturi D, Batinic-Haberle I, Fridovich I, Goldstein S, Czapski G, and Radi R. Reactions of manganese porphyrins with peroxynitrite and carbonate radical anion. *J Biol Chem* 278: 27432–27438, 2003.
87. Filipovic MR, Duerr K, Mojovic M, Simeunovic V, Zimmermann R, Niketic V, and Ivanovic-Burmazovic I. NO dismutase activity of seven-coordinate manganese(II) pentaazamacrocyclic complexes. *Angew Chem Int Ed* 47: 8735–8739, 2008.
88. Floyd RA, Towner RA, Wu D, Abbott A, Cranford R, Branch D, Guo WX, Foster SB, Jones I, Alam R, Moore D, Allen T, and Huycke M. Anti-cancer activity of nitrones in the Apc(Min/+) model of colorectal cancer. *Free Radic Res* 44: 108–117, 2010.
89. Forman HJ, Davies KJ, and Ursini F. How do Nutritional antioxidants really work: nucleophilic tone and parahormesis versus free radical scavenging *in vivo*. *Free Radic Biol Med* pii: S0891-5849(13)00273-6, 2013.
90. Forman HJ, Maiorino M, and Ursini F. Signaling functions of reactive oxygen species. *Biochemistry* 49: 835–842, 2010.
91. Fuller TF, Rose F, Singleton KD, Linde Y, Hoff U, Freise CE, Dragun D, and Niemann CU. Glutamine donor pretreatment in rat kidney transplants with severe preservation reperfusion injury. *J Surg Res* 140: 77–83, 2007.
92. Gad SC, Sullivan DW, Jr., Crapo JD, and Spainhour CB. A nonclinical safety assessment of MnTE-2-PyP, a manganese porphyrin. *Int J Toxicol* 32: 274–287, 2013..
93. Gao MC, Jia XD, Wu QF, Cheng Y, Chen FR, and Zhang J. Silencing Prx1 and/or Prx5 sensitizes human esophageal cancer cells to ionizing radiation and increases apoptosis via intracellular ROS accumulation. *Acta Pharmacol Sin* 32: 528–536, 2011.
94. Garteiser P, Doblas S, Watanabe Y, Saunders D, Hoyle J, Lerner M, He T, Floyd RA, and Towner RA. Multiparametric assessment of the anti-glioma properties of OKN007 by magnetic resonance imaging. *J Magn Reson Imaging* 31: 796–806, 2010.
95. Gauter-Fleckenstein B, Fleckenstein K, Owzar K, Jiang C, Batinic-Haberle I, and Vujaskovic Z. Comparison of two Mn porphyrin-based mimics of superoxide dismutase in pulmonary radioprotection. *Free Radic Biol Med* 44: 982–989, 2008.
96. Gauter-Fleckenstein B, Fleckenstein K, Owzar K, Jiang C, Reboucas JS, Batinic-Haberle I, and Vujaskovic Z. Early and late administration of MnTE-2-PyP5+ in mitigation and treatment of radiation-induced lung damage. *Free Radic Biol Med* 48: 1034–1043, 2010.
97. Getzoff ED, Tainer JA, Weiner PK, Kollman PA, Richardson JS, and Richardson DC. Electrostatic recognition between superoxide and copper, zinc superoxide dismutase. *Nature* 306: 287–290, 1983.
98. Giblin GM, Box PC, Campbell IB, Hancock AP, Roomans S, Mills GI, Molloy C, Tranter GE, Walker AL, Doctrow SR, Huffman K, and Malfroy B. 6,6′-Bis(2-hydroxyphenyl)-2,2′-bipyridine manganese(III) complexes: a novel series of superoxide dismutase and catalase mimetics. *Bioorg Med Chem Lett* 11: 1367–1370, 2001.
99. Goldstein S, Czapski G, and Heller A. Osmium tetroxide, used in the treatment of arthritic joints, is a fast mimic of superoxide dismutase. *Free Radic Biol Med* 38: 839–845, 2005.
100. Gridley DS, Makinde AY, Luo X, Rizvi A, Crapo JD, Dewhirst MW, Moeller BJ, Pearlstein RD, and Slater JM. Radiation and a metalloporphyrin radioprotectant in a mouse prostate tumor model. *Anticancer Res* 27: 3101–3109, 2007.
101. Gu M and Imlay JA. Superoxide poisons mononuclear iron enzymes by causing mismetallation. *Mol Microbiol* 89: 123–134, 2013.
102. Gur S, Kadowitz PJ, and Hellstrom WJ. A critical appraisal of erectile function in animal models of diabetes mellitus. *Int J Androl* 32: 93–114, 2009.
103. Haber A, Angel I, Mahammed A, and Gross Z. Combating diabetes complications by 1-Fe, a corrole-based catalytic antioxidant. *J Diabetes Complications* 27: 316–321, 2013.
104. Haber A, Aviram M, Gross Z. Variables that influence cellular uptake and cytotoxic/cytoprotective effects of macrocyclic iron complexes. Inorg Chem 51: 28–30, 2012.
105. Haber A, Mahammed A, Fuhrman B, Volkova N, Coleman R, Hayek T, Aviram M, and Gross Z. Amphiphilic/bipolar metallocorroles that catalyze the decomposition of reactive oxygen and nitrogen species, rescue lipoproteins from oxidative damage, and attenuate atherosclerosis in mice. *Angew Chem Int Ed* 47: 7896–7900, 2008.

106. Hahn SM, DeLuca AM, Coffin D, Krishna CM, and Mitchell JB. *In vivo* radioprotection and effects on blood pressure of the stable free radical nitroxides. *Int J Radiat Oncol Biol Phys* 42: 839–842, 1998.
107. Halliwell B. Dietary polyphenols: good, bad, or indifferent for your health? *Cardiovasc Res* 73: 341–347, 2007.
108. Halliwell B. Are polyphenols antioxidants or pro-oxidants? What do we learn from cell culture and *in vivo* studies? *Arch Biochem Biophys* 476: 107–112, 2008.
109. Halliwell B and Gutteridge JMC. *Free Radicals in Biology and Medicine.* New York: Oxford University Press, 2007.
110. Hamilton KL, Mbai FN, Gupta S, and Knowlton AA. Estrogen, heat shock proteins, and NFkappaB in human vascular endothelium. *Arterioscler Thromb Vasc Biol* 24: 1628–1633, 2004.
111. Hay N and Sonenberg N. Upstream and downstream of mTOR. *Genes Dev* 18: 1926–1945, 2004.
112. He Z, Subramaniam D, Ramalingam S, Dhar A, Postier RG, Umar S, Zhang Y, and Anant S. Honokiol radiosensitizes colorectal cancer cells: enhanced activity in cells with mismatch repair defects. *Am J Physiol Gastrointest Liver Physiol* 301: G929–G937, 2011.
113. Heckert EG, Karakoti AS, Seal S, and Self WT. The role of cerium redox state in the SOD mimetic activity of nanoceria. *Biomaterials* 29: 2705–2709, 2008.
114. Hempel N, Carrico PM, and Melendez JA. Manganese superoxide dismutase (Sod2) and redox-control of signaling events that drive metastasis. *Anticancer Agents Med Chem* 11: 191–201, 2011.
115. Hill RP, Zaidi A, Mahmood J, and Jelveh S. Investigations into the role of inflammation in normal tissue response to irradiation. *Radiother Oncol* 101: 73–79, 2011.
116. Hoffer LJ, Levine M, Assouline S, Melnychuk D, Padayatty SJ, Rosadiuk K, Rousseau C, Robitaille L, and Miller WH, Jr. Phase I clinical trial of i.v. ascorbic acid in advanced malignancy. *Ann Oncol* 19: 1969–1974, 2008.
117. Holley AK, Xu Y, Noel T, Bakthavatchalu V, Batinic-Haberle I, and St. Clair DK. Manganese superoxide dismutase-mediated inside-out signaling in HaCaT human keratinocytes and SKH-1 mouse skin. *Antioxid Redox Signal* 20: 2347–2360, 2014.
118. Hudnell HK. Effects from environmental Mn exposures: a review of the evidence from non-occupational exposure studies. *Neurotoxicology* 20: 379–397, 1999.
119. Hyman LM and Franz KJ. Probing oxidative stress: small molecule fluorescent sensors of metal ions, reactive oxygen species, and thiols. *Coord Chem Rev* 256: 2333–2356, 2012.
120. Inano H, Onoda M, Inafuku N, Kubota M, Kamada Y, Osawa T, Kobayashi H, and Wakabayashi K. Chemoprevention by curcumin during the promotion stage of tumorigenesis of mammary gland in rats irradiated with gamma-rays. *Carcinogenesis* 20: 1011–1018, 1999.
121. Jackson IL, Gaunter-Fleckenstein BM, Batinic-Haberle I, Poulton S, Zhao Y, Dewhirst MW, and Vujaskovic Z. Hyperthermia enhances the anti-angiogenic effect of metalloporphyrin mimetic of superoxide dismutase. *24th Annual Meeting of the European Society for Hyperthermic Oncology*, Prague, Czech Republic, 2007.
122. Jackson IL, Zhang X, Hadley C, Rabbani ZN, Zhang Y, Marks S, and Vujaskovic Z. Temporal expression of hypoxia-regulated genes is associated with early changes in redox status in irradiated lung. *Free Radic Biol Med* 53: 337–346, 2012.
123. Jagetia GC and Rajanikant GK. Acceleration of wound repair by curcumin in the excision wound of mice exposed to different doses of fractionated gamma radiation. *Int Wound J* 9: 76–92, 2012.
124. Jaramillo MC, Briehl MM, Batinic Haberle I, and Tome ME. Inhibition of the electron transport chain via the pro-oxidative activity of manganese porphyrin-based SOD mimetics modulates bioenergetics and enhances the response to chemotherapy. *Free Radic Biol Med* 65: S25, 2013.
125. Jaramillo MC, Briehl MM, Crapo JD, Batinic-Haberle I, and Tome ME. Manganese porphyrin, MnTE-2-PyP5+, Acts as a pro-oxidant to potentiate glucocorticoid-induced apoptosis in lymphoma cells. *Free Radic Biol Med* 52: 1272–1284, 2012.
126. Jaramillo MC, Briehl MM, and Tome ME. Manganese porphyrin glutathionylates the p65 subunit of NF-κB to potentiate glucocorticoid-induced apoptosis in lymphoma. *Free Radic Biol Med* 49: S63, 2010.
127. Jaramillo MC, Frye JB, Crapo JD, Briehl MM, and Tome ME. Increased manganese superoxide dismutase expression or treatment with manganese porphyrin potentiates dexamethasone-induced apoptosis in lymphoma cells. *Cancer Res* 69: 5450–5457, 2009.
128. Jin N, Lahaye DE, and Groves JT. A "push-pull" mechanism for heterolytic o-o bond cleavage in hydroperoxo manganese porphyrins. *Inorg Chem* 49: 11516–11524, 2010.
129. Joanny E, Ding Q, Gong L, Kong P, Saklatvala J, and Clark AR. Anti-inflammatory effects of selective glucocorticoid receptor modulators are partially dependent on up-regulation of dual specificity phosphatase 1. *Br J Pharmacol* 165: 1124–1136, 2012.
130. Jumbo-Lucioni PP, Ryan EL, Hopson ML, Bishop HM, Weitner T, Tovmasyan A, Spasojevic I, Batinic-Haberle I, Liang Y, Jones DP, and Fridovich-Keil JL. Manganese-based superoxide dismutase mimics modify both acute and long-term outcome severity in a *Drosophila melanogaster* model of classic galactosemia. *Antioxid Redox Signal* 20: 2361–2371, 2014.
131. Kachadourian R, Johnson CA, Min E, Spasojevic I, and Day BJ. Flavin-dependent antioxidant properties of a new series of meso-N,N′-dialkyl-imidazolium substituted manganese(III) porphyrins. *Biochem Pharmacol* 67: 77–85, 2004.
132. Keaney M, Matthijssens F, Sharpe M, Vanfleteren J, and Gems D. Superoxide dismutase mimetics elevate superoxide dismutase activity *in vivo* but do not retard aging in the nematode *Caenorhabditis elegans*. *Free Radic Biol Med* 37: 239–250, 2004.
133. Kelly S, Lancon D, and Kadish KM. Electron-transfer and ligand-addition reactions of (Tpp)Mn(No) and (Tpp)Co(-No) in nonaqueous media. *Inorg Chem* 23: 1451–1458, 1984.
134. Kim A, Joseph S, Khan A, Epstein CJ, Sobel R, and Huang TT. Enhanced expression of mitochondrial superoxide dismutase leads to prolonged *in vivo* cell cycle progression and up-regulation of mitochondrial thioredoxin. *Free Radic Biol Med* 48: 1501–1512, 2010.
135. Kim HY, Wang J, Lu Y, Chung JM, and Chung K. Superoxide signaling in pain is independent of nitric oxide signaling. *Neuroreport* 20: 1424–1428, 2009.
136. Kimura M, Rabbani ZN, Zodda AR, Yan H, Jackson IL, Polascik TJ, Donatucci CF, Moul JW, Vujaskovic Z, and Koontz BF. Role of oxidative stress in a rat model of radiation-induced erectile dysfunction. *J Sex Med* 9: 1535–1549, 2012.
137. Klug-Roth D, Fridovich I, and Rabani J. Pulse radiolytic investigations of superoxide catalyzed disproportionation. Mechanism for bovine superoxide dismutase. *J Am Chem Soc* 95: 2786–2790, 1973.
138. Korsvik C, Patil S, Seal S, and Self WT. Superoxide dismutase mimetic properties exhibited by vacancy en-

gineered ceria nanoparticles. *Chem Commun (Camb)* 1056–1058, 2007.
139. Kos I, Benov L, Spasojevic I, Reboucas JS, and Batinic-Haberle I. High lipophilicity of meta Mn(III) N-alkylpyridylporphyrin-based superoxide dismutase mimics compensates for their lower antioxidant potency and makes them as effective as ortho analogues in protecting superoxide dismutase-deficient *Escherichia coli*. *J Med Chem* 52: 7868–7872, 2009.
140. Kos I, Reboucas JS, Sheng H, Warner DS, Spasojevic I, and Batinic-Haberle I. Oral availability of MnTE-2-PyP^{5+}, a potent antioxidant and cellular redox modulator. *Free Radic Biol Med* 45: S86, 2008.
141. Kuiper C, Molenaar IG, Dachs GU, Currie MJ, Sykes PH, and Vissers MC. Low ascorbate levels are associated with increased hypoxia-inducible factor-1 activity and an aggressive tumor phenotype in endometrial cancer. *Cancer Res* 70: 5749–5758, 2010.
142. Kwei KA, Finch JS, Thompson EJ, and Bowden GT. Transcriptional repression of catalase in mouse skin tumor progression. *Neoplasia* 6: 440–448, 2004.
143. Lan KL, Lan KH, Sheu ML, Chen MY, Shih YS, Hsu FC, Wang HM, Liu RS, and Yen SH. Honokiol inhibits hypoxia-inducible factor-1 pathway. *Int J Radiat Biol* 87: 579–590, 2011.
144. Landauer MR, Srinivasan V, and Seed TM. Genistein treatment protects mice from ionizing radiation injury. *J Appl Toxicol* 23: 379–385, 2003.
145. Langan AR, Khan MA, Yeung IW, Van Dyk J, and Hill RP. Partial volume rat lung irradiation: the protective/mitigating effects of Eukarion-189, a superoxide dismutase-catalase mimetic. *Radiother Oncol* 79: 231–238, 2006.
146. Lange M, Szabo C, Enkhbaatar P, Connelly R, Horvath E, Hamahata A, Cox RA, Esechie A, Nakano Y, Traber LD, Herndon DN, and Traber DL. Beneficial pulmonary effects of a metalloporphyrinic peroxynitrite decomposition catalyst in burn and smoke inhalation injury. *Am J Physiol Lung Cell Mol Physiol* 300: L167–L175, 2011.
147. Lee JB, Hunt JA, and Groves JT. Manganese porphyrins as redox-coupled peroxynitrite reductases. *J Am Chem Soc* 120: 6053–6061, 1998.
148. Lee JB, Hunt JA, and Groves JT. Mechanisms of iron porphyrin reactions with peroxynitrite. *J Am Chem Soc* 120: 7493–7501, 1998.
149. Lee JH, Lee YM, and Park JW. Regulation of ionizing radiation-induced apoptosis by a manganese porphyrin complex. *Biochem Biophys Res Commun* 334: 298–305, 2005.
150. Lee JH and Park JW. A manganese porphyrin complex is a novel radiation protector. *Free Radic Biol Med* 37: 272–283, 2004.
151. Levine M, Espey MG, and Chen Q. Losing and finding a way at C: new promise for pharmacologic ascorbate in cancer treatment. *Free Radic Biol Med* 47: 27–29, 2009.
152. Li H, Wang Y, Pazhanisamy SK, Shao L, Batinic-Haberle I, Meng A, and Zhou D. Mn(III) meso-tetrakis-(N-ethylpyridinium-2-yl) porphyrin mitigates total body irradiation-induced long-term bone marrow suppression. *Free Radic Biol Med* 51: 30–37, 2011.
153. Li W, Sun L, Liang Q, Wang J, Mo W, and Zhou B. Yeast AMID homologue Ndi1p displays respiration-restricted apoptotic activity and is involved in chronological aging. *Mol Biol Cell* 17: 1802–1811, 2006.
154. Lim P, Mahammed A, Okun Z, Saltsman I, Gross Z, Gray HB, and Termini J. Differential cytostatic and cytotoxic action of Metallocorroles against human cancer cells: potential platforms for anticancer drug development. *Chem Res Toxicol* 25: 400–409, 2012.
155. Limtrakul P, Lipigorngoson S, Namwong O, Apisariyakul A, and Dunn FW. Inhibitory effect of dietary curcumin on skin carcinogenesis in mice. *Cancer Lett* 116: 197–203, 1997.
156. Lin HS, Lin TS, Lai RS, D'Rosario T, and Luh TY. Fullerenes as a new class of radioprotectors. *Int J Radiat Biol* 77: 235–239, 2001.
157. Little JW, Chen Z, Doyle T, Porreca F, Ghaffari M, Bryant L, Neumann WL, and Salvemini D. Supraspinal peroxynitrite modulates pain signaling by suppressing the endogenous opioid pathway. *J Neurosci* 32: 10797–10808, 2012.
158. Lopez-Jornet P, Camacho-Alonso F, and Gomez-Garcia F. Effect of curcumin and irradiation in PE/CA-PJ15 oral squamous cell carcinoma. *Acta Odontol Scand* 69: 269–273, 2011.
159. Ma Q. Role of nrf2 in oxidative stress and toxicity. *Annu Rev Pharmacol Toxicol* 53: 401–426, 2013.
160. Madero-Visbal RA, Alvarado BE, Colon JF, Baker CH, Wason MS, Isley B, Seal S, Lee CM, Das S, and Manon R. Harnessing nanoparticles to improve toxicity after head and neck radiation. *Nanomedicine* 8: 1223–1231, 2012.
161. Mahammed A and Gross Z. Highly efficient catalase activity of metallocorroles. *Chem Commun (Camb)* 46: 7040–7042, 2010.
162. Mahammed A, Tumanskii B, and Gross Z. Effect of bromination on the electrochemistry, frontier orbitals, and spectroscopy of metallocorroles. *J Porphyr Phthalocya* 15: 1275–1286, 2011.
163. Mahmood J, Jelveh S, Calveley V, Zaidi A, Doctrow SR, and Hill RP. Mitigation of radiation-induced lung injury by genistein and EUK-207. *Int J Radiat Biol* 87: 889–901, 2011.
164. Makinde AY, Luo-Owen X, Rizvi A, Crapo JD, Pearlstein RD, Slater JM, and Gridley DS. Effect of a metalloporphyrin antioxidant (MnTE-2-PyP) on the response of a mouse prostate cancer model to radiation. *Anticancer Res* 29: 107–118, 2009.
165. Makinde AY, Rizvi A, Crapo JD, Pearlstein RD, Slater JM, and Gridley DS. A metalloporphyrin antioxidant alters cytokine responses after irradiation in a prostate tumor model. *Radiat Res* 173: 441–452, 2010.
166. Mao XW, Crapo JD, Mekonnen T, Lindsey N, Martinez P, Gridley DS, and Slater JM. Radioprotective effect of a metalloporphyrin compound in rat eye model. *Curr Eye Res* 34: 62–72, 2009.
167. Maroz A, Kelso GF, Smith RA, Ware DC, and Anderson RF. Pulse radiolysis investigation on the mechanism of the catalytic action of Mn(II)-pentaazamacrocycle compounds as superoxide dismutase mimetics. *J Phys Chem A* 112: 4929–4935, 2008.
168. Marshall KR, Gong M, Wodke L, Lamb JH, Jones DJL, Farmer PB, Scrutton NS, and Munro AW. The human apoptosis-inducing protein AMID is an oxidoreductase with a modified flavin cofactor and DNA binding activity. *J Biol Chem* 280: 30735–30740, 2005.
169. Martell AE and Motekaitis RJ. *The Determination and Use of Stability Constants*. New York: VCH Publishers, Inc., 1992.
170. Martins EN, Pessano NT, Leal L, Roos DH, Folmer V, Puntel GO, Rocha JB, Aschner M, Avila DS, and Puntel RL. Protective effect of Melissa officinalis aqueous extract against Mn-induced oxidative stress in chronically exposed mice. *Brain Res Bull* 87: 74–79, 2012.
171. Masini E, Bani D, Vannacci A, Pierpaoli S, Mannaioni PF, Comhair SA, Xu W, Muscoli C, Erzurum SC, and Salvemini D. Reduction of antigen-induced respiratory abnormalities and airway inflammation in sensitized

guinea pigs by a superoxide dismutase mimetic. *Free Radic Biol Med* 39: 520–531, 2005.
172. Maybauer DM, Maybauer MO, Szabo C, Cox RA, Westphal M, Kiss L, Horvath EM, Traber LD, Hawkins HK, Salzman AL, Southan GJ, Herndon DN, and Traber DL. The peroxynitrite catalyst WW-85 improves pulmonary function in ovine septic shock. *Shock* 35: 148–155, 2011.
173. Maybauer DM, Maybauer MO, Szabo C, Westphal M, Traber LD, Salzman AL, Herndon DN, and Traber DL. The peroxynitrite catalyst WW-85 improves microcirculation in ovine smoke inhalation injury and septic shock. *Burns* 37: 842–850, 2011.
174. McGovern T, Day BJ, White CW, Powell WS, and Martin JG. AEOL10150: a novel therapeutic for rescue treatment after toxic gas lung injury. *Free Radic Biol Med* 50: 602–608, 2011.
175. Metz JM, Smith D, Mick R, Lustig R, Mitchell J, Cherakuri M, Glatstein E, and Hahn SM. A phase I study of topical Tempol for the prevention of alopecia induced by whole brain radiotherapy. *Clin Cancer Res* 10: 6411–6417, 2004.
176. Miljkovic J, Ivanovic-Burmazovic I, Filipovic M. H2S generates HNO and HSNO from nitrite by a heme iron-catalyzed metabolism in mitochondria. *Free Radic Biol Med* 65: S98, 2013.
177. Miriyala S, Spasojevic I, Tovmasyan A, Salvemini D, Vujaskovic Z, St Clair D, and Batinic-Haberle I. Manganese superoxide dismutase, MnSOD and its mimics. *Biochim Biophys Acta* 1822: 794–814, 2012.
178. Miriyala S, Thipakkorn C, Xu Y, Noel T, Kooi CV, Batinic-Haberle I, Prachayasittikul V, and Clair DK. 4-Hydroxy-2-nonenal mediates Aifm2 release from mitochondria: an insight into the mechanism of oxidative stress mediated retrograde signaling. *Free Radic Biol Med* 51: S30, 2011.
179. Miriyala S, Thippakorn C, Chaiswing L, Xu Y, Noel T, Tovmasyan A, Batinic-Haberle I, Kooi CV, Chi W, Latif AA, Reda H, Oberley T, Prachayasittikul V, and Clair DK. 4-hydroxy-2-nonenal triggers AIFM2-mediated retrograde signaling by activating its translocation and function switching. Submitted 2013.
180. Moeller BJ, Batinic-Haberle I, Spasojevic I, Rabbani ZN, Anscher MS, Vujaskovic Z, and Dewhirst MW. A manganese porphyrin superoxide dismutase mimetic enhances tumor radioresponsiveness. *Int J Radiat Oncol Biol Phys* 63: 545–552, 2005.
181. Monti DA, Mitchell E, Bazzan AJ, Littman S, Zabrecky G, Yeo CJ, Pillai MV, Newberg AB, Deshmukh S, and Levine M. Phase I evaluation of intravenous ascorbic acid in combination with gemcitabine and erlotinib in patients with metastatic pancreatic cancer. *PLoS One* 7: e29794, 2012.
182. Moon EJ, Sonveaux P, Porporato PE, Danhier P, Gallez B, Batinic-Haberle I, Nien YC, Schroeder T, and Dewhirst MW. NADPH oxidase-mediated reactive oxygen species production activates hypoxia-inducible factor-1 (HIF-1) via the ERK pathway after hyperthermia treatment. *Proc Natl Acad Sci U S A* 107: 20477–20482, 2010.
183. Mouraviev V, Venkatraman T, Tovmasyan A, Kimura M, Tsivian M, Mouravieva V, Polascik T, Wang H, Amrhein TJ, Batinic-Haberle I, and Lascola C. Mn porphryins as novel molecular MRI contrast agents. *J Endourol* 1420–1424, 2011.
184. Mu XH and Kadish KM. Insitu Ftir and Uv-visible spectroelectrochemical studies of iron nitrosyl porphyrins in nonaqueous media. *Inorg Chem* 27: 4720–4725, 1988.
185. Murphy AJ, Guyre PM, and Pioli PA. Estradiol suppresses NF-kappa B activation through coordinated regulation of let-7a and miR-125b in primary human macrophages. *J Immunol* 184: 5029–5037, 2010.
186. Murphy CK, Fey EG, Watkins BA, Wong V, Rothstein D, and Sonis ST. Efficacy of superoxide dismutase mimetic M40403 in attenuating radiation-induced oral mucositis in hamsters. *Clin Cancer Res* 14: 4292–4297, 2008.
187. Muscoli C, Cuzzocrea S, Ndengele MM, Mollace V, Porreca F, Fabrizi F, Esposito E, Masini E, Matuschak GM, and Salvemini D. Therapeutic manipulation of peroxynitrite attenuates the development of opiate-induced antinociceptive tolerance in mice. *J Clin Invest* 117: 3530–3539, 2007.
188. Nangle MR, Cotter MA, and Cameron NE. Effects of the peroxynitrite decomposition catalyst, FeTMPyP, on function of corpus cavernosum from diabetic mice. *Eur J Pharmacol* 502: 143–148, 2004.
189. Negi G, Kumar A, and Sharma SS. Concurrent targeting of nitrosative stress-PARP pathway corrects functional, behavioral and biochemical deficits in experimental diabetic neuropathy. *Biochem Biophys Res Commun* 391: 102–106, 2010.
190. Nilakantan V, Liang H, Maenpaa CJ, and Johnson CP. Differential patterns of peroxynitrite mediated apoptosis in proximal tubular epithelial cells following ATP depletion recovery. *Apoptosis* 13: 621–633, 2008.
191. Nonn L, Berggren M, and Powis G. Increased expression of mitochondrial peroxiredoxin-3 (thioredoxin peroxidase-2) protects cancer cells against hypoxia and drug-induced hydrogen peroxide-dependent apoptosis. *Mol Cancer Res* 1: 682–689, 2003.
192. Oberley-Deegan RE, Steffan JJ, Rove KO, Pate KM, Weaver MW, Spasojevic I, Frederick B, Raben D, Meacham RB, Crapo JD, and Koul HK. The antioxidant, MnTE-2-PyP, prevents side-effects incurred by prostate cancer irradiation. *PLoS One* 7: e44178, 2012.
193. Obrosova IG, Mabley JG, Zsengeller Z, Charniauskaya T, Abatan OI, Groves JT, and Szabo C. Role for nitrosative stress in diabetic neuropathy: evidence from studies with a peroxynitrite decomposition catalyst. *FASEB J* 19: 401–403, 2005.
194. Ohiro Y, Garkavtsev I, Kobayashi S, Sreekumar KR, Nantz R, Higashikubo BT, Duffy SL, Higashikubo R, Usheva A, Gius D, Kley N, and Horikoshi N. A novel p53-inducible apoptogenic gene, PRG3, encodes a homologue of the apoptosis-inducing factor (AIF). *FEBS Lett* 524: 163–171, 2002.
195. Okado-Matsumoto A, Batinic-Haberle I, and Fridovich I. Complementation of SOD-deficient *Escherichia coli* by manganese porphyrin mimics of superoxide dismutase activity. *Free Radic Biol Med* 37: 401–410, 2004.
196. Okun Z and Gross Z. Fine tuning the reactivity of corrole-based catalytic antioxidants. *Inorg Chem* 51: 8083–8090, 2012.
197. Okun Z, Kuperschmidt L, Youdim MB, and Gross Z. Cellular uptake and organ accumulation of amphipolar metallocorroles with cytoprotective and cytotoxic properties. *Anticancer Agents Med Chem* 11: 380–384, 2011.
198. Orrell RW. AEOL-10150 (Aeolus). *Curr Opin Investig Drugs* 7: 70–80, 2006.
199. Padayatty SJ and Levine M. Reevaluation of ascorbate in cancer treatment: emerging evidence, open minds and serendipity. *J Am Coll Nutr* 19: 423–425, 2000.

200. Palomares SM, Gardner-Morse I, Sweet JG, and Cipolla MJ. Peroxynitrite decomposition with FeTMPyP improves plasma-induced vascular dysfunction and infarction during mild but not severe hyperglycemic stroke. *J Cereb Blood Flow Metab* 32: 1035–1045, 2012.
201. Para AE, Bezjak A, Yeung IW, Van Dyk J, and Hill RP. Effects of genistein following fractionated lung irradiation in mice. *Radiother Oncol* 92: 500–510, 2009.
202. Park W and Lim D. Effect of the oligo(ethylene glycol) group on the antioxidant activity of manganese salen complexes. *Bioorg Med Chem Lett* 19: 614–617, 2009.
203. Pasternack RF and Halliwell B. Superoxide dismutase activities of an iron porphyrin and other iron complexes. *J Am Chem Soc* 101: 1026–1031, 1979.
204. Pate K, Dunham K, Padgett L, Tse H, Floyd C, and Crapo J. MnTnBuOE-2-PyP^{5+} is neuroprotective following acute cervical spinal cord injury in rats. *Free Radic Biol Med* 53: S114, 2012.
204a. Pickens J, Savage K, Tse H, Batinic-Haberle I, Floyd C. A metalloporphyrin catalytic oxidoreductant is protective after spinal cord injury in a rat model. 31st Annual National Neurotrauma Symposium, Nashville, TN. D-162, 2013.
205. Pazhanisamy SK, Li H, Wang Y, Batinic-Haberle I, and Zhou D. NADPH oxidase inhibition attenuates total body irradiation-induced haematopoietic genomic instability. *Mutagenesis* 26: 431–435, 2011.
206. Pearlstein RD, Higuchi Y, Moldovan M, Johnson K, Fukuda S, Gridley DS, Crapo JD, Warner DS, and Slater JM. Metalloporphyrin antioxidants ameliorate normal tissue radiation damage in rat brain. *Int J Radiat Biol* 86: 145–163, 2010.
207. Pieper GM, Nilakantan V, Chen M, Zhou J, Khanna AK, Henderson JD, Jr., Johnson CP, Roza AM, and Szabo C. Protective mechanisms of a metalloporphyrinic peroxynitrite decomposition catalyst, WW85, in rat cardiac transplants. *J Pharmacol Exp Ther* 314: 53–60, 2005.
208. Piganelli JD, Mathews CE. Autoreactive T-cell responses: new technology in pursuit of an old nemesis. *Pediatr Diabetes* 8: 249–51, 2007.
208a. Delmastro-Greenwood MM, Tse HM, Piganelli JD. Effects of metalloporphyrins on reducing inflammation and autoimmunity. *Antioxid Redox Signal* 20: 2465–2477, 2014.
209. Piganelli JD, Flores SC, Cruz C, Koepp J, Batinic-Haberle I, Crapo J, Day B, Kachadourian R, Young R, Bradley B, and Haskins K. A metalloporphyrin-based superoxide dismutase mimic inhibits adoptive transfer of autoimmune diabetes by a diabetogenic T-cell clone. *Diabetes* 51: 347–355, 2002.
210. Pollard JM, Reboucas JS, Durazo A, Kos I, Fike F, Panni M, Gralla EB, Valentine JS, Batinic-Haberle I, and Gatti RA. Radioprotective effects of manganese-containing superoxide dismutase mimics on ataxia-telangiectasia cells. *Free Radic Biol Med* 47: 250–260, 2009.
211. Rabbani ZN, Batinic-Haberle I, Anscher MS, Huang J, Day BJ, Alexander E, Dewhirst MW, and Vujaskovic Z. Long-term administration of a small molecular weight catalytic metalloporphyrin antioxidant, AEOL 10150, protects lungs from radiation-induced injury. *Int J Radiat Oncol Biol Phys* 67: 573–580, 2007.
212. Rabbani ZN, Salahuddin FK, Yarmolenko P, Batinic-Haberle I, Thrasher BA, Gauter-Fleckenstein B, Dewhirst MW, Anscher MS, and Vujaskovic Z. Low molecular weight catalytic metalloporphyrin antioxidant AEOL 10150 protects lungs from fractionated radiation. *Free Radic Res* 41: 1273–1282, 2007.
213. Rabbani ZN, Spasojevic I, Zhang X, Moeller BJ, Haberle S, Vasquez-Vivar J, Dewhirst MW, Vujaskovic Z, and Batinic-Haberle I. Antiangiogenic action of redox-modulating Mn(III) meso-tetrakis(N-ethylpyridinium-2-yl)porphyrin, MnTE-2-PyP(5+), via suppression of oxidative stress in a mouse model of breast tumor. *Free Radic Biol Med* 47: 992–1004, 2009.
214. Radovits T, Beller CJ, Groves JT, Merkely B, Karck M, Szabo C, and Szabo G. Effects of FP15, a peroxynitrite decomposition catalyst on cardiac and pulmonary function after cardiopulmonary bypass. *Eur J Cardiothorac Surg* 41: 391–396, 2012.
215. Radovits T, Seres L, Gero D, Lin LN, Beller CJ, Chen SH, Zotkina J, Berger I, Groves JT, Szabo C, and Szabo G. The peroxynitrite decomposition catalyst FP15 improves ageing-associated cardiac and vascular dysfunction. *Mech Ageing Dev* 128: 173–181, 2007.
216. Rajic Z, Tovmasyan A, Spasojevic I, Sheng H, Lu M, Li AM, Gralla EB, Warner DS, Benov L, and Batinic-Haberle I. A new SOD mimic, Mn(III) ortho N-butoxyethylpyridylporphyrin, combines superb potency and lipophilicity with low toxicity. *Free Radic Biol Med* 52: 1828–1834, 2012.
217. Rausaria S, Ghaffari MM, Kamadulski A, Rodgers K, Bryant L, Chen Z, Doyle T, Shaw MJ, Salvemini D, and Neumann WL. Retooling manganese(III) porphyrin-based peroxynitrite decomposition catalysts for selectivity and oral activity: a potential new strategy for treating chronic pain. *J Med Chem* 54: 8658–8669, 2011.
218. Rausaria S, Kamadulski A, Rath NP, Bryant L, Chen Z, Salvemini D, and Neumann WL. Manganese(III) complexes of bis(hydroxyphenyl)dipyrromethenes are potent orally active peroxynitrite scavengers. *J Am Chem Soc* 133: 4200–4203, 2011.
219. Ravizza R, Cereda E, Monti E, and Gariboldi MB. The piperidine nitroxide Tempol potentiates the cytotoxic effects of temozolomide in human glioblastoma cells. *Int J Oncol* 25: 1817–1822, 2004.
220. Rawal M, Schroeder SR, Wagner BA, Cushing CM, Welsh JL, Button AM, Du J, Sibenaller ZA, Buettner GR, Cullen JJ. Manganoporphyrins Increase Ascorbate-Induced Cytotoxicity by Enhancing H_2O_2 Generation. *Cancer Res.* 73: 5232–5241, 2013.
221. Reboucas JS, DeFreitas-Silva G, Spasojevic I, Idemori YM, Benov L, and Batinic-Haberle I. Impact of electrostatics in redox modulation of oxidative stress by Mn porphyrins: protection of SOD-deficient *Escherichia coli* via alternative mechanism where Mn porphyrin acts as a Mn carrier. *Free Radic Biol Med* 45: 201–210, 2008.
222. Reboucas JS, Kos I, Vujaskovic Z, and Batinic-Haberle I. Determination of residual manganese in Mn porphyrin-based superoxide dismutase (SOD) and peroxynitrite reductase mimics. *J Pharm Biomed Anal* 50: 1088–1091, 2009.
223. Reboucas JS, Spasojevic I, and Batinic-Haberle I. Pure manganese(III) 5,10,15,20-tetrakis(4-benzoic acid)porphyrin (MnTBAP) is not a superoxide dismutase mimic in aqueous systems: a case of structure-activity relationship as a watchdog mechanism in experimental therapeutics and biology. *J Biol Inorg Chem* 13: 289–302, 2008.
224. Reboucas JS, Spasojevic I, and Batinic-Haberle I. Quality of potent Mn porphyrin-based SOD mimics and peroxynitrite

scavengers for pre-clinical mechanistic/therapeutic purposes. *J Pharm Biomed Anal* 48: 1046–1049, 2008.
225. Reboucas JS, Spasojevic I, Tjahjono DH, Richaud A, Mendez F, Benov L, and Batinic-Haberle I. Redox modulation of oxidative stress by Mn porphyrin-based therapeutics: the effect of charge distribution. *Dalton Trans* 1233–1242, 2008.
226. Riley DP. Rational design of synthetic enzymes and their potential utility as human pharmaceuticals: development of manganese(II)-based superoxide dismutase mimics. In: *Advances in Supramolecular Chemistry*. Stanford, JAI Press Inc. 2000, pp. 217–244.
227. Riley DP, Henke SL, Lennon PJ, and Aston K. Computer-aided design (CAD) of synzymes: use of molecular mechanics (MM) for the rational design of superoxide dismutase mimics. *Inorg Chem* 38: 1908–1917, 1999.
228. Riley DP, Lennon PJ, Neumann WL, and Weiss RH. Toward the rational design of superoxide dismutase mimics: mechanistic studies for the elucidation of substituent effects on the catalytic activity of macrocyclic manganese(II) complexes. *J Am Chem Soc* 119: 6522–6528, 1997.
229. Rosenthal RA, Fish B, Hill RP, Huffman KD, Lazarova Z, Mahmood J, Medhora M, Molthen R, Moulder JE, Sonis ST, Tofilon PJ, and Doctrow SR. Salen Mn complexes mitigate radiation injury in normal tissues. *Anticancer Agents Med Chem* 11: 359–372, 2011.
230. Roth JA. Homeostatic and toxic mechanisms regulating manganese uptake, retention, and elimination. *Biol Res* 39: 45–57, 2006.
231. Saito S, Hasegawa S, Sekita A, Bakalova R, Furukawa T, Murase K, Saga T, and Aoki I. Manganese-enhanced MRI reveals early-phase radiation-induced cell alterations *in vivo*. *Cancer Res* 73: 3216–3224, 2013.
232. Salvemini D, Wang ZQ, Zweier JL, Samouilov A, Macarthur H, Misko TP, Currie MG, Cuzzocrea S, Sikorski JA, and Riley DP. A nonpeptidyl mimic of superoxide dismutase with therapeutic activity in rats. *Science* 286: 304–306, 1999.
233. Sampson N, Koziel R, Zenzmaier C, Bubendorf L, Plas E, Jansen-Durr P, and Berger P. ROS signaling by NOX4 drives fibroblast-to-myofibroblast differentiation in the diseased prostatic stroma. *Mol Endocrinol* 25: 503–515, 2011.
234. Sharpe MA, Ollosson R, Stewart VC, and Clark JB. Oxidation of nitric oxide by oxomanganese-salen complexes: a new mechanism for cellular protection by superoxide dismutase/catalase mimetics. *Biochem J* 366: 97–107, 2002.
235. Shen KK, Ji LL, Chen Y, Yu QM, and Wang ZT. Influence of glutathione levels and activity of glutathione-related enzymes in the brains of tumor-bearing mice. *Biosci Trends* 5: 30–37, 2011.
236. Sheng H, Chaparro RE, Sasaki T, Izutsu M, Pearlstein RD, Tovmasyan A, and Warner DS. Metalloporphyrins as therapeutic catalytic oxidoreductants in central nervous system disorders. *Antioxid Redox Signal* 20: 2437–2464, 2014.
237. Sheng H, Enghild JJ, Bowler R, Patel M, Batinic-Haberle I, Calvi CL, Day BJ, Pearlstein RD, Crapo JD, and Warner DS. Effects of metalloporphyrin catalytic antioxidants in experimental brain ischemia. *Free Radic Biol Med* 33: 947–961, 2002.
238. Sheng H, Spasojevic I, Tse HM, Jung JY, Hong J, Zhang Z, Piganelli JD, Batinic-Haberle I, and Warner DS. Neuroprotective efficacy from a lipophilic redox-modulating Mn(III) N-Hexylpyridylporphyrin, MnTnHex-2-PyP: rodent models of ischemic stroke and subarachnoid hemorrhage. *J Pharmacol Exp Ther* 338: 906–916, 2011.
239. Sheng H, Spasojevic I, Warner DS, and Batinic-Haberle I. Mouse spinal cord compression injury is ameliorated by intrathecal cationic manganese(III) porphyrin catalytic antioxidant therapy. *Neurosci Lett* 366: 220–225, 2004.
240. Sheng H, Yang W, Fukuda S, Tse HM, Paschen W, Johnson K, Batinic-Haberle I, Crapo JD, Pearlstein RD, Piganelli J, and Warner DS. Long-term neuroprotection from a potent redox-modulating metalloporphyrin in the rat. *Free Radic Biol Med* 47: 917–923, 2009.
241. Shimanovich R and Groves JT. Mechanisms of peroxynitrite decomposition catalyzed by FeTMPS, a bioactive sulfonated iron porphyrin. *Arch Biochem Biophys* 387: 307–317, 2001.
242. Shimanovich R, Hannah S, Lynch V, Gerasimchuk N, Mody TD, Magda D, Sessler J, and Groves JT. Mn(II)-texaphyrin as a catalyst for the decomposition of peroxynitrite. *J Am Chem Soc* 123: 3613–3614, 2001.
243. Siriphorn A, Dunham KA, Chompoopong S, and Floyd CL. Postinjury administration of 17beta-estradiol induces protection in the gray and white matter with associated functional recovery after cervical spinal cord injury in male rats. *J Comp Neurol* 520: 2630–2646, 2012.
244. Soriano FG, Lorigados CB, Pacher P, and Szabo C. Effects of a potent peroxynitrite decomposition catalyst in murine models of endotoxemia and sepsis. *Shock* 35: 560–566, 2011.
245. Sorokina LV, Solyanik GI, and Pyatchanina TV. The evaluation of prooxidant and antioxidant state of two variants of lewis lung carcinoma: a comparative study. *Exp Oncol* 32: 249–253, 2010.
246. Soule BP, Hyodo F, Matsumoto K, Simone NL, Cook JA, Krishna MC, and Mitchell JB. The chemistry and biology of nitroxide compounds. *Free Radic Biol Med* 42: 1632–1650, 2007.
247. Spasojevic I and Batinic-Haberle I. Manganese(III) complexes with porphyrins and related compounds as catalytic scavengers of superoxide (vol 317, pg 230, 2001). *Inorg Chim Acta* 328: 263–263, 2002.
248. Spasojevic I, Batinic-Haberle I, and Fridovich I. Nitrosylation of manganese(II) tetrakis(N-ethylpyridinium-2-yl)porphyrin: a simple and sensitive spectrophotometric assay for nitric oxide. *Nitric Oxide* 4: 526–533, 2000.
249. Spasojevic I, Batinic-Haberle I, Stevens RD, Hambright P, Thorpe AN, Grodkowski J, Neta P, and Fridovich I. Manganese(III) biliverdin IX dimethyl ester: a powerful catalytic scavenger of superoxide employing the Mn(III)/Mn(IV) redox couple. *Inorg Chem* 40: 726–739, 2001.
250. Spasojevic I, Chen Y, Noel TJ, Fan P, Zhang L, Reboucas JS, St Clair DK, and Batinic-Haberle I. Pharmacokinetics of the potent redox-modulating manganese porphyrin, MnTE-2-PyP(5+), in plasma and major organs of B6C3F1 mice. *Free Radic Biol Med* 45: 943–949, 2008.
251. Spasojevic I, Kos I, Benov LT, Rajic Z, Fels D, Dedeugd C, Ye X, Vujaskovic Z, Reboucas JS, Leong KW, Dewhirst MW, and Batinic-Haberle I. Bioavailability of metalloporphyrin-based SOD mimics is greatly influenced by a single charge residing on a Mn site. *Free Radic Res* 45: 188–200, 2011.
252. Spasojevic I, Li AM, Tovmasyan A, Rajic Z, Salvemini D, St. Clair D, Valentine JS, Vujaskovic Z, Gralla EB, and Batinic-Haberle I. Accumulation of porphyrin-based SOD mimics

in mitochondria is proportional to their lipophilicity. *Free Radic Biol Med* 49: S199, 2010.
253. Spasojevic I, Menzeleev R, White PS, and Fridovich I. Rotational isomers of N-alkylpyridylporphyrins and their metal complexes. HPLC separation, H-1 NMR and X-ray structural characterization, electrochemistry, and catalysis of O-2(center dot-) disproportionation. *Inorg Chem* 41: 5874–5881, 2002.
254. Spasojevic I, Miryala S, Tovmasyan A, Salvemini D, Vujaskovic Z, Batinic-Haberle I, and St. Clair D. Lipophilicity of Mn(III) *N*-alkylpyridylporphyrins dominates their accumulation within mitochondria and therefore *in vivo* efficacy. A mouse study. *Free Radic Biol Med* 51: S98, 2011.
255. Srinivasan V, Doctrow S, Singh VK, and Whitnall MH. Evaluation of EUK-189, a synthetic superoxide dismutase/catalase mimetic as a radiation countermeasure. *Immunopharmacol Immunotoxicol* 30: 271–290, 2008.
256. Stefanutti G, Pierro A, Smith VV, Klein NJ, and Eaton S. Peroxynitrite decomposition catalyst FeTMPyP provides partial protection against intestinal ischemia and reperfusion injury in infant rats. *Pediatr Res* 62: 43–48, 2007.
257. Suofu Y, Clark J, Broderick J, Wagner KR, Tomsick T, Sa Y, and Lu A. Peroxynitrite decomposition catalyst prevents matrix metalloproteinase activation and neurovascular injury after prolonged cerebral ischemia in rats. *J Neurochem* 115: 1266–1276, 2010.
258. Szabo C, Ischiropoulos H, and Radi R. Peroxynitrite: biochemistry, pathophysiology and development of therapeutics. *Nat Rev Drug Discov* 6: 662–680, 2007.
259. Szabo G, Loganathan S, Merkely B, Groves JT, Karck M, Szabo C, and Radovits T. Catalytic peroxynitrite decomposition improves reperfusion injury after heart transplantation. *J Thorac Cardiovasc Surg* 143: 1443–1449, 2012.
260. Tang SY and Halliwell B. Medicinal plants and antioxidants: what do we learn from cell culture and *Caenorhabditis elegans* studies? *Biochem Biophys Res Commun* 394: 1–5, 2010.
261. Tantra R, Cackett A, Peck R, Gohil D, and Snowden J. Measurement of redox potential in nanoecotoxicological investigations. *J Toxicol* 2012: 270651, 2012.
262. Tareen B, Summers JL, Jamison JM, Neal DR, McGuire K, Gerson L, and Diokno A. A 12 week, open label, phase I/IIa study using apatone for the treatment of prostate cancer patients who have failed standard therapy. *Int J Med Sci* 5: 62–67, 2008.
263. Tarnuzzer RW, Colon J, Patil S, and Seal S. Vacancy engineered ceria nanostructures for protection from radiation-induced cellular damage. *Nano Lett* 5: 2573–2577, 2005.
264. Thamsen M and Jakob U. The redoxome: proteomic analysis of cellular redox networks. *Curr Opin Chem Biol* 15: 113–119, 2011.
265. Theriot CA, Casey RC, Moore VC, Mitchell L, Reynolds JO, Burgoyne M, Partha R, Huff JL, Conyers JL, Jeevarajan A, and Wu H. Dendro[C(60)]fullerene DF-1 provides radioprotection to radiosensitive mammalian cells. *Radiat Environ Biophys* 49: 437–445, 2010.
266. Thomas R and Sharifi N. SOD mimetics: a novel class of androgen receptor inhibitors that suppresses castration-resistant growth of prostate cancer. *Mol Cancer Ther* 11: 87–97, 2012.
267. Thompson JS, Chu Y, Glass J, Tapp AA, and Brown SA. The manganese superoxide dismutase mimetic, M40403, protects adult mice from lethal total body irradiation. *Free Radic Res* 44: 529–540, 2010.
268. Tian J, Peehl DM, and Knox SJ. Metalloporphyrin synergizes with ascorbic acid to inhibit cancer cell growth through fenton chemistry. *Cancer Biother Radiopharm* 25: 439–448, 2010.
269. Tome ME, Lee K, Jaramillo MC, and Briehl MM. Mitochondria are the primary source of the H(2)O(2) signal for glucocorticoid-induced apoptosis of lymphoma cells. *Exp Ther Med* 4: 237–242, 2012.
270. Tovmasyan A, Reboucas JS, and Benov L. Simple biological systems for assessing the activity of superoxide dismutase mimics. *Antioxid Redox Signal* 20: 2416–2436, 2014.
271. Tovmasyan A, Sheng H, Weitner T, Arulpragasam A, Lu M, Warner DS, Vujaskovic Z, Spasojevic I, and Batinic-Haberle I. Design, mechanism of action, bioavailability and therapeutic effects of Mn porphyrin-based redox modulators. *Med Princ Pract* 22: 103–130, 2013.
272. Tovmasyan A, Weitner T, Roberts E, Jaramillo M, Spasojevic I, Leong K, Tome M, Benov L, and Batinic-Haberle I. Understanding differences in mechanisms of action of Fe vs Mn porphyrins: comparison of their reactivities towards cellular reductants and reactive species. *Free Radic Biol Med* 53: S120, 2012.
273. Tovmasyan A, Weitner T, Sheng H, Lu M, Rajic Z, Warner DS, Spasojevic I, Reboucas JS, Benov L, and Batinic-Haberle I. Differential coordination demands in Fe versus Mn water-soluble cationic metalloporphyrins translate into remarkably different aqueous redox chemistry and biology. *Inorg Chem* 52: 5677–5691, 2013.
274. Tovmasyan AG, Rajic Z, Spasojevic I, Reboucas JS, Chen X, Salvemini D, Sheng H, Warner DS, Benov L, and Batinic-Haberle I. Methoxy-derivatization of alkyl chains increases the *in vivo* efficacy of cationic Mn porphyrins. Synthesis, characterization, SOD-like activity, and SOD-deficient *E. coli* study of meta Mn(III) N-methoxyalkylpyridylporphyrins. *Dalton Trans* 40: 4111–4121, 2011.
275. Trajkovic S, Dobric S, Jacevic V, Dragojevic-Simic V, Milovanovic Z, and Dordevic A. Tissue-protective effects of fullerenol C60(OH)24 and amifostine in irradiated rats. *Colloids Surf B Biointerfaces* 58: 39–43, 2007.
276. Trofimova NS, Safronov AY, and Ikeda O. Electrochemical and spectral studies on the reductive nitrosylation of water-soluble iron porphyrin. *Inorg Chem* 42: 1945–1951, 2003.
277. Trostchansky A, Ferrer-Sueta G, Batthyany C, Botti H, Batinic-Haberle I, Radi R, and Rubbo H. Peroxynitrite flux-mediated LDL oxidation is inhibited by manganese porphyrins in the presence of uric acid. *Free Radic Biol Med* 35: 1293–1300, 2003.
278. Tse HM, Milton MJ, and Piganelli JD. Mechanistic analysis of the immunomodulatory effects of a catalytic antioxidant on antigen-presenting cells: implication for their use in targeting oxidation-reduction reactions in innate immunity. *Free Radic Biol Med* 36: 233–247, 2004.
279. Valsecchi V, Pignataro G, Sirabella R, Matrone C, Boscia F, Scorziello A, Sisalli MJ, Esposito E, Zambrano N, Cataldi M, Di Renzo G, and Annunziato L. Transcriptional regulation of ncx1 gene in the brain. *Adv Exp Med Biol* 961: 137–145, 2013.
280. Vance CK and Miller AF. A simple proposal that can explain the inactivity of metal-substituted superoxide dismutases. *J Am Chem Soc* 120: 461–467, 1998.
281. Vance CK and Miller AF. Novel insights into the basis for *Escherichia coli* superoxide dismutase's metal ion specificity

from Mn-substituted FeSOD and its very high E(m). *Biochemistry* 40: 13079–13087, 2001.
282. Vander Heiden MG, Cantley LC, and Thompson CB. Understanding the Warburg effect: the metabolic requirements of cell proliferation. *Science* 324: 1029–1033, 2009.
283. Varecha M, Amrichova J, Zimmermann M, Ulman V, Lukasova E, and Kozubek M. Bioinformatic and image analyses of the cellular localization of the apoptotic proteins endonuclease G, AIF, and AMID during apoptosis in human cells. *Apoptosis* 12: 1155–1171, 2007.
284. Verrax J, Beck R, Dejeans N, Glorieux C, Sid B, Pedrosa RC, Benites J, Vasquez D, Valderrama JA, and Calderon PB. Redox-active quinones and ascorbate: an innovative cancer therapy that exploits the vulnerability of cancer cells to oxidative stress. *Anticancer Agents Med Chem* 11: 213–221, 2011.
285. Vorotnikova E, Rosenthal RA, Tries M, Doctrow SR, and Braunhut SJ. Novel synthetic SOD/catalase mimetics can mitigate capillary endothelial cell apoptosis caused by ionizing radiation. *Radiat Res* 173: 748–759, 2010.
286. Vujaskovic Z, Batinic-Haberle I, Rabbani ZN, Feng QF, Kang SK, Spasojevic I, Samulski TV, Fridovich I, Dewhirst MW, and Anscher MS. A small molecular weight catalytic metalloporphyrin antioxidant with superoxide dismutase (SOD) mimetic properties protects lungs from radiation-induced injury. *Free Radic Biol Med* 33: 857–863, 2002.
287. Weaver MR, Venkatraman S, Venkataraman S, and Oberley-Deegan RE. The SOD mimetic, MnTE-2-PyP, Inhibits prostate tumor growth and metastasis. *Free Radic Biol Med* 53: S48, 2012.
288. Weitner T, Kos I, Sheng H, Tovmasyan A, Reboucas JS, Fan P, Warner DS, Vujaskovic Z, Batinic-Haberle I, and Spasojevic I. Comprehensive pharmacokinetic studies and oral bioavailability of two Mn porphyrin-based SOD mimics, MnTE-2-PyP(5+) and MnTnHex-2-PyP(5+). *Free Radic Biol Med* 58: 73–80, 2013.
289. Weitner T, Sheng H, Miriyala S, Leu D, Tovmasyan A, Kos I, Reboucas JS, Fan P, Vujaskovic Z, Batinic-Haberle I, Huang TT, Clair DK, Warner DS, and Spasojevic I. Comprehensive pharmocokinetic studies and biodistribution of two cationic Mn porphyrins-based catalysts, MnTE-2-PyP^{5+} and MnTnHex-2-PyP^{5+}: plasma and organ oral availability, mitochondrial, cytosolic, whole brain, hippocampus and cortex distribution. *Free Radic Biol Med* 53: S118, 2012.
290. Welsh JJ, Du J, Sibenaller ZA, Kalen AL, Wagner BA, Allen BG, Spitz DR, Goswami PC, Buettner GR, and Cullen JJ. Ascorbate is a radiosensitizer in pancreatic caner. *Free Rad Biol Med* 53: S52, 2012.
291. Welsh JL, Wagner BA, van't Erve TJ, Zehr PS, Berg DJ, Halfdanarson TR, Yee NS, Bodeker KL, Du J, Roberts LJ, 2nd, Drisko J, Levine M, Buettner GR, and Cullen JJ. Pharmacological ascorbate with gemcitabine for the control of metastatic and node-positive pancreatic cancer (PACMAN): results from a phase I clinical trial. *Cancer Chemother Pharmacol* 71: 765–775, 2013.
292. Winterbourn CC. Superoxide as an intracellular radical sink. *Free Radic Biol Med* 14: 85–90, 1993.
293. Winterbourn CC. The challenges of using fluorescent probes to detect and quantify specific reactive oxygen species in living cells. *Biochim Biophys Acta* 2013.
294. Winterbourn CC, Peskin AV, and Parsons-Mair HN. Thiol oxidase activity of copper, zinc superoxide dismutase. *J Biol Chem* 277: 1906–1911, 2002.
295. Wu M, Xu LG, Li X, Zhai Z, and Shu HB. AMID, an apoptosis-inducing factor-homologous mitochondrion-associated protein, induces caspase-independent apoptosis. *J Biol Chem* 277: 25617–25623, 2002.
296. Wu M, Xu LG, Su T, Tian Y, Zhai Z, and Shu HB. AMID is a p53-inducible gene downregulated in tumors. *Oncogene* 23: 6815–6819, 2004.
297. Yakovlev VA, Rabender CS, Sankala H, Gauter-Fleckenstein B, Fleckenstein K, Batinic-Haberle I, Jackson I, Vujaskovic Z, Anscher MS, Mikkelsen RB, and Graves PR. Proteomic analysis of radiation-induced changes in rat lung: Modulation by the superoxide dismutase mimetic MnTE-2-PyP(5+). *Int J Radiat Oncol Biol Phys* 78: 547–554, 2010.
298. Yallapu MM, Maher DM, Sundram V, Bell MC, Jaggi M, and Chauhan SC. Curcumin induces chemo/radio-sensitization in ovarian cancer cells and curcumin nanoparticles inhibit ovarian cancer cell growth. *J Ovarian Res* 3: 11, 2010.
299. Ye X, Fels D, Tovmasyan A, Aird KM, Dedeugd C, Allensworth JL, Kos I, Park W, Spasojevic I, Devi GR, Dewhirst MW, Leong KW, and Batinic-Haberle I. Cytotoxic effects of Mn(III) N-alkylpyridylporphyrins in the presence of cellular reductant, ascorbate. *Free Radic Res* 45: 1289–1306, 2011.
300. Yikilmaz E, Xie J, Brunold TC, and Miller AF. Hydrogen-bond-mediated tuning of the redox potential of the nonheme Fe site of superoxide dismutase. *J Am Chem Soc* 124: 3482–3483, 2002.
301. Young HK, Floyd RA, Maidt ML, and Dynlacht JR. Evaluation of nitrone spin-trapping agents as radioprotectors. *Radiat Res* 146: 227–231, 1996.
302. Zhang Y, Zhang X, Rabbani ZN, Jackson IL, and Vujaskovic Z. Oxidative stress mediates radiation lung injury by inducing apoptosis. *Int J Radiat Oncol Biol Phys* 83: 740–748, 2012.
303. Zhao Q, Li Y, Xu J, Liu R, and Li W. Radioprotection by fullerenols of Stylonychia mytilus exposed to gamma-rays. *Int J Radiat Biol* 81: 169–175, 2005.
304. Zhao Y, Chaiswing L, Oberley TD, Batinic-Haberle I, St Clair W, Epstein CJ, and St Clair D. A mechanism-based antioxidant approach for the reduction of skin carcinogenesis. *Cancer Res* 65: 1401–1405, 2005.
305. Zheng H, Nagaraja GM, Kaur P, Asea EE, and Asea A. Chaperokine function of recombinant Hsp72 produced in insect cells using a baculovirus expression system is retained. *J Biol Chem* 285: 349–356, 2010.

Address correspondence to:
Dr. Ines Batinic-Haberle
Department of Radiation Oncology
Duke University Medical Center
Research Drive
281b/285 MSRB I
Box 3455
Durham, NC 27710

E-mail: ibatinic@duke.edu

Date of first submission to ARS Central, January 2, 2013; date of final revised submission, June 30, 2013; date of acceptance, July 22, 2013.

Abbreviations Used

2-DG = 2-deoxy-D-glucose
8-OHdG = 8-oxo-2′-deoxyguanosine
AP-1 = activator protein-1
AUC = pharmacokinetic parameter, area under the curve up to the last measurement at 24h
BBB = blood brain barrier
Ceo^- = hypochlorous acid, deprotonoted
$CO_3^{\bullet-}$ = carbonate radical
DMEM = Dulbecco's modified Eagle medium-low glucose
$E_{1/2}$ = half-wave reduction potential
EDTA = ethylenediaminetetraacetic acid
EUK-8 = Mn(III) salen
FeP = Fe porphyrin
FeTE-2(or 3)-PyP^{5+} = Fe(III) *meso*-tetrakis(*N*-ethylpyridinium-2(or 3)-yl)porphyrin
FeTM-4-PyP^{5+} = Fe(III) *meso*-tetrakis(*N*-methylpyridinium-4-yl)porphyrin
$FeTMSP^{7-}$ = Fe(III) *meso*-tetrakis(2,4,6-trimethyl-3,5-disulfonatophenyl)porphyrin
FeTnBuOE-2-PyP^{5+} = Fe(III) *meso*-tetrakis(*N*-(n-butoxyethyl)pyridinium-2-yl)porphyrin
$FeTSPP^{3-}$ = (Fe(III) *meso*-tetrakis(4-sulfonatophenyl)porphyrin
GALT = galactose-P uridylyltransferase
HA^- = ascorbic acid, deprotonated
HO_2^- = hydrogen peroxide, deprotonated
$(H_2O)_2Mn^{III}P$ = Mn(III) diaqua porphyrin
$(H_2O)Mn^{II}P$ = Mn(II) monoaqua porphyrin [when cationic porphyrins bear 5+ charge they have Mn in +3 oxidation state ($Mn^{III}P^{5+}$), and with 4+ total charge Mn is in +2 ($Mn^{II}P^{4+}$) or +4 oxidation states ($O{=}Mn^{IV}P^{4+}$)]
HIF-1α = hypoxia inducible factor-1
HSC = hematopoietic stem cell
ip = intraperitoneal
iv = intravenous
M40403 = cyclic polyamine
MC = metallocorrole
MCAO = middle cerebral artery occlusion
Mito-CP = Mito-carboxypropyl
MitoQ = mitochondrially targeted redox cycling qunone
$MnBr_8TM\text{-}3\text{-}PyP^{4+}$ = Mn(II) β-octabromo-*meso*-tetrakis(*N*-methylpyridinium-3-yl)porphyrin
$[MnBV^{2-}]_2$ = Mn(III) biliverdin
$MnDiM\text{-}4\text{-}PyMAn\text{-}Corrole^{3+}$ = Mn(III) *meso*-*trans*-di(*N*-methylpyridinium-4-yl)-mono(anisyl)corrole
MnHalTAlkyl-2(3, 4)-PyP^{5+}s = Mn(III) β-halogenated *meso*-tetrakis(*N*-alkylpyridinium-2(3, 4)-yl)porphyrins
$Mn^{II}Br_8TM\text{-}4\text{-}PyP^{4+}$ = Mn(II) β-octabromo-*meso*-tetrakis(*N*-methylpyridinium-4-yl)porphyrin
$Mn^{III}Br_8TCPP^{3-}$ = Mn(III) β-octabromo-*meso*-tetrakis(4-carboxylatophenyl)porphyrin (also $Mn^{III}Br_8TBAP^{3-}$)
$Mn^{III}Br_8TSPP^{3-}$ = Mn(III) β-octabromo-*meso*-tetrakis (4-sulfonatophenyl)porphyrin
$Mn^{III}C$ = Mn(III) corrole
$Mn^{IV}C$ = Mn(IV) corrole
MnP = Mn porphyrin
MnT-2-PyP^+ = Mn(III) *meso*-tetrakis(2-pyridyl)porphyrin
MnTAlkoxyalkyl-2-PyP^{5+}s = Mn(III) *meso*-tetrakis(*N*-alkoxyalkylpyridinium-2-yl)porphyrins
MnTAlkoxyalkyl-3-PyP^{5+}s = Mn(III) *meso*-tetrakis(*N*-alkoxyalkylpyridinium-3-yl)porphyrins
MnTAlkyl-2(3 or 4)-PyPs = Mn(III) *meso*-tetrakis(*N*-alkylpyridinium-2(3 or 4)-yl)porphyrins [Alkyl being methyl (M, AEOL10112), ethyl (E, AEOL10113, BMX-010, FBC-007), n-hexyl (nHex), n-heptyl (nHep), n-octyl (nOct); 2, 3 and 4 relate to *ortho*, *meta* and *para* isomers, respectively]
$MnTBAP^{3-}$ = Mn(III) *meso*-tetrakis(4-carboxyphenyl)porphyrin
$MnTDE\text{-}2\text{-}ImP^{5+}$ = Mn(III) *meso*-tetrakis(*N*,*N*′-diethylimidazolium-2-yl)porphyrin [AEOL10150]
MnTnBuOE-2-PyP^{5+} = Mn(III) *meso*-tetrakis(*N*-(n-butoxyethyl)pyridinium-2-yl)porphyrin
MnTN-sub-2-ImP^{5+}s = Mn(III) *meso*-tetrakis(*N*,*N*′-disubstituted imidazolium-2-yl)porphyrins
$MnTrF_5Ph\text{-}\beta(SO_3)_2\text{-}Corrole^{2-}$ = Mn(III) *meso*-tris(pentafluorophenyl)-β-bis(sulfonato)corrole
$MnTSPP^{3-}$ = Mn(III) *meso*-tetrakis(4-sulfonatophenyl)porphyrin
MPs = metalloporphyrins
$^{\bullet}NO$ = nitric oxide
NF-κB = nuclear factor κB

NHE = normal hydrogen electrode
Nrf-2 = nuclear factor-erythroid-derived 2-like 2
$O_2^{\bullet-}$ = superoxide
$(OH)(H_2O)Fe^{III}P$ = Fe(III) monohydroxo monoaqua porphyrin
$(OH)Fe^{II}P$ = Fe(II) monohydroxo porphyrin
peroxynitrite = $ONOO^-$+ONOOH, given its pKa = 6.6 at pH 7.8 peroxynitrite exists predominantly as $ONOO^-$
PK = pharmacokinetic
PTEN = phosphoinositide 3-phosphatase
RS^- = thiol, deprotonated
salen = *N*,*N*′-bis-(salicylideneamino)ethane
SAR = structure-activity relationship
SOD = superoxide dismutase
SVCT1 and SVCT2 = sodium-dependent vitamin C transporters 1 and 2
TBI = total body radiation
TD50 = median toxic dose of a drug which toxicity occurs in 50% of cases
tempol = 4-OH-2,2,6,6,-tetramethylpiperidine-1-oxyl
TF = transcription factor
VEGF = vascular endothelial growth factor